

**PRESSURE DISTRIBUTION DURING  
PARACHUTE OPENING**

**PHASE II. FINITE MASS OPERATING CASE**

*by*

*H. D. MELZIG*

*C. SALIARIS*

\*\*\* Export controls have been removed \*\*\*

This document is subject to special export controls and each transmittal to foreign governments or foreign nationals may be made only with prior approval of the Vehicle Equipment Division (FDF), Air Force Flight Dynamics Laboratory, Wright-Patterson AFB, Ohio 45433.

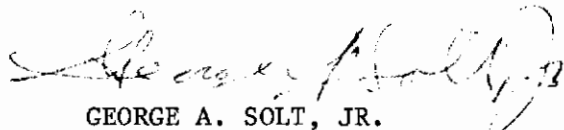
FOREWORD

This technical report was prepared by the Institut fuer Flugmechanik of the Deutsche Forschungsanstalt fuer Luft-und Raumfahrt E. V. (DFLR) under USAF Contract No. AF61(052)-922. The work was sponsored by the Air Force Flight Dynamics Laboratory, Wright-Patterson Air Force Base, Ohio, Air Force Systems Command, through the European Office of Aerospace Research, USAF. The work was administered by the European Office of Aerospace Research, USAF, in Brussels, Belgium, Captain William D. Higgins and Captain Ronald L. Carlberg, Contracting Officers, and was directed technically by the Recovery and Crew Station Branch, Air Force Flight Dynamics Laboratory. Mr. Rudi J. Berndt was the project engineer.

The research effort was initiated in February 1966 and completed in February 1968, and was conducted under Project No. 6065, "Design and Performance of Deployable Aerodynamic Decelerators;" Task 606503, "Parachute Aerodynamics and Structures."

This report was submitted by the authors in August 1968.

This technical report has been reviewed and is approved.



GEORGE A. SOLT, JR.  
Chief, Recovery & Crew Station Branch  
Vehicle Equipment Division  
Air Force Flight Dynamics Laboratory

# Contrails

## ABSTRACT

An experimental investigation was conducted to determine the differential pressure distribution over the surface of parachute canopies during the period of inflation under finite mass conditions.

Full scale parachute canopies of the Circular Flat, 10% Extended Skirt, Ringslot and Ribbon types were utilized during the free-flight test program, and differential pressures on the gore centerline and on the cord line were measured by means of four pressure transducers distributed over the canopy in equal distances from the skirt to the vent.

In order to analyze the relationships and dependencies between the pressure distribution, projected canopy area, canopy shape, generated force, and dynamic pressure, graphical displays of these quantities were made as a function of time for each type of parachute canopy.

The results of the pressure distribution measurements permit a better understanding of the physical nature of the dynamic process of parachute inflation. The stress distribution in a parachute canopy can be calculated if the corresponding canopy shape is known. For this purpose, the evolution of the canopy shape with the corresponding time is presented for each of the canopy types.

(The distribution of this Abstract is unlimited.)

# *Contrails*

# Contrails

## TABLE OF CONTENTS

SECTION	PAGE
1. INTRODUCTION	1
2. TEST CONDITIONS	1
2.1 Parachute Types	1
2.2 Test Vehicles and Test Method	2
2.3 Test Procedures	3
3. RESULTS AND ANALYSIS	4
3.1 Canopy Pressure Distribution and Corresponding Projected Canopy Area, Force, and Dynamic Pressure as Functions of Time	4
3.2 Evolvement of the Canopy Shape	6
4. CONCLUSIONS	7
5. REFERENCES	9
6. APPENDIX - Original Oscillographic Recordings of the Differential Pressures, Force, Dynamic Pressure, Opening of the Camera Shutters and Time Base	54

## ILLUSTRATIONS

FIGURE		PAGE
1.	Parachute Test Vehicle FB1A	10
2.	Parachute Test Vehicle FB1B	10
3.	Components of the Test System	11
4.	On-Board Telemetry System	12
5.	Telemetry Ground Station	12
6.	Pressure Transducer Attached to Canopy	13

Graphical presentations of the differential pressure coefficient,  $C_p = \Delta P/q_s$ , the corresponding canopy area ratio,  $S_p/S_o$ , the opening shock factor,  $F/C_{D_o} S_o q_s$ , and the dynamic pressure coefficient,  $q/q_s$ , as a function of the time ratio,  $T = t/t_f$ , for:

7.	Test No. AF1, Circular Flat Type Canopy. Filling Time, $t_f = 1.14$ sec.; Measurement on the Cord Line	18
8.	Test No. AF 2, Circular Flat Type Canopy. Filling Time, $t_f = 1.05$ sec.; Measurement on the Cord Line	19
9.	Test No. AF 5, Circular Flat Type Canopy. Filling Time, $t_f = 1.28$ sec., Measurement on the Gore Center Line	20
10.	Test No. AF 7, Circular Flat Type Canopy. Filling Time, $t_f = 1.16$ sec.; Measurement on the Gore Center Line	21
11.	Test No. AF 24, Extended Skirt Type Canopy. Filling Time, $t_f = 1.72$ sec.; Measurement on the Cord line	22
12.	Test No. AF 26, Extended Skirt Type Canopy. Filling Time, $t_f = 1.609$ sec.; Measurement on the Cord Line	23
13.	Test No. AF 14, Extended Skirt Type Canopy. Filling Time, $t_f = 1.795$ sec.; Measurement on the Gore Center Line	24

# Contrails

## ILLUSTRATIONS (CONT'D)

FIGURE		PAGE
14.	Test No. AF 16, Extended Skirt Type Canopy. Filling Time, $t_f = 2.158$ sec.; Measurement on the Gore Center Line	25
15.	Test No. AF 33, Ringslot (G) Type Canopy. Filling Time, $t_f = 3.68$ sec.; Measurement on the Cord Line	26
16.	Test No. AF 35, Ringslot (G) Type Canopy. Filling Time, $t_f = 3.21$ sec.; Measurement on the Cord Line	27
17.	Test No. AF 34, Ringslot (US) Type Canopy. Filling Time, $t_f = 2.83$ sec.; Measurement on the Cord Line	28
18.	Test No. AF 36, Ringslot (US) Type Canopy. Filling Time, $t_f = 2.77$ sec.; Measurement on the Cord Line	29
19.	Test No. AF 51, Ringslot (G) Type Canopy. Filling Time, $t_f = 2.99$ sec.; Measurement on the Gore Center Line	30
20.	Test No. AF 55, Ringslot (G) Type Canopy. Filling Time, $t_f = 3.79$ sec.; Measurement on the Gore Center Line	31
21.	Test No. AF 40, Ringslot (US) Type Canopy. Filling Time, $t_f = 3.37$ sec.; Measurement on the Gore Center Line	32
22.	Test No. AF 43, Ringslot (US) Type Canopy. Filling Time, $t_f = 3.62$ sec.; Measurement on the Gore Center Line	33
23.	Test No. AF 72, Circular Flat Ribbon (G) Type Canopy. Filling Time, $t_f = 2.04$ sec.; Measurement on the Cord Line	34
24.	Test No. AF 73, Circular Flat Ribbon (G) Type Canopy. Filling Time, $t_f = 2.32$ sec.; Measure- ment on the Cord Line	35

# Contrails

## ILLUSTRATIONS (CONT'D)

FIGURE		PAGE
25.	Test No. AF 42, Circular Flat Ribbon (US) Type Canopy. Filling Time, $t_f = 9.37$ sec.; Measurement on the Cord Line	36
26.	Test No. AF 54, Circular Flat Ribbon (US) Type Canopy. Filling Time, $t_f = 10.98$ sec.; Measurement on the Cord Line	37
27.	Test No. AF 75, Circular Flat Ribbon (G) Type Canopy. Filling Time, $t_f = 2.26$ sec.; Measurement on the Gore Center Line	38
28.	Test No. AF 77, Circular Flat Ribbon (G) Type Canopy. Filling Time, $t_f = 1.94$ sec.; Measurement on the Gore Center Line	39
29.	Test No. AF 60, Circular Flat Ribbon (US) Type Canopy. Filling Time, $t_f = 4.46$ sec.; Measurement on the Gore Center Line	40
30.	Test No. AF 66, Circular Flat Ribbon Type Canopy (US). Filling Time, $t_f = 4.18$ sec.; Measurement on the Gore Center Line	41
Evolution of the Canopy Shape for:		
31.	Test No. AF 2, Circular Flat Type Canopy. Filling Time, $t_f = 1.05$ sec.; Measurement on the Cord Line	42
32.	Test No. AF 7, Circular Flat Type Canopy. Filling Time, $t_f = 1.16$ sec; Measurement on Gore Center Line	43
33.	Test No. AF 26, Extended Skirt Type Canopy. Filling Time, $t_f = 1.609$ sec.; Measurement on the Cord line	44
34.	Test No. AF 16, Extended Skirt Type Canopy. Filling Time, $t_f = 2.158$ sec.; Measurement on the Gore Center Line	45
35.	Test No. AF 35, Ringslot (G) Type Canopy. Filling Time, $t_f = 3.21$ sec.; Measurement on the Cord Line	46



## ILLUSTRATIONS (CONT'D)

FIGURE		PAGE
36.	Test No. AF 34, Ringslot (US) Type Canopy. Filling Time, $t_f = 2.83$ sec.; Measurement on the Cord Line	47
37.	Test No. AF 51, Ringslot (G) Type Canopy. Filling Time, $t_f = 2.99$ sec.; Measurement on the Gore Center Line	48
38.	Test No. AF 40, Ringslot (US) Type Canopy. Filling Time, $t_f = 3.37$ sec.; Measurement on the Gore Center Line	49
39.	Test No. AF 72, Circular Flat Ribbon (G) Type Canopy. Filling Time, $t_f = 2.04$ sec.; Measurement on the Cord Line	50
40.	Test No. AF 42, Circular Flat Ribbon (US) Type Canopy. Filling Time, $t_f = 9.37$ sec.; Measurement on the Cord Line	51
41.	Test No. AF 77, Circular Flat Ribbon (G) Type Canopy. Filling Time, $t_f = 1.94$ sec.; Measure- ment on the Gore Center Line	52
42.	Test No. AF 66, Circular Flat Ribbon (US) Type Canopy. Filling Time, $t_f = 4.18$ sec.; Measurement on the Gore Center Line	53
Original oscillographic recordings of the differential pressures, force, dynamic pressure, openings of the camera shutters and time base for:		
43.	Test No. AF 1, Circular Flat Type Canopy. Pressure Transducers on Cord Line	55
44.	Test No. AF 2, Circular Flat Type Canopy. Pressure Transducers on the Cord Line	56
45.	Test No. AF 5, Circular Flat Type Canopy. Pressure Transducers on the Gore Center Line	57
46.	Test No. AF 7, Circular Flat Type Canopy. Pressure Transducers on the Gore Center Line	58
47.	Test No. AF 24, Extended Skirt Type Canopy. Pressure Transducers on the Cord Line	59

# Contracts

## ILLUSTRATIONS (CONT'D)

FIGURE		PAGE
48	Test No. AF 26, Extended Skirt Type Canopy. Pressure Transducers on the Cord Line	60
49.	Test No. AF 14, Extended Skirt Type Canopy. Pressure Transducers on the Gore Center Line	61
50.	Test No. AF 16, Extended Skirt Type Canopy. Pressure Transducers on the Gore Center Line	62
51.	Test No. AF 33, Ringslot (G) Type Canopy. Pressure Transducers on the Cord Line	63
52.	Test No. AF 35, Ringslot (G) Type Canopy. Pressure Transducers on the Cord Line	64
53.	Test No. AF 34, Ringslot (US) Type Canopy. Pressure Transducers on the Cord Line	65
54.	Test No. AF 36, Ringslot (US) Type Canopy. Pressure Transducers on the Cord Line	66
55.	Test No. AF 51, Ringslot (G) Type Canopy. Pressure Transducers on the Gore Center Line	67
56.	Test No. AF 55, Ringslot (G) Type Canopy. Pressure Transducers on the Gore Center Line	68
57.	Test No. AF 40, Ringslot (US) Type Canopy. Pressure Transducers on the Gore Center Line	69
58.	Test No. AF 43, Ringslot (US) Type Canopy. Pressure Transducers on the Gore Center Line	70
59.	Test No. AF 72, Circular Flat Ribbon (G) Type Canopy. Pressure Transducers on the Cord Line	71
60.	Test No. AF 73, Circular Flat Ribbon (G) Type Canopy. Pressure Transducers on the Cord Line	72
61.	Test No. AF 42, Circular Flat Ribbon (US) Type Canopy. Pressure Transducers on the Cord Line	73
62.	Test No. AF 54, Circular Flat Ribbon (US) Type Canopy. Pressure Transducers on the Cord Line	74
63.	Test No. AF 75, Circular Flat Ribbon (G) Type Canopy. Pressure Transducers on the Gore Center Line	75

ILLUSTRATIONS (CONT'D)

FIGURE		PAGE
64.	Test No. AF 77, Circular Flat Ribbon (G) Type Canopy. Pressure Transducers on the Gore Center Line	76
65.	Test No. AF 60, Circular Flat Ribbon (US) Type Canopy. Pressure Transducers on the Gore Center Line	77
66.	Test No. AF 66, Circular Flat Ribbon (US) Type Canopy. Pressure Transducers on the Gore Center Line	78

# Contrails

## TABLES

TABLE NO.		PAGE
1	Peak Values for Differential Pressure Coefficients, $C_p = \Delta p/q_s$ and corresponding times, $T = t/t_f$	14
2	Snatch Force and Opening Shock Values with Corresponding Times for all Parachute Types	16

## SYMBOLS

$C_{D_0}$	Drag coefficient of parachute based on nominal canopy surface area
$D_0$	Nominal diameter of parachute canopy
$S_0$	Nominal surface area of parachute canopy
$S_p$	Instantaneous projected area of parachute canopy
$t$	Time
$t_f$	Filling time
$T$	Time ratio, $t/t_f$
$q$	Instantaneous dynamic pressure
$q_s$	Dynamic pressure at the time of suspension line stretch or occurrence of snatch force
$F$	Instantaneous force acting between suspension lines and test vehicle
$\Delta p$	Differential pressure between internal and external side of the canopy surface
$C_p$	Differential pressure coefficient, $\Delta p/q_s$
(G)	Parachute fabricated in Germany
(US)	Parachute fabricated in USA

### Subscripts:

- 1 Location of canopy skirt
- 2 Location 1/3 of distance  $\bar{14}$  from canopy skirt
- 3 Location 2/3 of distance  $\bar{14}$  from canopy skirt
- 4 Location at canopy vent

# *Contrails*

## 1. INTRODUCTION

The determination of stresses in a parachute canopy, their distribution over the canopy and their time history during the inflation phase has as yet not been successful, neither through analytical methods nor through actual measurements. The common method for the sensing of stresses in a structure by means of strain measurements fails to work in a parachute canopy fabricated from nylon material. The reasons are the high breaking elongation and the nonelastic behavior of the nylon material.

Theoretical attempts for the calculation of stresses are all restricted to the steady state phase of an idealized rigid shape (Ref. 1 and 2). The application of these methods to the unsteady phase requires simplifications and assumptions which do no longer reflect the realities of the dynamic process of parachute inflation.

As an alternative, the magnitude and history of stresses in a parachute canopy can be reasonably closely approximated if the pressure distribution over the canopy in relation to the instantaneous canopy shape is known. The stresses can then be calculated, using experimentally acquired pressure distributions and corresponding canopy shapes gained from photographic recordings.

The measurement of the differential pressure over the parachute canopy and its time history was made possible by the availability of a special small size, lightweight, acceleration insensitive pressure transducer. The feasibility of the measurement of differential pressures on inflating parachutes was successfully demonstrated during a series of wind tunnel tests on scale model parachute canopies opening under infinite mass conditions (Ref. 3 and 4).

This report documents the procedures for and the results of measurements of differential pressures and correlating canopy shapes on full scale parachutes during free-flight tests and while opening under finite mass conditions.

## 2. TEST CONDITIONS

### 2.1 Parachute Types

Four basic types of parachute canopies were investigated:

- Circular Flat Type Canopy, Type C-9
- 10% Extended Skirt Type Canopy, Type T-10
- Ringslot Type Canopy
- Circular Flat Ribbon Type Canopy

The Type C-9 and T-10 parachute canopies were purchased from Brueggemann & Brand KG, Volmarstein, Germany. Their design parameters were based on Military Specifications.

# Contracts

The design of the Ringslot (G) type canopy was based on Specification MIL-C-9401A. The canopies had a nominal diameter of 32 ft. (9.76 meter), and incorporated 32 gores, 10 concentric cloth rings, and a geometric porosity of 15%.

Two other Ringslot (U.S.) type canopies were furnished by the United States Air Force Flight Dynamics Laboratory. This canopy type had the same dimensions and porosity as the type (G), but was constructed of 11 cloth rings.

The design of the Circular Flat Ribbon (G) type parachute was based on Specification MIL-P-6653. The canopies had a nominal diameter of 34 ft. (10.38 meter), and incorporated 34 gores, 83 concentric ribbons, and a geometric porosity of 15%.

Two other Circular Flat Ribbon (U.S.) type canopies were furnished by the United States Air Force Flight Dynamics Laboratory. These canopies were of the same dimensions and had the same geometric porosity as the type (G), but were constructed of 76 concentric ribbons and had a larger vent.

The cloth used in the fabrication of the Circular Flat and 10% Extended Skirt type parachute canopies was made in accordance with Specification MIL-C-7020, Type I; and for the Ringslot type canopies cloth made in accordance with Specification MIL-C-7350, Type I was used. The ribbons used for the fabrication of the Circular Flat Ribbon type canopies were made in accordance with Specification MIL-T-5608, Type V, Class C.

## 2.2 Test Vehicles and Test Method

The DFL Parachute Test Vehicles, Type FB1A and Type FB1B, fully instrumented and recoverable by an independent parachute recovery system, were used throughout the experimental test program. The Type FB1A test vehicle (Figure 1) was used for the testing of the solid cloth type parachute canopies; the Type FB1B test vehicle (Figure 2), which is the basic Type FB1A test vehicle with an enlarged test parachute compartment, was utilized for the testing of the geometric porosity type parachute canopies.

The components of the test system are shown in Figure 3. The front compartment of the test vehicle contains the on-board 7-Channel FM/FM type telemetry system (Figure 4). The telemetry system is composed of subcarrier oscillators, Vector Type TL61B; a mixer-amplifier, Vector Type TA48; and a transmitter, Vector Type T1225. The front compartment also contains the power supply and a command receiver.

The telemetry ground station (Figure 5) contains the receiver and discriminators. All conditioned signals were recorded on a Honeywell Visicorder.

A 16mm on-board photographic camera of the Photo Sonics type recorded the frontal view of the test parachute canopy at a rate of 100 frames per



second. The growth of the projected canopy area was determined from this recording. A 32mm ground based photographic camera of the Vinten type recorded the profile shapes of the inflating and inflated canopy at a rate of 100 frames per second.

Initially, the flight path of the parachute-load configuration was recorded by two cinetheodolite stations. From these recordings, the velocity of the system and the dynamic pressure were determined. Subsequently, the dynamic pressure was measured directly by means of a vehicle-borne pitot-static probe and pressure transducer arrangement since this method proved to be as accurate as the data derived from the cinetheodolite measurements.

Four pressure transducers were affixed to the test parachute canopy (see Figure 6) from skirt to vent in equal distances. For one test series they were located along one of the canopy cord lines, for another test series along a gore center line.

Equal numbers of suspension lines were connected to two short risers. The risers were attached to the test vehicle at two opposite points at the aft end of the parachute compartment. A strain gage type force transducer was inserted in each of the two risers and the two signals were added electrically.

All pertinent data were recorded on the same recording medium. The recordings rendered by the Visicorder contain the telemetered and conditioned signals of the four differential pressures as sensed by the DFL pressure transducers, the force transmitted from the parachute to the test vehicle as sensed by the two tensiometer links, the dynamic pressure as sensed by the test vehicle-borne pitot-static tube and pressure transducer arrangement, and the shutter opening of the on-board camera. In addition, the shutter openings of the cinetheodolite and ground based cameras were recorded. The time base of the recording is given by lines spanning the width of the recording medium and produced by a 100 Hz signal generator. By this method, an accurate correlation of all recorded quantities is possible.

### 2.3 Test Procedure

The test vehicle was released from the test aircraft (Dornier 27) at a velocity of 110 knots IAS (205 km/hr) and at an altitude of 1000 ft. (300 meters).

An electronic timer initiated two pyrotechnic cartridges which released the cover of the test parachute compartment. A small pilot chute was attached to the cover and was deployed during cover release. The pilot chute deployed a 7.8 ft (2.4 meter) diameter extraction parachute which, in turn, pulled the packed test parachute from the stowage compartment and aided in test parachute deployment.

As long as the test vehicle was carried by the aircraft, it was connected to the aircraft's power supply. Two seconds before drop, the ground based recording system was activated; one second later, the ground camera started to operate. At the moment of drop, the test vehicle was disconnected

# Contrails

from the aircraft power supply and the on-board instrumentation system was connected to the test vehicle-borne power supply. The event of power transfer from external to internal was telemetered and recorded on the recording medium. A fraction of a second later, an electronic timer initiated the firing of the explosive bolts which served to keep the parachute compartment cover attached to the test vehicle, and activated the on-board camera.

Measurement of all quantities was continued to the moment of test vehicle ground impact. In order to allow re-use of the pitot-static tube, the probe was separated from the test vehicle at a point 200 ft. (61 meter) above ground and recovered by a separate parachute.

During tests where cinetheodolite measurements were made, time synchronization with other transmitted signals was accomplished in the same manner: the openings of the camera shutters were transmitted and recorded on the same medium.

Four identical deployment tests were made with each parachute canopy type and location of pressure sensing element arrangement. Reproductions of selected frames showing the evolution of the canopy profile shapes during the filling process, as rendered by the ground-based camera, are shown in Figures 31 through 42. Reproductions of the original recordings of all telemetered and other signals are given in the Appendix.

### 3. RESULTS AND ANALYSIS

#### 3.1 Canopy Pressure Distribution and Corresponding Projected Canopy Area, Force, and Dynamic Pressure as Functions of Time

Two of each four identical tests on a specific parachute canopy type and pressure transducer arrangement were selected for detailed analysis. The results of this analysis are presented in Tables 1 and 2 and in Figures 7 through 30. The dynamic pressure at time of snatch, the parachute filling time, and the maximum pressure coefficients for each of the four pressure sensing locations are listed in Table 1. Table 2 is a tabulation of the measured snatch and opening forces as well as of the time of occurrence of the maximum opening force for each of the tests selected for analysis. Figures 7 through 30 are graphical presentations of the evaluated quantities as functions of the dimensionless time,  $T$ . The reference time is the respective parachute filling time,  $t_f$ .

The four differential pressures,  $\Delta p$ , are made dimensionless by the dynamic pressure at the time of snatch,  $q_s$ , and presented as differential pressure coefficients,  $C_{p1}$  (skirt),  $C_{p2}$ ,  $C_{p3}$ , and  $C_{p4}$  (vent).

The instantaneous projected canopy area,  $S_p$ , was determined from the on-board photographic recordings and made dimensionless by the nominal canopy area,  $S_0$ .

The instantaneous dynamic pressure,  $q$ , is made dimensionless by the dynamic pressure at the time of snatch,  $q_s$ , and the instantaneous

# Contrails

force,  $F$ , is divided by the steady state drag force for the dynamic pressure at time of snatch,  $(C_D S) \rho v^2$ . This permits the direct determination of the value of the opening shock factor of the parachute canopy from the plotted function. The opening shock factor is equivalent to the maximum value shown after occurrence of snatch.

The time histories of the differential pressures are shown in the graphical presentations in Figures 7 through 30. The peak pressure values appear shortly before or after the occurrence of the snatch force. At this time, the quarter bag is already partially or fully removed from the canopy. The pressure fluctuates between positive and negative values. This is due to high local dynamic pressures caused by the flutter of the canopy material during this early stage of filling. The highest peak can be positive or negative at random. This peak appears first in the skirt area and then moves along the canopy towards the vent area.

The solid cloth type parachute canopies exhibit higher pressure peaks than the geometric porosity type canopies. The highest values are associated with the Circular Flat Type canopy, the lowest values with the Ringslot type canopy. On the average, the peak pressure coefficients for the solid cloth type canopies are between the values of 2 and 3; for the geometric porosity type canopies they are between the values of 1 and 2.

The history of the differential pressure with respect to both amplitude and frequency is different for the solid cloth and for the geometric porosity type parachute canopies. As sensed along the cord line of the geometric porosity type parachute canopies, the time history of the differential pressure at the skirt and at the two adjacent points of measurement is very smooth. Only the vent area shows considerable pressure variations. This indicates that sufficient differential pressures are difficult to build-up in geometric porosity type canopies due to the relatively large openings between ribbons or concentric rings. As a consequence, the filling time is longer for these canopy types. Especially the United States version of the Circular Flat Ribbon type canopy exhibited extremely long filling times, between 4 and 11 seconds; however, these long filling times may be partially attributed to the fact that the United States canopy version had a somewhat larger vent than the German version of the canopy.

In general, the pressure distribution and pressure time histories of all four types of parachutes show the same tendencies. There are violent fluctuations between positive and negative pressure peaks caused by flutter of the material during the inflation phase. As the canopy fills in the vent area, the material flutter ends very soon in areas adjacent to the vent. After a few early negative peaks, the differential pressure at the vent remains mainly positive. As the canopy filling continues toward the skirt, the material flutter diminishes correspondingly. The time where the canopy vent area is filled corresponds to the end of the "initial" filling period. The dynamic pressure has decreased to 20% of its value at time of snatch, the projected canopy area has increased to approximately 6.2% of its steady state value, and for geometric porosity type parachutes, the opening shock has occurred. The pressure history in the vent area differs markedly from

those at the other points of measurement. It has high positive values during the entire "initial" filling phase.

Comparing all the test results, one exception becomes evident. The pressure histories measured on the Circular Flat Ribbon (G) type canopy show the same trends, but to the negative side (compare tests AF72, 73, 75 and 77 and Figures 23, 24, 27 and 28). No explanation can be offered for this result. Everything possible was checked, but no mistake in electrical connections, calibration or sensors could be ascertained. Since all other test parachute canopies, even the Circular Flat Ribbon (U. S.) type show pressure trends to the positive side, a mistake in data acquisition has to be assumed.

In general, the pressure measurements revealed that the pressure fluctuations are more violent along the gore centerline than along the cord line. This, again, may be attributed to the flutter of the material in the gores.

### 3.2 Evolvement of Canopy Shape

The evolvement of the shape of each of the four parachute canopy types is shown in a series of pictures selected from the photographic recordings rendered by the ground based camera. These pictures are reproduced in Figures 31 through 42. Two series of pictures are shown for each canopy type. One series represents tests where the pressure transducers were attached to a gore centerline of the canopy, the other series was taken during tests where the pressure transducers were attached to one of the canopy cord lines.

Twelve characteristic stages of filling were selected for each series of pictures. The first picture in each series reflects the canopy configuration at time of snatch (T=0), the following pictures show several consecutive stages of filling, the canopy shape at the time the maximum force occurs, the first attainment of the steady state projected diameter ( $T = 1.0$ ), the maximum projected area shape (overinflation), and the last picture shows the canopy shape under steady descent conditions. Each of the shapes represented by these pictures can be coordinated to the instantaneous pressure values by virtue of the common time base.

Overall, the characteristic canopy shapes during the filling process are reproducible with good regularity for the same initial conditions.

Idealizations of the canopy shapes can be made using basic bodies of revolution such as cylinders, truncated cones, spherical segments, or hemispheroids (Ref. 3 and 4). For a dimensional determination of the canopy shape, the length of the test vehicle (without pitot-static tube) may be used. For the Type FB1A test vehicle, which was used for tests on the solid cloth type parachute canopy, this length is 6.9 ft. (2.26 meter); for the Type FB1B test vehicle used for the testing of geometric porosity type canopies, this length is 6.75 ft. (2.208 meter).

# Contrails

The previously mentioned fluttering of the canopy material during the early filling phase may be seen from these pictures.

## 4. CONCLUSIONS

An experimental test program was conducted to determine the values and the time history of the differential pressure at different locations over the surface of four types of parachute canopies while opening under finite mass conditions. To permit a more complete analysis of the canopy pressure distribution, the dynamic pressure and the forces generated by the inflating canopies were measured as a function of time, and the canopy profile shapes were derived and related to a common time base. The results of this test phase supplement the measurements made during an earlier phase under which similar quantities were acquired and analyzed for model parachute canopies opening under infinite mass conditions.

The results of the experimental test program confirm the expected difference in the frequency and amplitude of the differential pressure values between solid cloth and geometric porosity type parachute canopies. The peak pressure coefficients for solid cloth type canopies are generally between the values of 2 and 3, while values between 1 and 2 were measured on the geometric porosity type canopies. Violent fluctuations of the differential pressures between positive and negative pressure peaks are evident during the early stage of canopy filling. These fluctuations are due to the flutter of the canopy material. As canopy filling progresses from the vent towards the skirt area, the material flutter diminishes and the differential pressures show mainly positive values.

Although a great deal of insight into the pressure distribution of inflating parachute canopies was gained from this test series, which will be of benefit to the formulation of stress analysis approaches for the unsteady phases of parachute operation, the absolute pressure values must be applied with caution. However, the results of these initial measurements of the dynamic differential pressure distribution over the surface of the parachute canopies tested will serve to gain a better understanding of the canopy stress loading history and its distribution. It is primarily a qualitative impression that can be gained about the stresses. For a quantitative evaluation, additional work has to be performed to improve upon methods for the numerical reduction of the measured pressure values into stress values. Difficulties result due to the dynamics of the parachute inflation process. For example, the highest pressure peaks were measured during the flutter phase of the canopy material, and the idealization of the canopy shapes during this phase and the correlation of the measured pressure values to these shapes may yield erroneous results. Longitudinal stresses will be predominant during the material flutter phase. During the steady state phase, the circumferential stresses will cause the main loading. This has to be considered in more detail during the formulation of stress analysis approaches.

Another problem for the formulation of a valid stress analysis approach is the visco-elastic behavior of the nylon material, which makes

# *Contrails*

the stress-strain relationship very complicated. The inclusion of this relationship into a practical stress analysis method should be avoided.

Additional experimental data should be acquired for differential pressures acting between points 3 and 4 on the canopies, since the vent area exhibits high continuous positive differential pressures. A series of tests should also be performed at dynamic pressures which are higher than those at which this test program was conducted and which are close to the strength limit of the canopy material.

## 5. REFERENCES

1. Topping, A. D.; Marketos, J. D.; Costakos, N. C.; A Study of Canopy Shapes and Stresses for Parachutes in Steady Descent, WADC TR 55-294, Wright Air Development Center, Wright-Patterson Air Force Base, Ohio, October 1955
2. Heinrich, H. G.; Jamison, L. R.; Parachute Stress Analysis During Inflation and at Steady State, Journal of Aircraft, Vol. 3, No. 1, January-February 1966
3. Melzig, H. D.; Schmidt, A. K.; Pressure Distribution During Parachute Opening; Phase I, Infinite Mass Operating Case, AFFDL TR 66-10, Air Force Flight Dynamics Laboratory, Wright-Patterson Air Force Base, Ohio, March 1966
4. Melzig, H. D.; Schmidt, P. K.; Parachute Canopies During Inflation, AD 631 777, September 1965

# Contrails

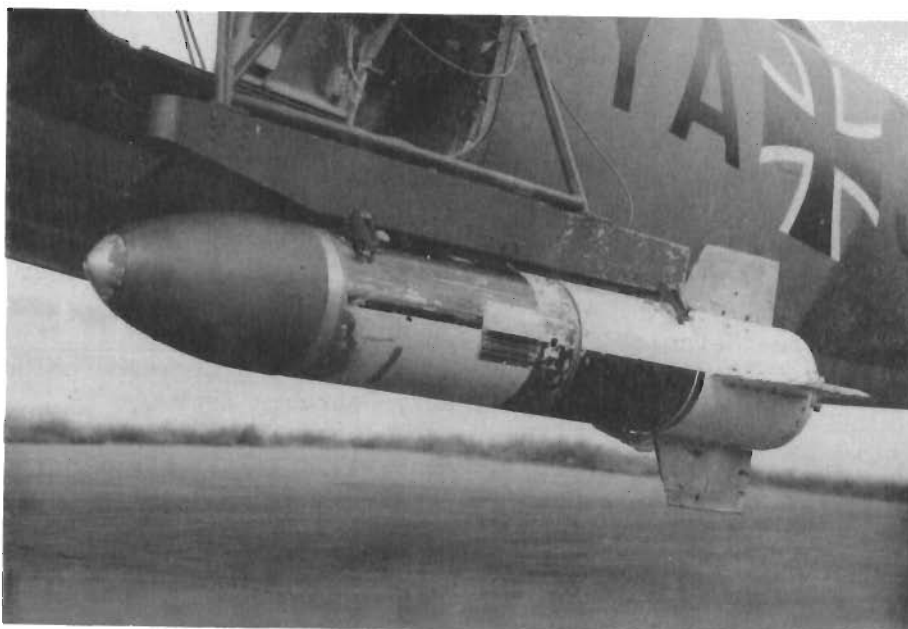


Fig. 1 Parachute test vehicle FB 1A

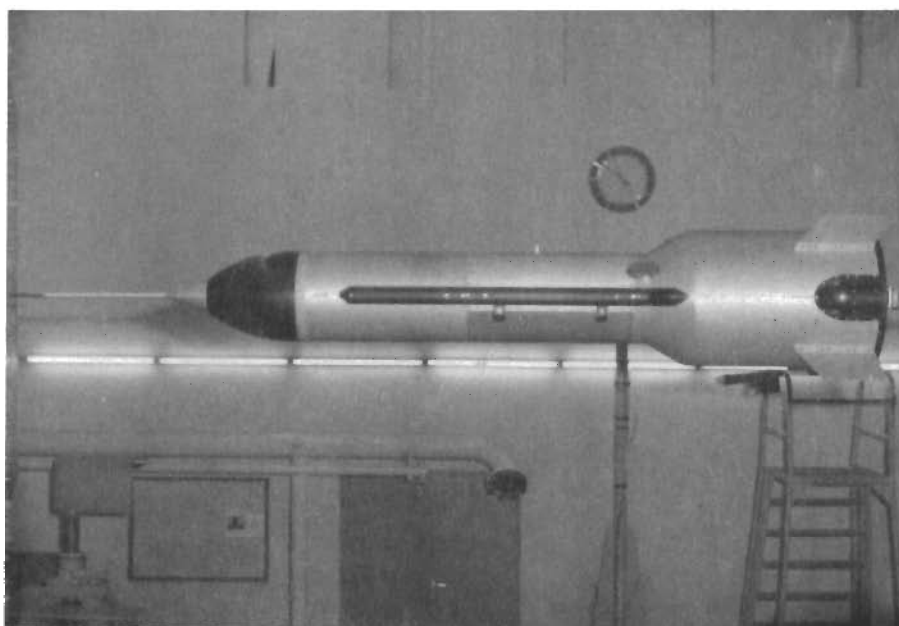
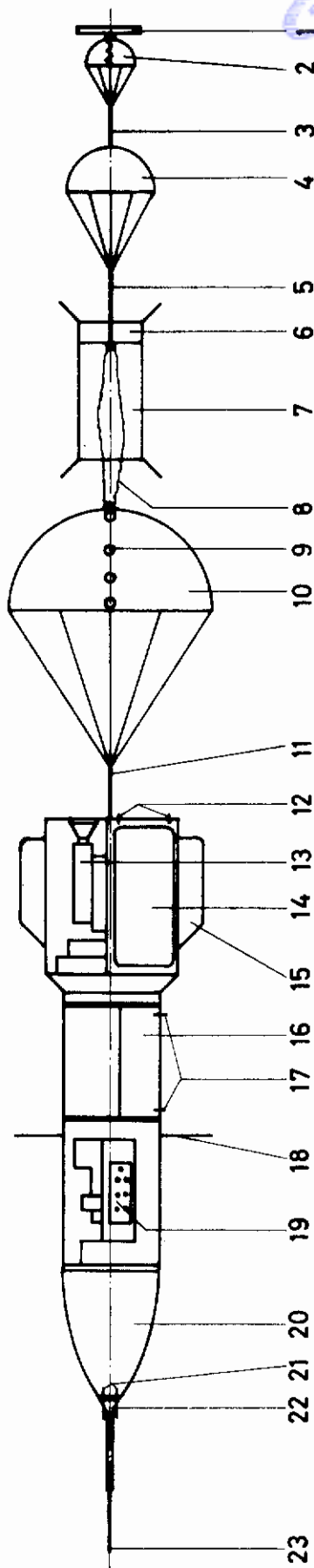


Fig. 2 Parachute test vehicle FB 1B





- |    |   |    |   |
|----|---|----|---|
| 1  | Parachute Compartment Cover   | 12 | 2 Explosive Screws for Parachute Compartment Cover                      |
| 2  | Pilot Chute, 3/2 inch Diameter Circular Flat Type Canopy (Kohake)         | 13 | On-Board Camera   |
| 3  | Bridle, 1 1500 lbs Nylon Webbing, 6.5 ft long                             | 14 | Parachute Compartment Stabilizer Pins                                   |
| 4  | Extraction Chute, 7.8 ft D <sub>0</sub> Ribbles Guide Surface Type Canopy | 15 | Emergency Recovery System   |
| 5  | Bridle, 1 1500 lbs Nylon Webbing, 5 ft long                               | 16 | 2 Explosive Screws for Emergency Recovery Parachute Compartment Cover   |
| 6  | Extraction Chute Bag  | 17 | Telemetry Antennas  |
| 7  | Deployment Bag  | 18 | Telemetry Equipment   |
| 8  | Breakcord, 2 Turns of 30 lbs Cotton Tape                                  | 19 | Elastic Nose  |
| 9  | 4 Pressure Transducers  | 20 | 2 Explosive Screws for Pitot-Static Tube Recovery Parachute Compartment |
| 10 | Test Parachute Canopy   | 21 | Pitot-Static Tube Recovery Parachute Compartment                        |
| 11 | 2 Risers, 2 Plies each of 5300 lbs Nylon webbing, 2 ft long.              | 22 | Pitot-Static Tube   |
| 12 |   | 23 | Pitot-Static Tube   |

FIG. 3 COMPONENTS OF THE TEST SYSTEM

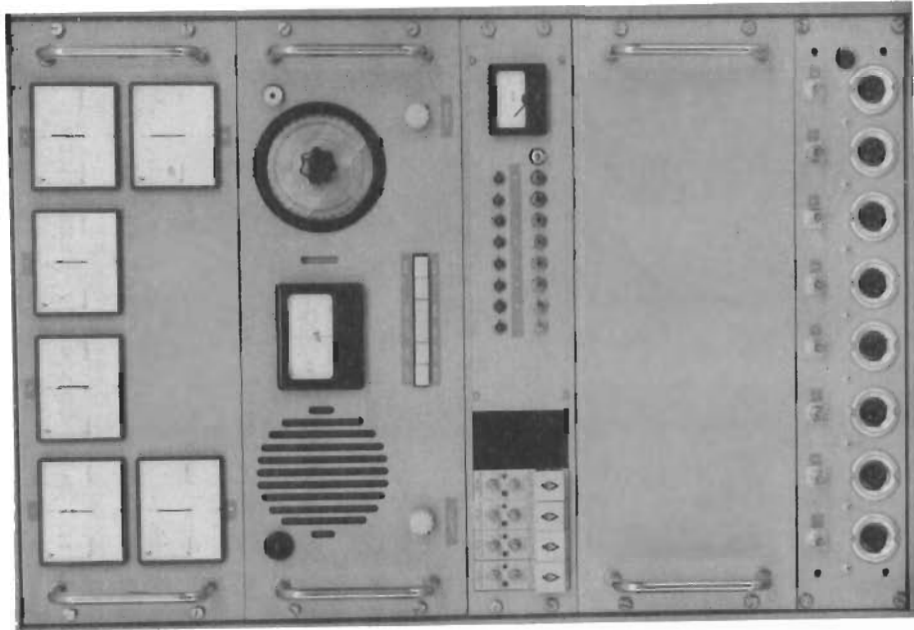


Fig. 5 Telemetry Ground Station



Fig. 4 Telemetry Onboard Station

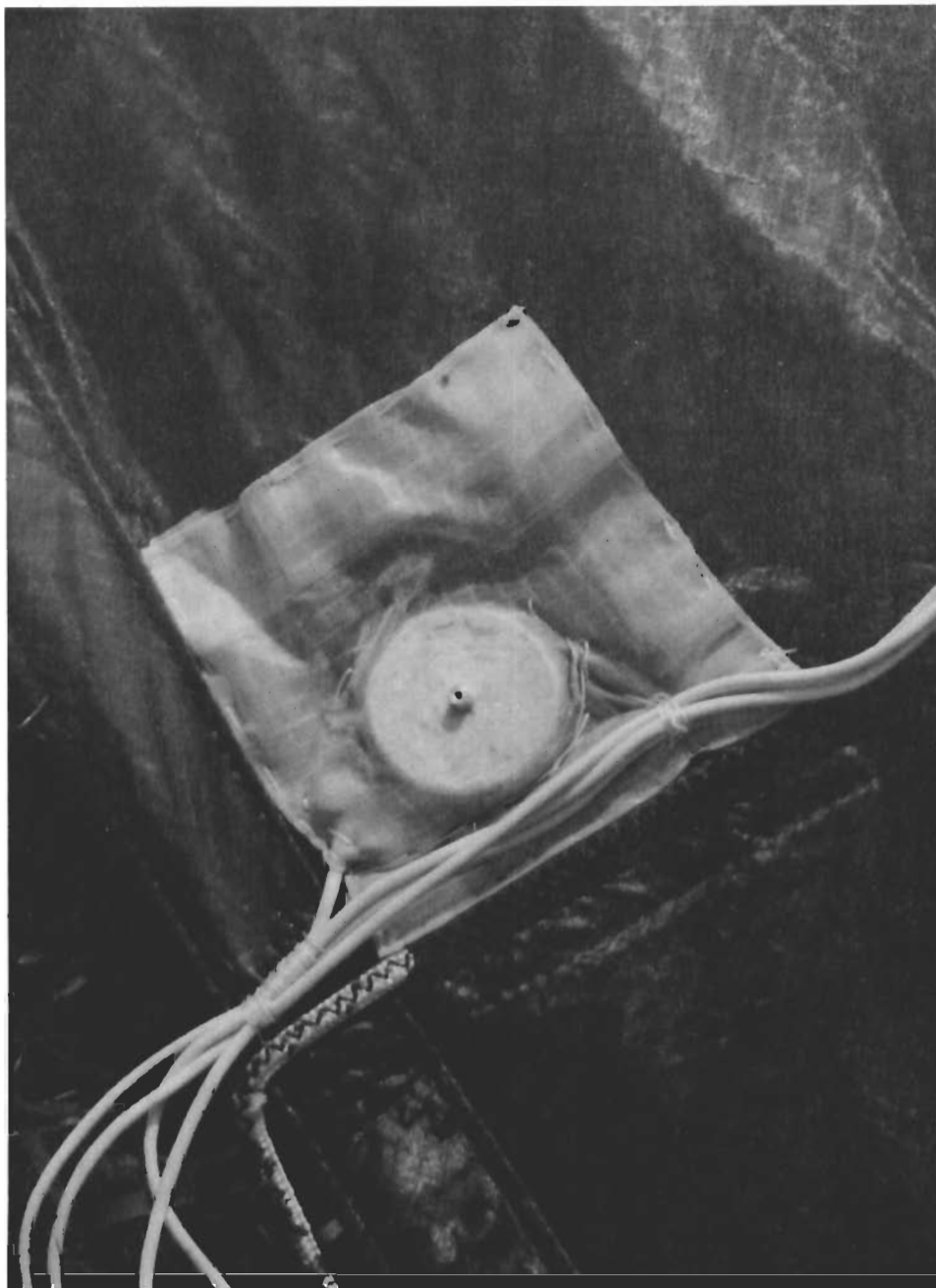


Fig. 6 Pressure transducer on canopy

*Contracts* **TABLE 1**

Peak values for differential pressure coefficients

$$c_p = \Delta p/q_s \text{ and corresponding times } T = t/t_f$$

Parachute Type	Location of pressure transducers	Test No. AF	$q_s$ [kp/m <sup>2</sup> ]	$t_f$ [sec]	$c_{p1}$ (skirt)	$c_{p2}$	$c_{p3}$	$c_{p4}$ (vent)
					$T_1$	$T_2$	$T_3$	$T_4$
CIRCULAR FLAT	cord	1	194	1.14	1.64 -0.018	-2.54 0.007	-2.35 0.035	-1.25 0.061
		2	188	1.05	-2.25 -0.029	-2.61 0.005	-1.18 0.038	0.890 0.357
	gore	5	186	1.28	2.19 -0.005	1.63 0.015	1.85 0.033	2.98 0.180
		7	201	1.16	-1.80 -0.009	-1.73 0.013	-1.20 0.243	1.30 0.300
	EXTENDED SKIRT	cord	24	172	1.72	-1.82 -0.007	-2.92 0.019	1.19 0.044
26			193	1.609	-1.15 0.011	1.24 0.032	1.05 0.034	0.94 0.248
gore		14	227	1.795	1.39 -0.003	-1.63 -0.015	1.54 0.038	-1.12 0.212
		16	206	2.158	-2.24 -0.005	-2.60 0.013	-2.00 0.029	1.02 0.248
RINGSLOT (G)		cord	33	198	3.68	-0.42 -0.015	-0.95 0.005	-0.51 0.050
	35		182	3.21	0.41 -0.017	0.51 0.061	0.57 0.098	-1.84 0.042
	gore	51	202	2.99	1.17 -0.012	-0.70 0.067	0.75 0.027	-1.23 0.095
		55	200	3.79	-1.56 0.021	-0.56 0.007	-1.15 0.071	1.03 0.094

*Confidential*  
TABLE 1 (cont.)

Peak values for differential pressure coefficients

$c_p = \Delta p / q_s$  and corresponding times  $T = t / t_f$

Parachute Type	Location of pressure transducers	Test No. AF	$q_s$ [ $kp/m^2$ ]	$t_f$ [sec]	$c_{p1}$ (skirt)	$c_{p2}$	$c_{p3}$	$c_{p4}$ (vent)	
					$T_1$	$T_2$	$T_3$	$T_4$	
RINGSLOT (US)	cord	34	214	2.83	-1.93 0.001	-0.84 0.008	1.24 0.034	-1.95 0.120	
		36	185	2.77	-0.77 -0.003	1.73 0.010	-1.97 0.080	2.76 0.116	
	gore	40	206	3.37	1.57 0.053	-0.85 0.007	-1.04 0.023	1.22 0.099	
		43	190	3.62	-1.78 0.019	-0.60 0.039	-0.79 0.063	-1.08 0.075	
	CIRCULAR FLAT RIBBON (G)	cord	72	181	2.04	0.74 -0.006	2.32 0.002	-0.88 0.022	-2.22 0.174
			73	186	2.32	1.07 -0.004	-0.59 0.012	0.56 0.117	-2.42 0.172
gore		75	166	2.26	1.13 0.049	1.71 0.022	0.67 0.053	-1.13 0.220	
		77	182	1.94	-1.38 0.083	1.48 0.004	0.72 0.131	-2.69 0.050	
CIRCULAR FLAT RIBBON (US)	cord	42	190	9.37	-0.47 0.000	-1.20 0.001	-0.68 0.020	1.04 0.027	
		54	206	10.98	-0.95 0.002	-1.74 0.001	-0.75 0.032	-2.00 0.016	
	gore	60	192	4.46	1.17 0.056	1.01 0.080	-1.45 -0.001	-1.88 0.081	
		66	170	4.18	-1.28 0.034	-0.90 0.090	-0.75 0.054	1.13 0.103	

Snatch Force and Opening Shock values with corresponding times  
for all parachute types

Parachute Type	Test No. AF	Snatch Force [lbs]	Opening Shock [lbs]	Filling time [sec]	Time of occurrence of Opening Shock [sec]
CIRCULAR FLAT	1	703	1695	1.140	0.720
	2	670	1728	1.050	0.770
	5	1000	1248	1.280	0.807
	7	984	1418	1.160	0.825
EXTENDED SKIRT	24	979	1573	1.720	0.478
	26	950	1615	1.609	0.464
	14	1064	2361	1.795	0.465
	16	947	1313	2.158	0.447
RINGSLOT (G)	33	440	1150	3.680	0.340
	35	1133	1035	3.210	0.330
	51	509	1074	2.990	0.775
	55	558	1429	3.790	0.326

*Continued*  
TABLE 2 (cont.)

Snatch Force and Opening Shock values in lbs with corresponding times in sec for all parachute types

Parachute Type	Test No. AF	Snatch Force [lbs]	Opening Shock [lbs]	Filling time [sec]	Time of occurrence of Opening Shock [sec]
RINGSLOT (US)	34	473	1396	2.830	0.330
	36	565	1275	2.770	0.350
	40	595	1071	3.370	0.319
	43	476	969	3.620	0.674
CIRCULAR FLAT RIBBON (G)	72	1304	1294	2.040	0.368
	73	493	1412	2.320	0.850
	75	460	1403	2.260	0.843
	77	1002	1445	1.940	0.835
CIRCULAR FLAT RIBBON (US)	42	394	936	9.370	0.494
	54	565	907	10.980	0.426
	60	1176	887	4.460	0.850
	66	466	936	4.180	0.990

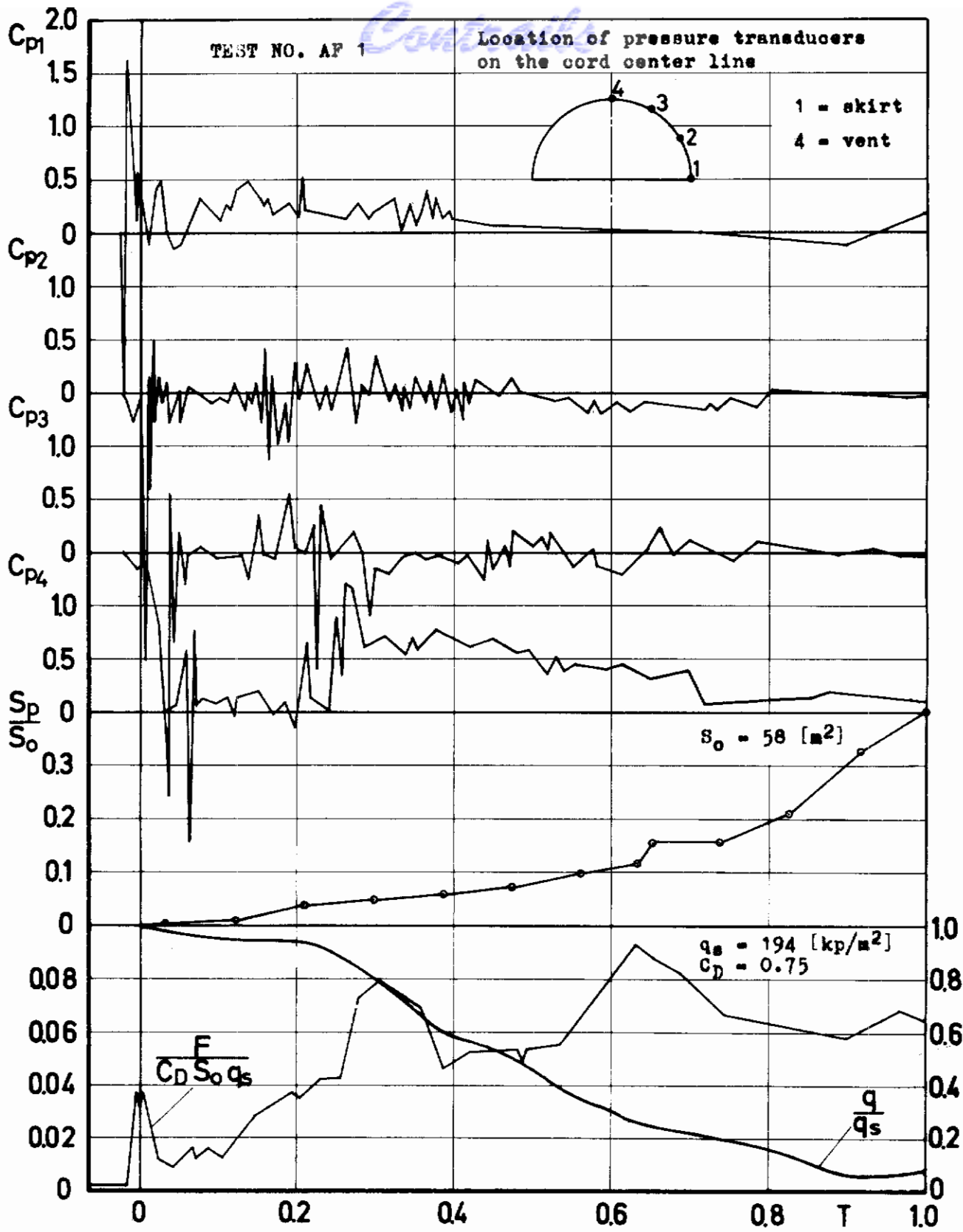
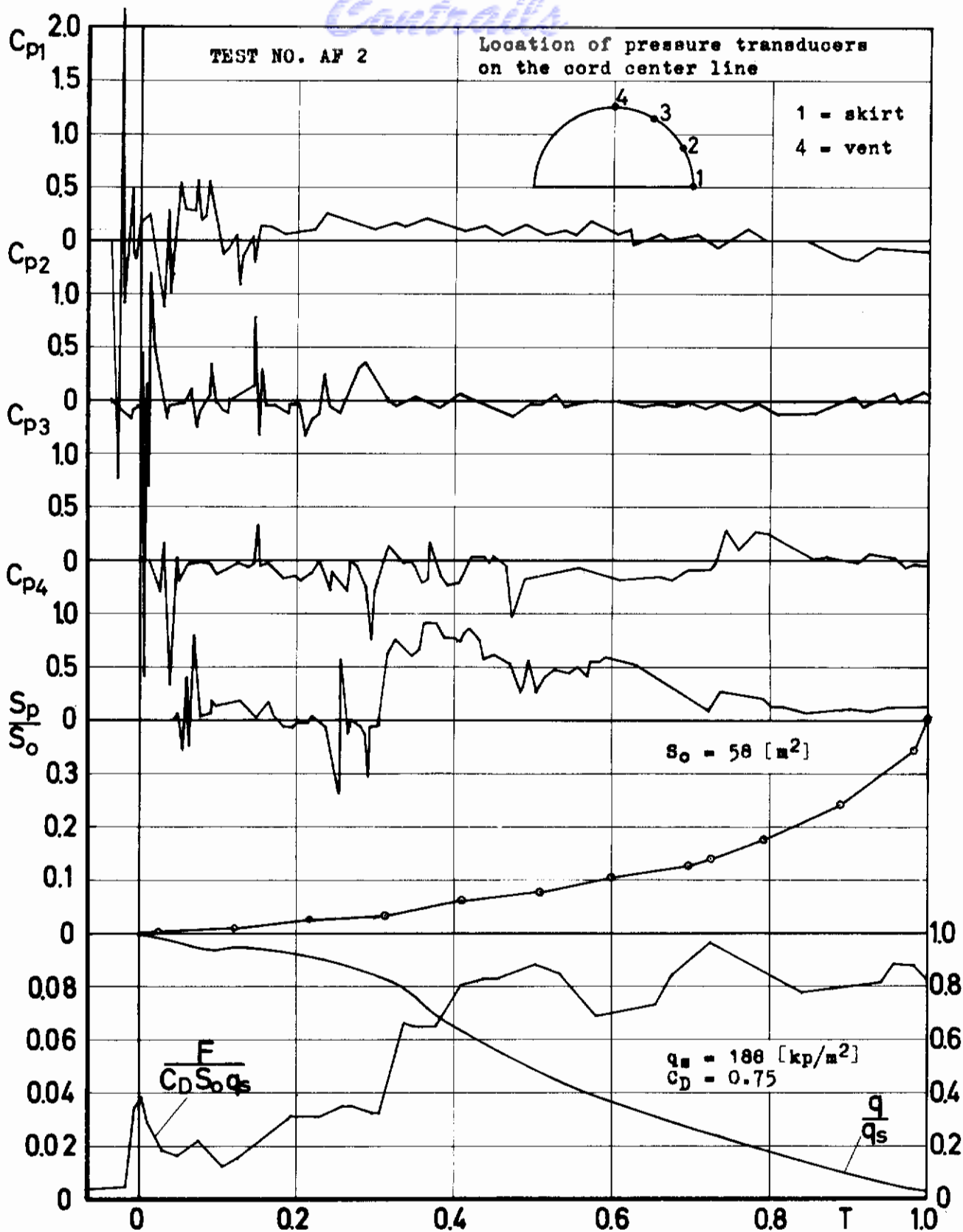


Fig. 7 Differential pressure coefficient  $C_p = \Delta p/q_s$  and corresponding projected area ratio  $S_p/S_0$ , opening shock factor  $F/C_D S_0 q_s$  and dynamic pressure coefficient  $q/q_s$  versus time ratio for 28 ft Circular Flat Parachute. Filling time  $t_f = 1.14$  [sec]





**Fig. 8** Differential pressure coefficient  $C_p = \Delta p/q_s$  and corresponding projected area ratio  $S_p/S_0$ , opening shock factor  $F/C_D S_0 q_s$  and dynamic pressure coefficient  $q/q_s$  versus time ratio for 28 ft Circular Flat Parachute. Filling time  $t_f = 1.05$  [sec]

# Contrails

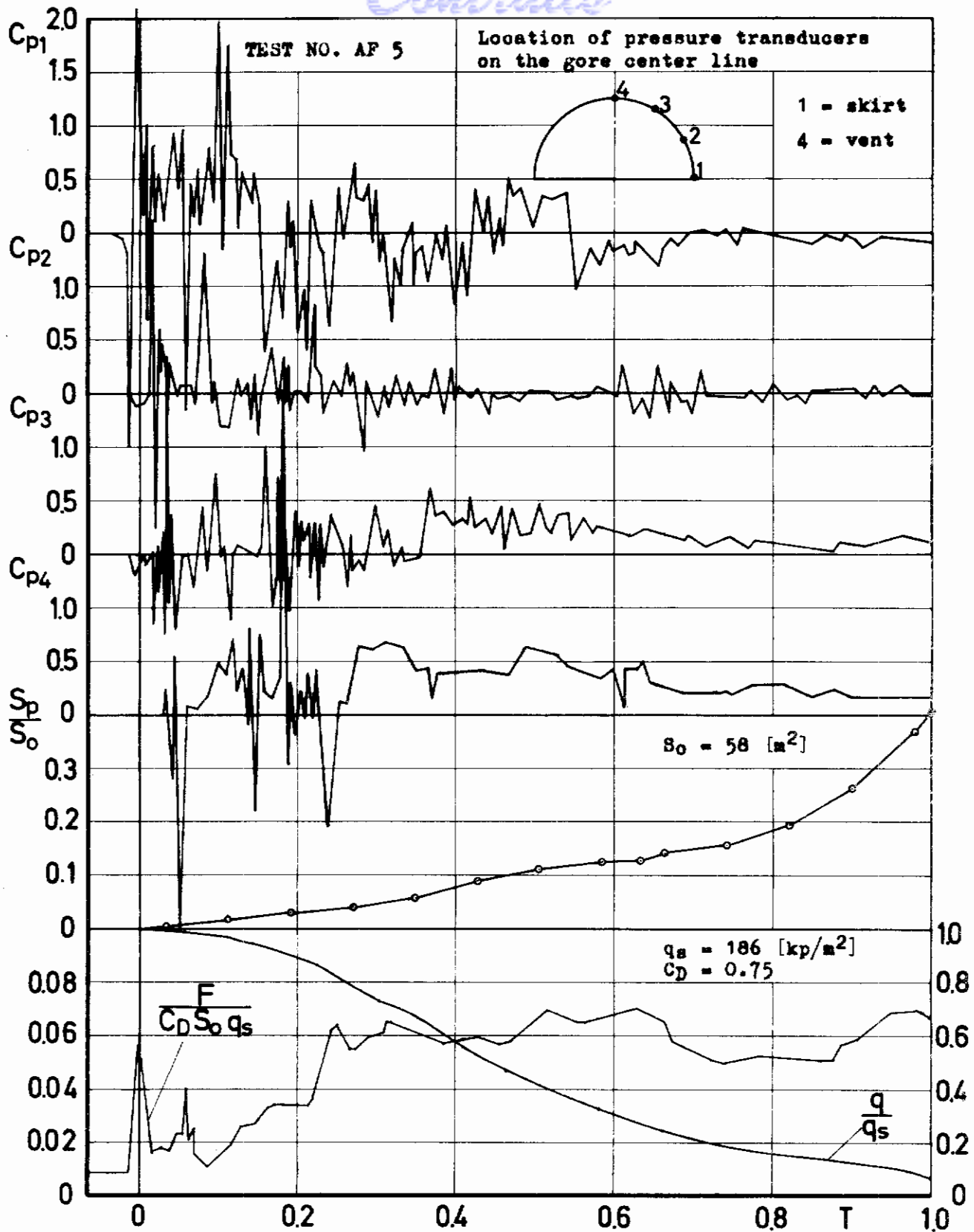


**Fig. 9** Differential pressure coefficient  $C_p = \Delta p/q_s$  and corresponding projected area ratio  $S_p/S_0$ , opening shock factor  $F/C_D S_0 q_s$  and dynamic pressure coefficient  $q/q_s$  versus time ratio for 28 ft Circular Flat Parachute. Filling time  $t_f = 1.28 \text{ [sec]}$

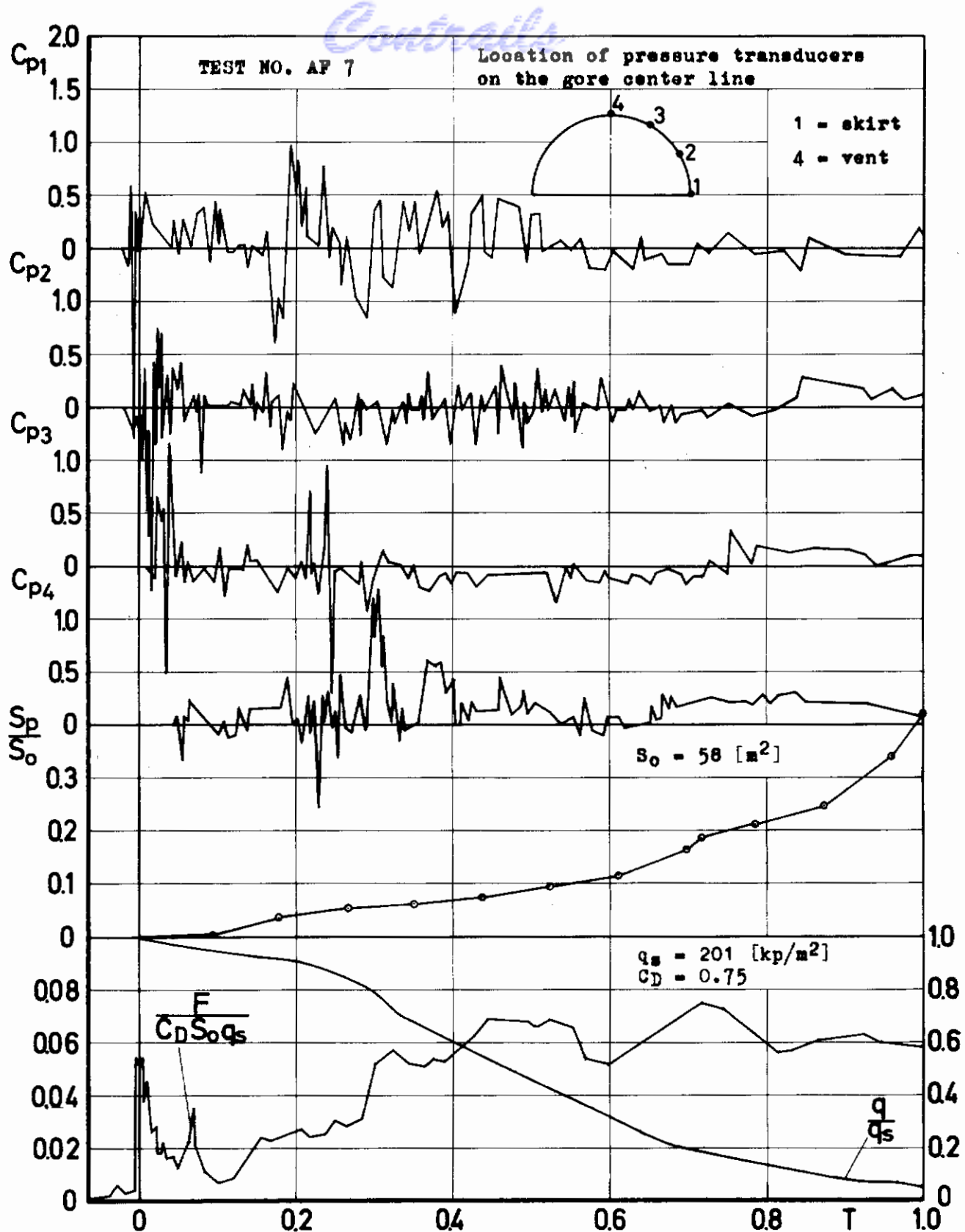


Fig.10 Differential pressure coefficient  $C_p = \Delta p/q_s$  and corresponding projected area ratio  $S_p/S_0$ , opening check factor  $F/C_D S_0 q_s$  and dynamic pressure coefficient  $q/q_s$  versus time ratio for 28 ft Circular Flat Parachute. Filling time  $t_f = 1.16$  [sec]

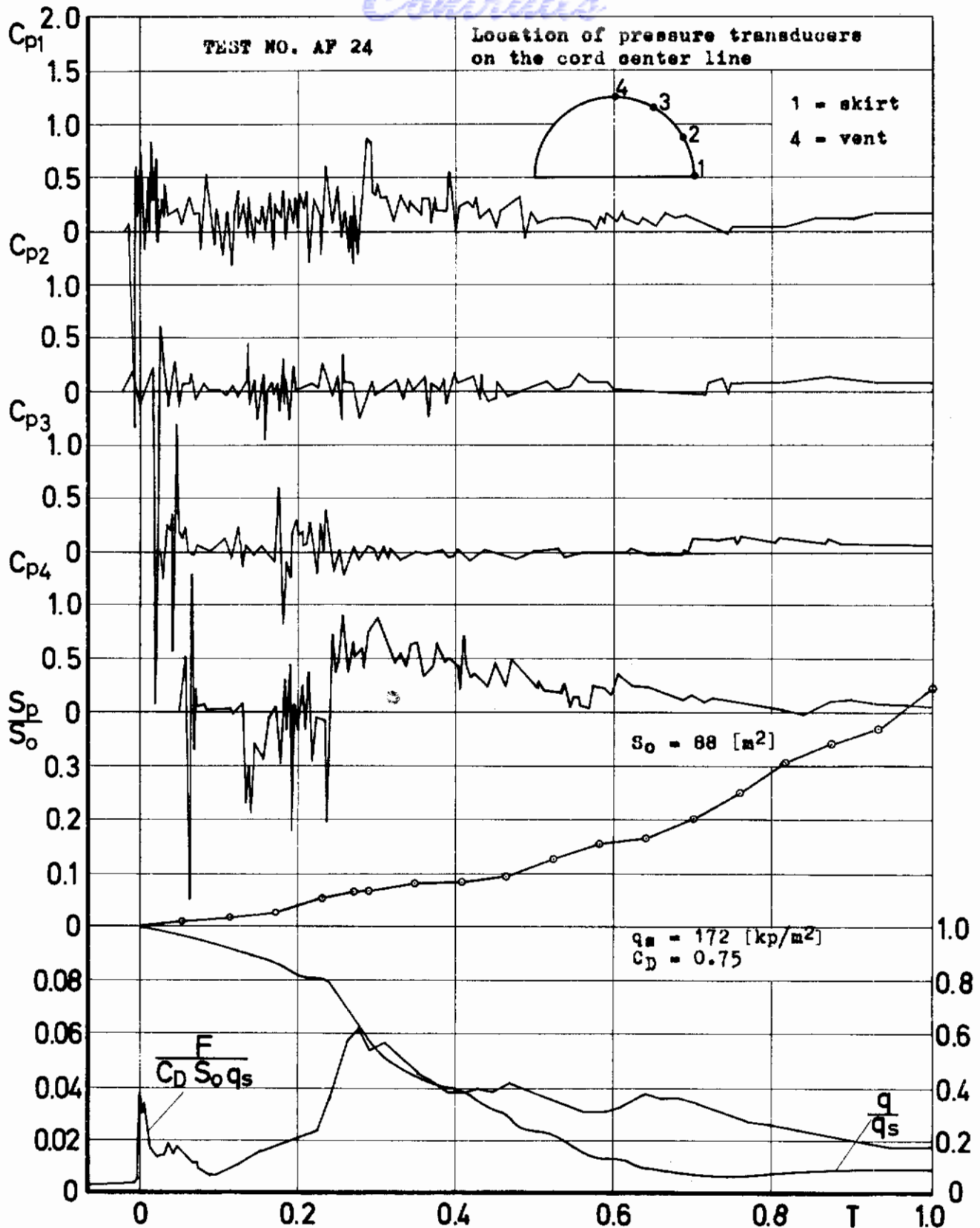


Fig.11 Differential pressure coefficient  $C_p = \Delta p/q_s$  and corresponding projected area ratio  $S_p/S_0$ , opening shock factor  $F/C_D S_0 q_s$  and dynamic pressure coefficient  $q/q_s$  versus time ratio for 35 ft Extended Skirt Parachute. Filling time  $t_f = 1.72$  [sec]

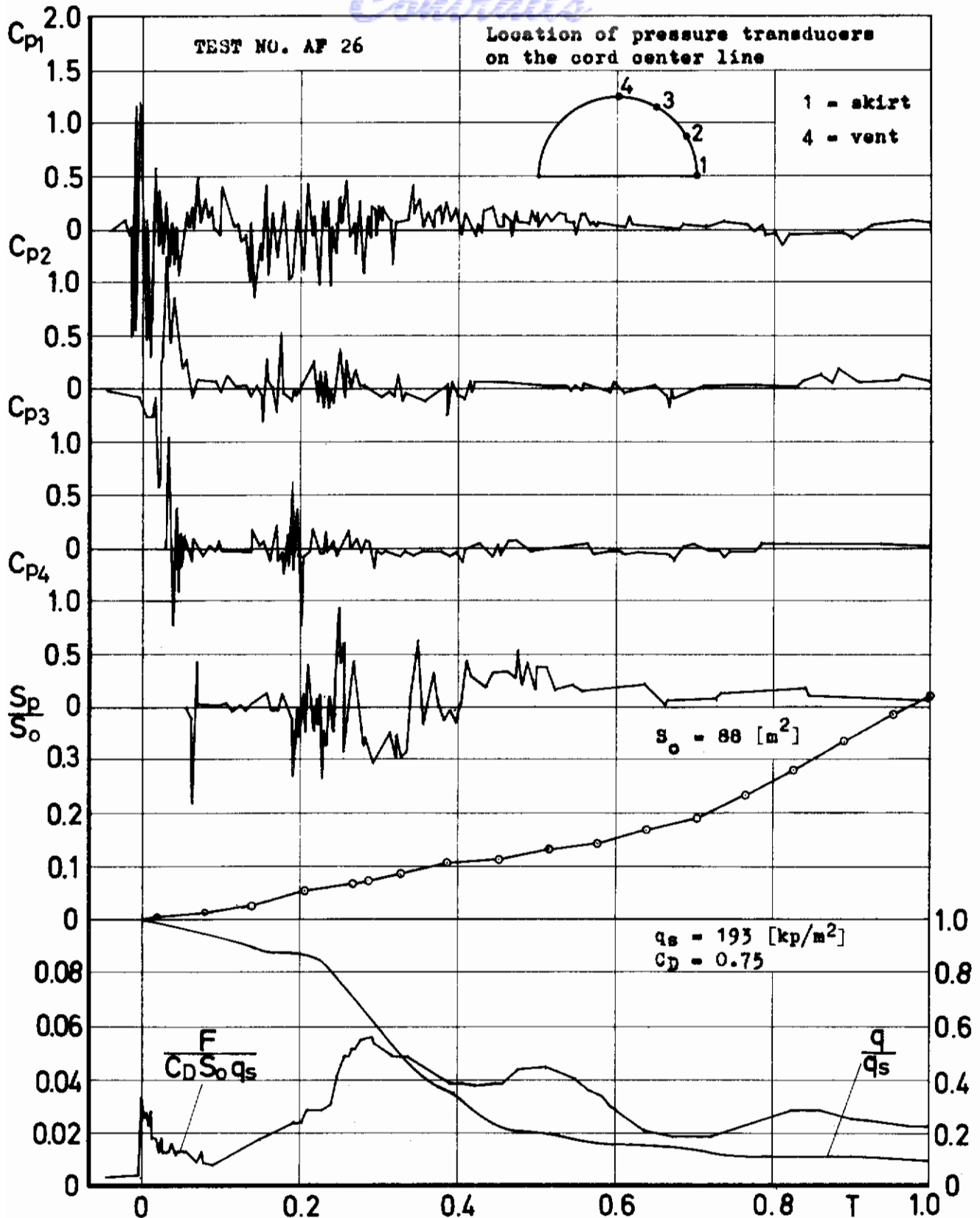


Fig. 12 Differential pressure coefficient  $C_p = \Delta p/q_s$  and corresponding projected area ratio  $S_p/S_0$ , opening shock factor  $F/C_D S_0 q_s$  and dynamic pressure coefficient  $q/q_s$  versus time ratio for 35 ft Extended Skirt Parachute. Filling time  $t_f = 1.609 \text{ [sec]}$

*Continails*

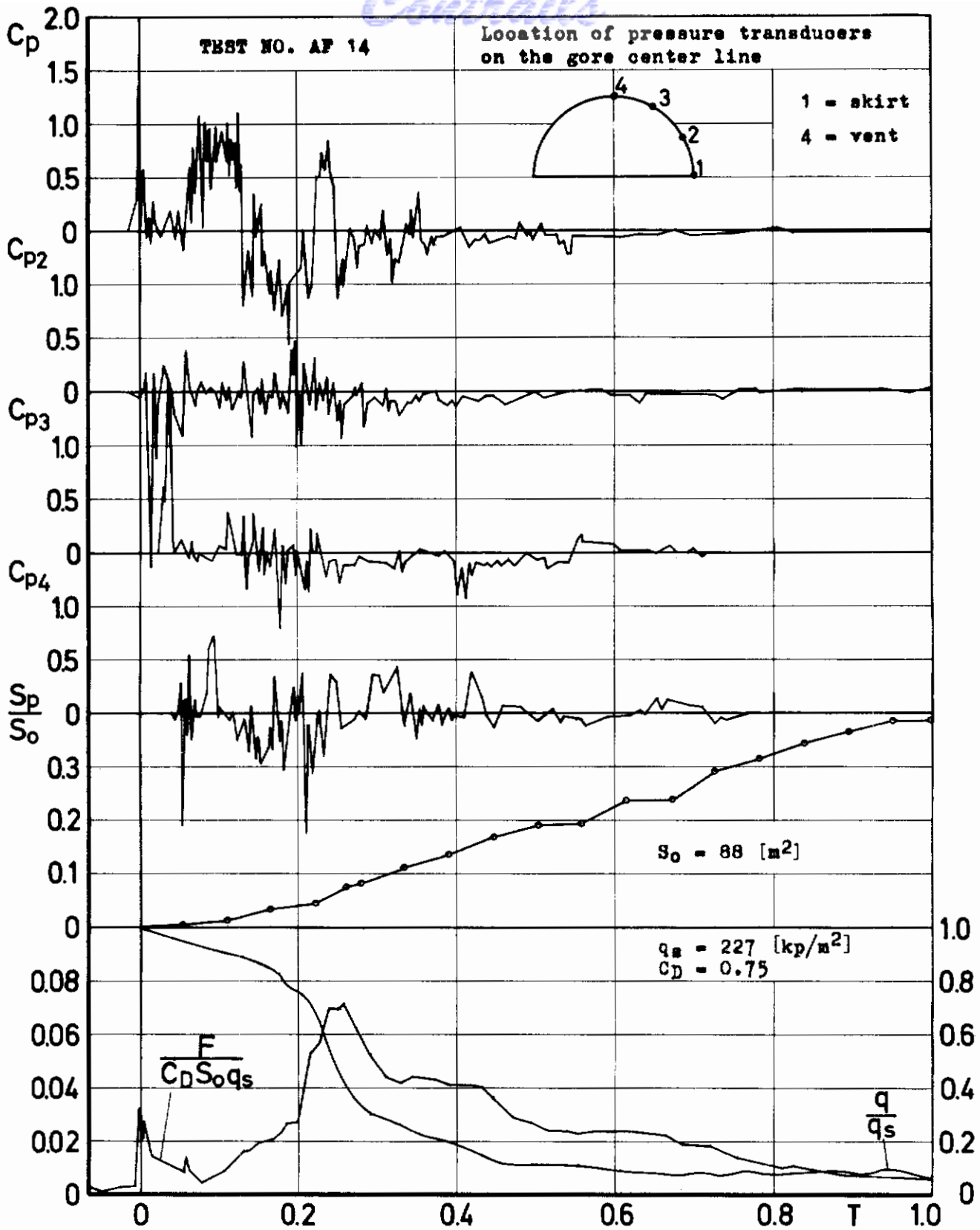


Fig.13 Differential pressure coefficient  $C_p = \Delta p/q_s$  and corresponding projected area ratio  $S_p/S_0$ , opening shock factor  $F/C_D S_0 q_s$  and dynamic pressure coefficient  $q/q_s$  versus time ratio for 35 ft Extended Skirt Parachute. Filling time  $t_f = 1.795 \text{ [sec]}$

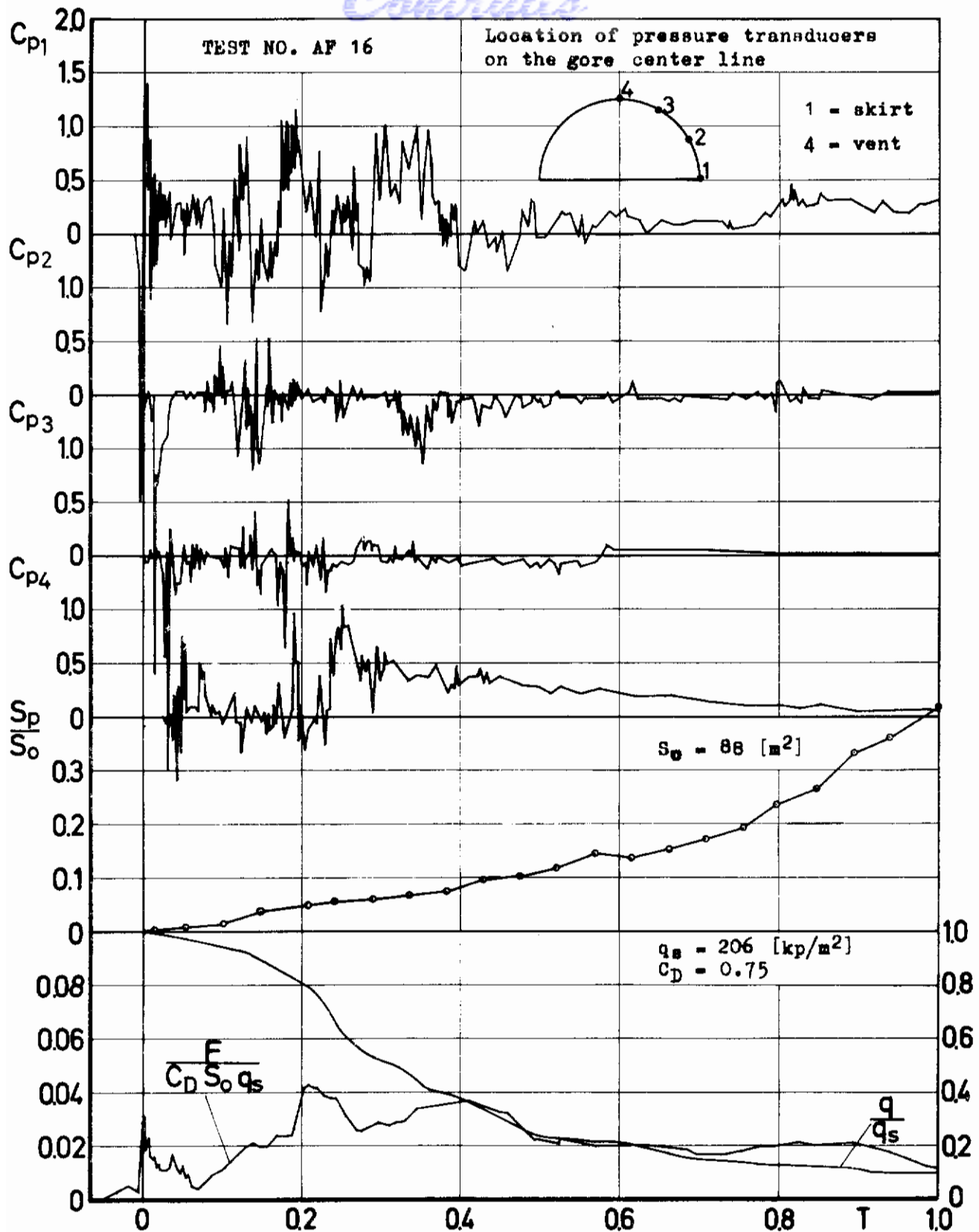


Fig.14 Differential pressure coefficient  $C_p = \Delta p/q_s$  and corresponding projected area ratio  $S_p/S_0$ , opening shock factor  $F/C_D S_0 q_s$  and dynamic pressure coefficient  $q/q_s$  versus time ratio for 35 ft Extended Skirt Parachute. Filling time  $t_f = 2.158 \text{ [sec]}$

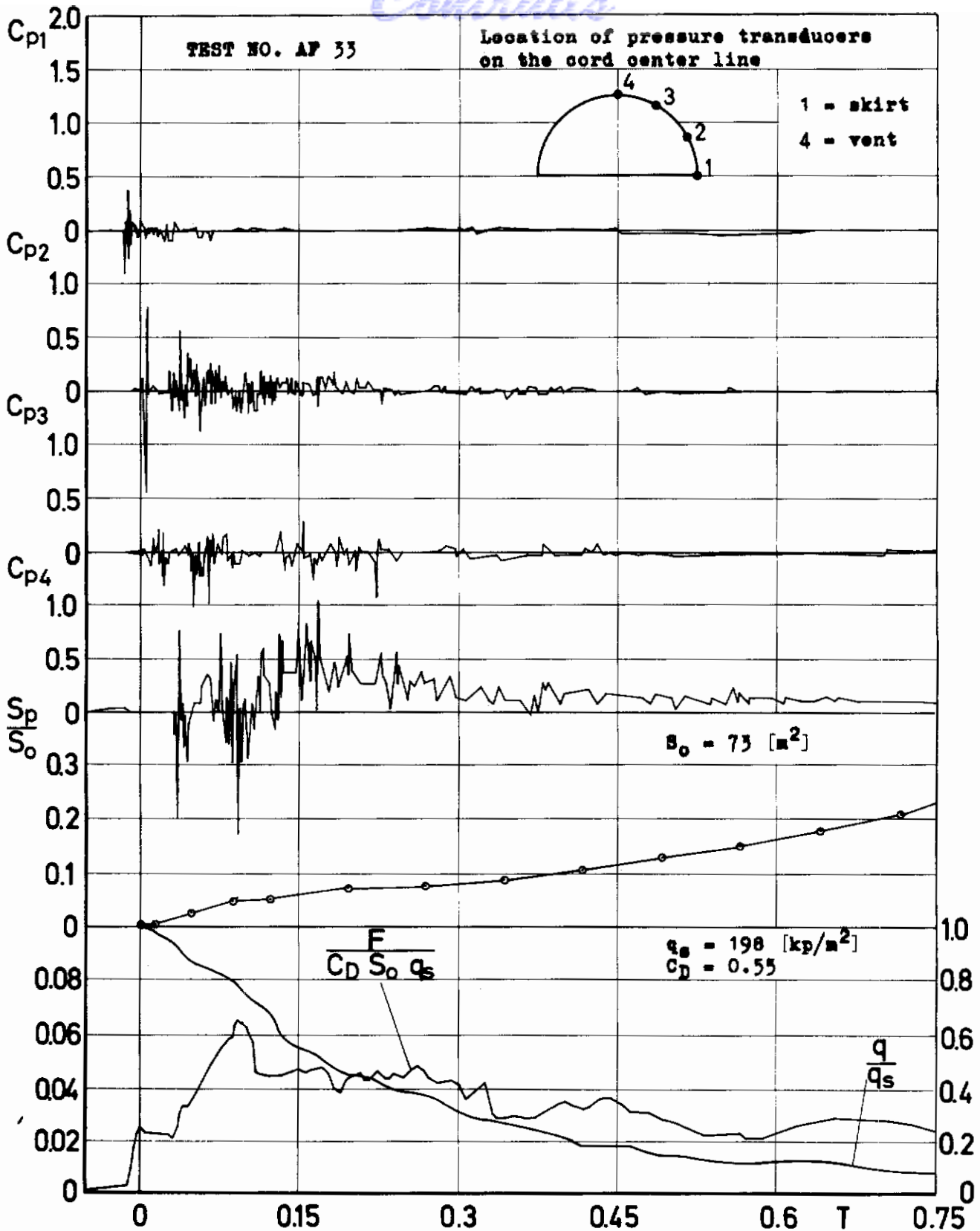


Fig.15 Differential pressure coefficient  $C_p = \Delta p/q_s$  and corresponding projected area ratio  $S_p/S_0$ , opening shock factor  $F/C_D S_0 q_s$  and dynamic pressure coefficient  $q/q_s$  versus time ratio for 32 ft Ringslot Parachute (O). Filling time  $t_f = 3.68$  [sec]



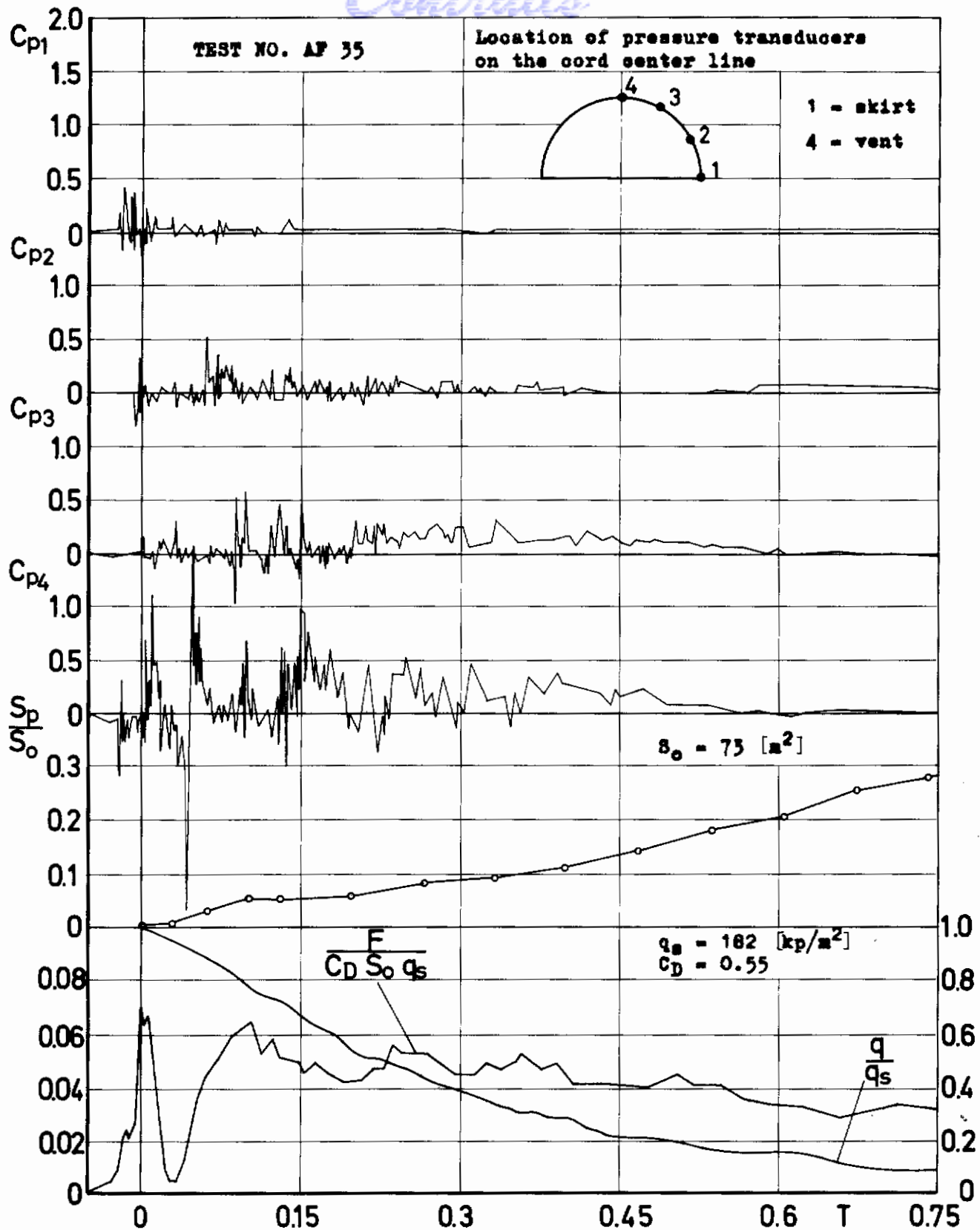


Fig. 16 Differential pressure coefficient  $C_p = \Delta p/q_s$  and corresponding projected area ratio  $S_p/S_0$ , opening shock factor  $F/C_D S_0 q_s$  and dynamic pressure coefficient  $q/q_s$  versus time ratio for 32 ft Ringslot Parachute (G). Filling time  $t_f = 3.21$  [sec]

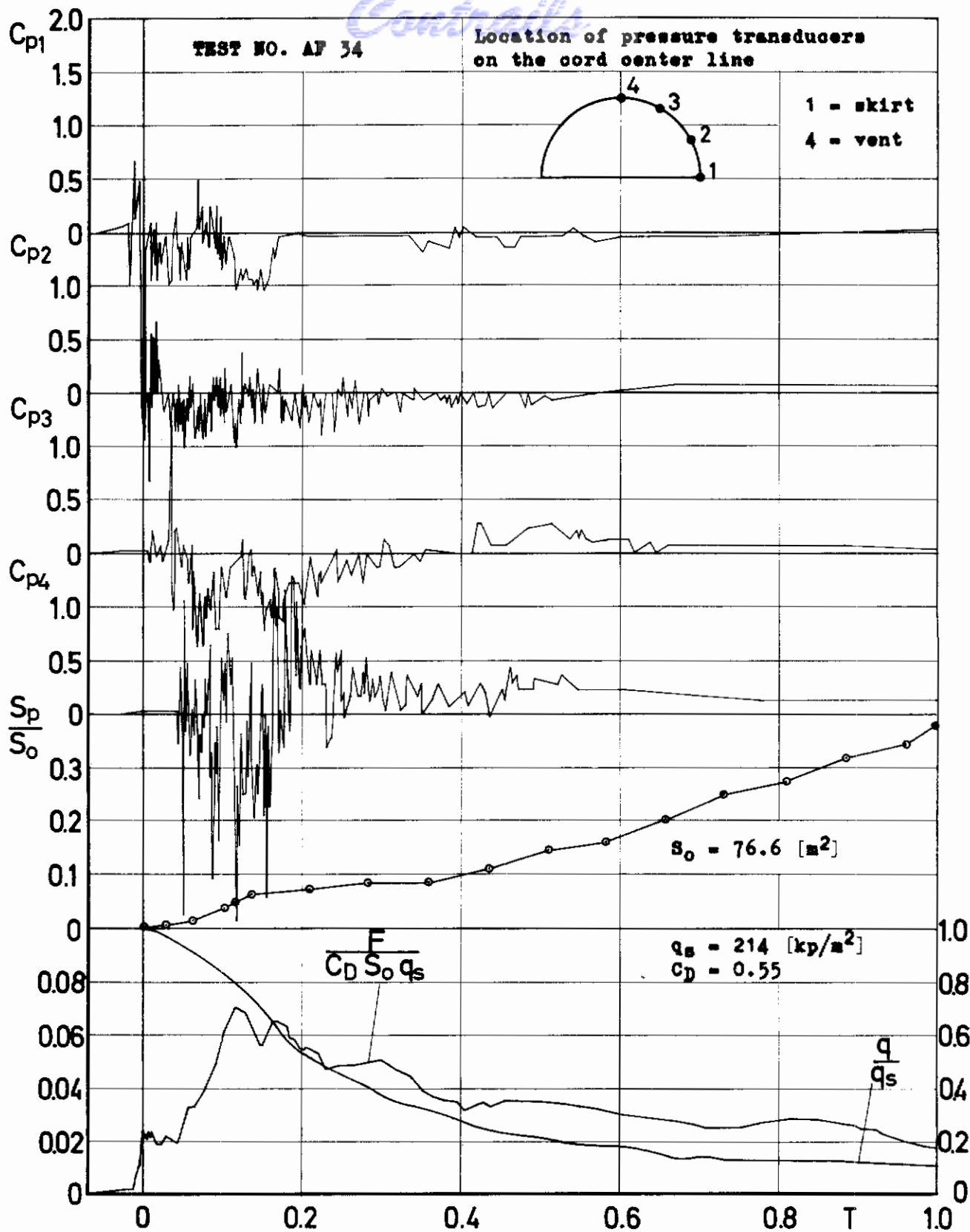


Fig.17 Differential pressure coefficient  $C_p = \Delta p/q_s$  and corresponding projected area ratio  $S_p/S_0$ , opening shock factor  $F/C_D S_0 q_s$  and dynamic pressure coefficient  $q/q_s$  versus time ratio for 32 ft Ringslot Parachute (US). Filling time  $t_f = 2.83 \text{ [sec]}$

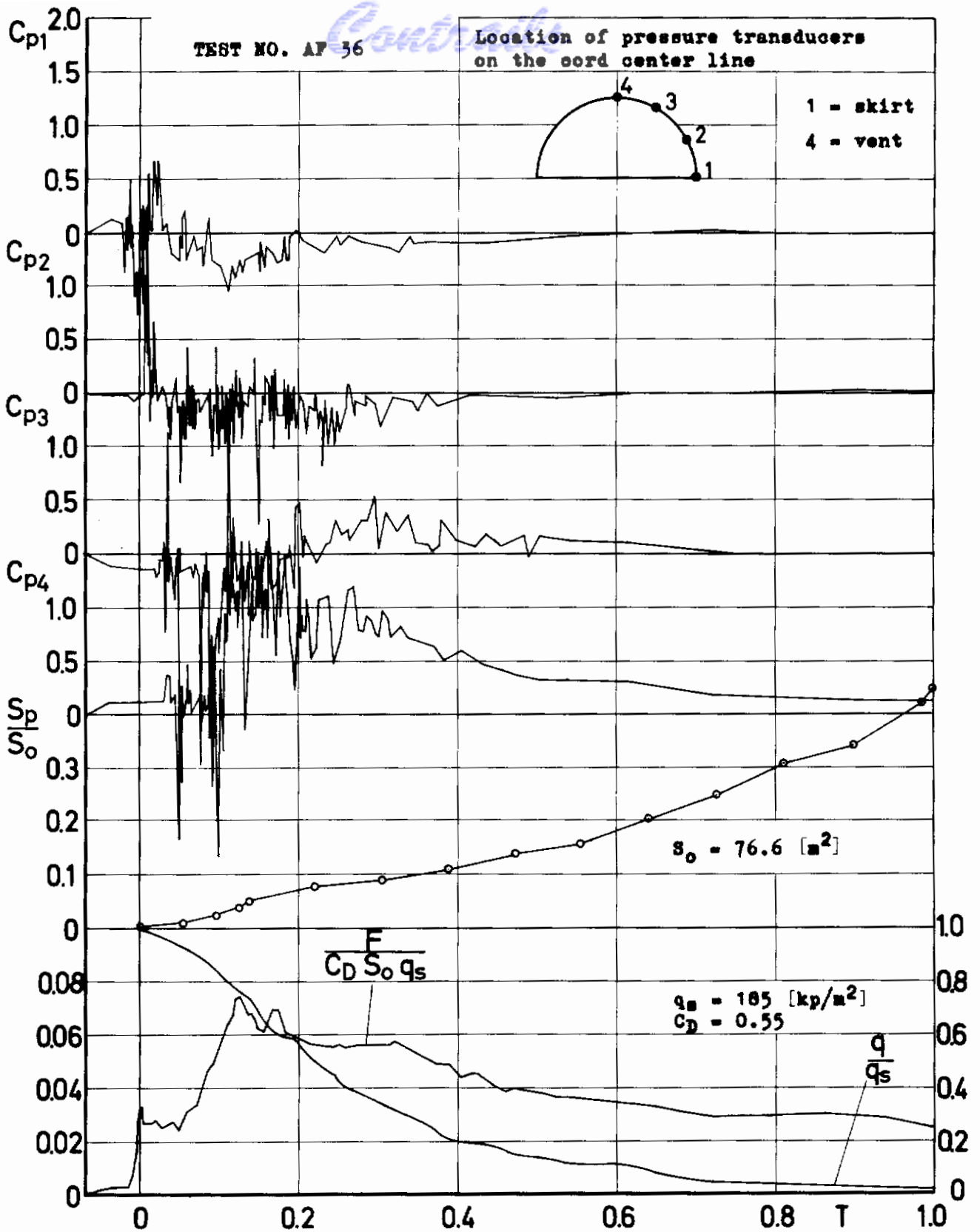


Fig.18 Differential pressure coefficient  $C_p = \Delta p/q_s$  and corresponding projected area ratio  $S_p/S_o$ , opening shock factor  $F/C_D S_o q_s$  and dynamic pressure coefficient  $q/q_s$  versus time ratio for 32 ft Ringslot Parachute (US). Filling time  $t_f = 2.77$  [sec]

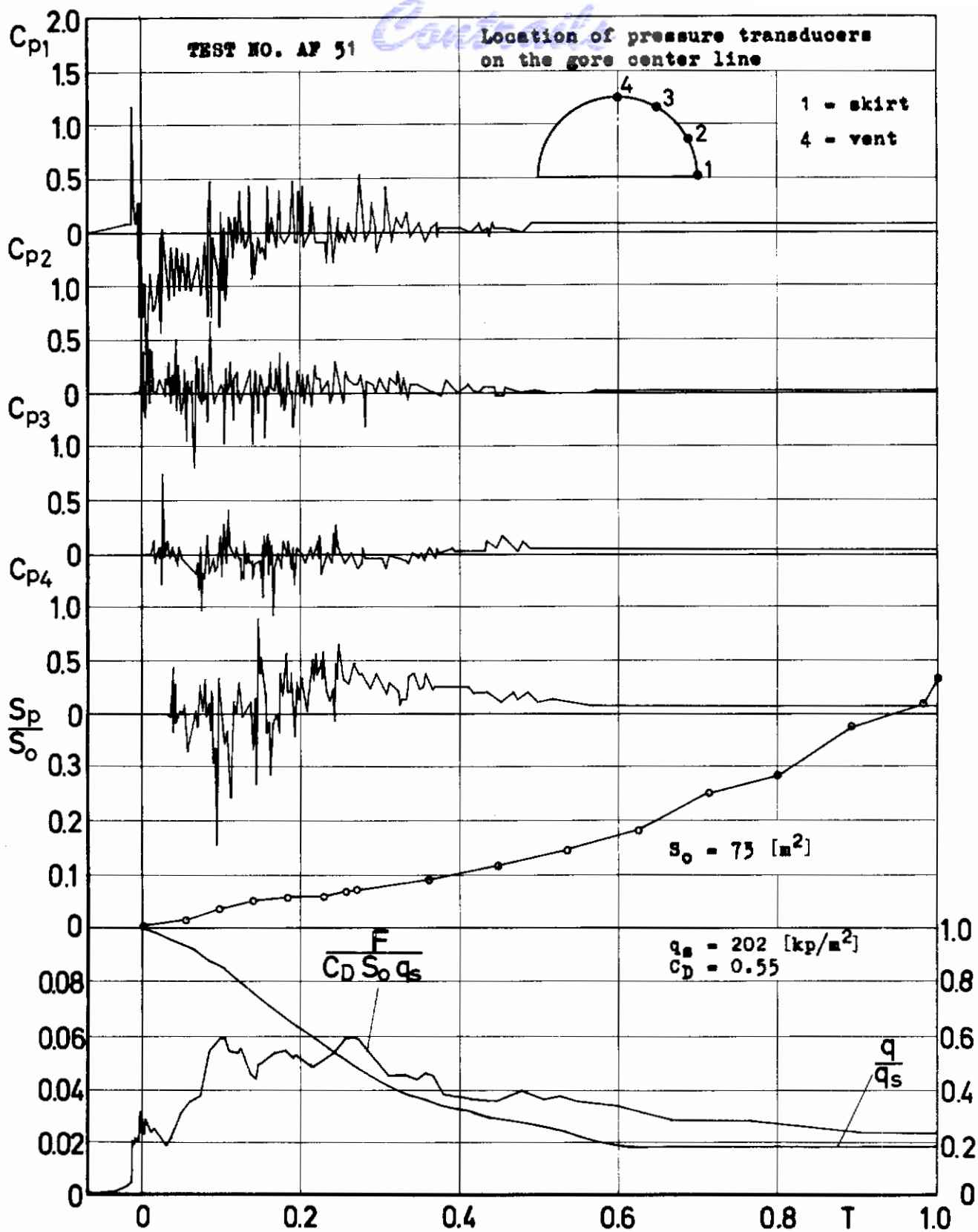


Fig. 19 Differential pressure coefficient  $C_p = \Delta p/q_s$  and corresponding projected area ratio  $S_p/S_o$ , opening shock factor  $F/C_D S_o q_s$  and dynamic pressure coefficient  $q/q_s$  versus time ratio for 32 ft Ringslot Parachute (G). Filling time  $t_f = 2.99$  [sec]

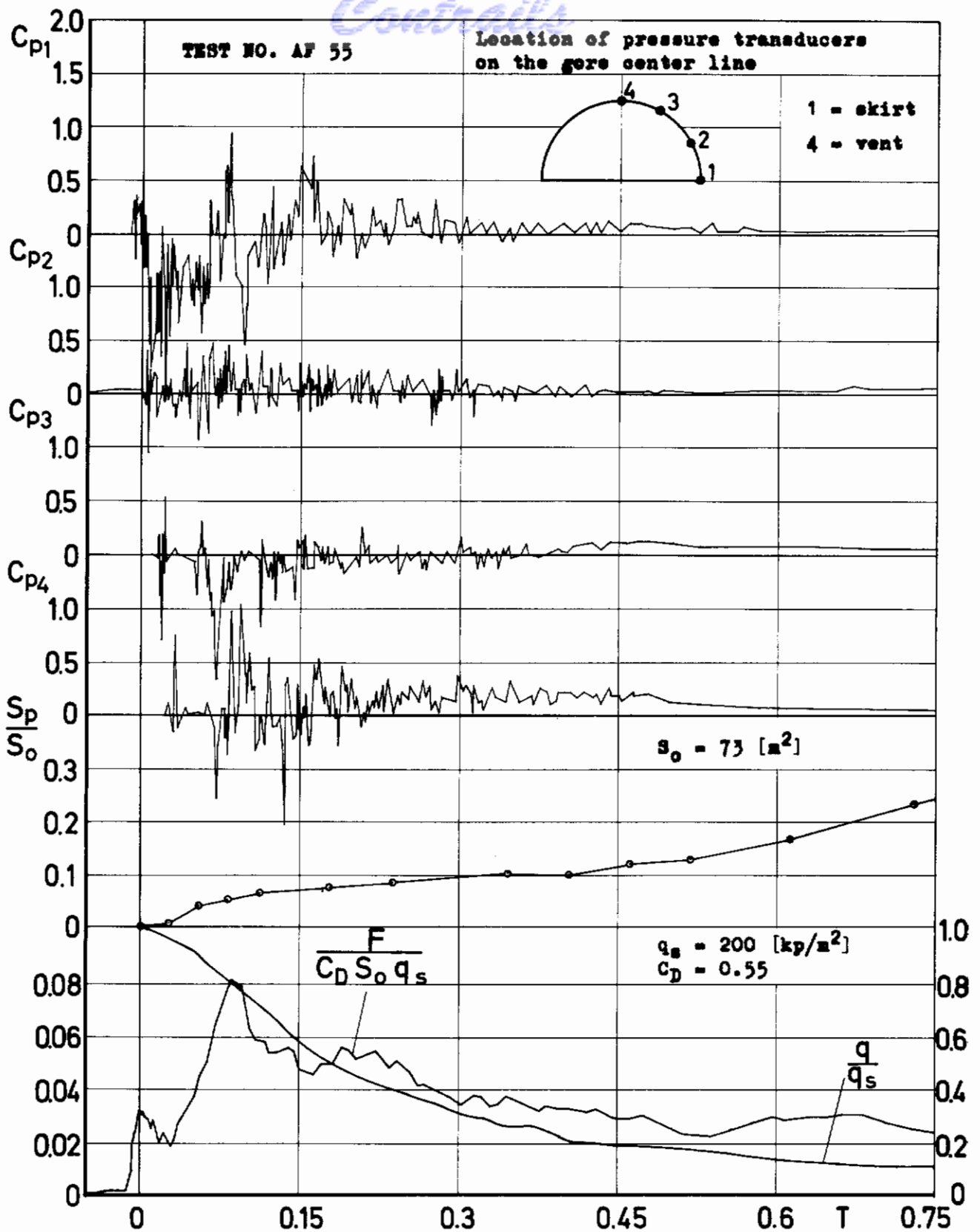
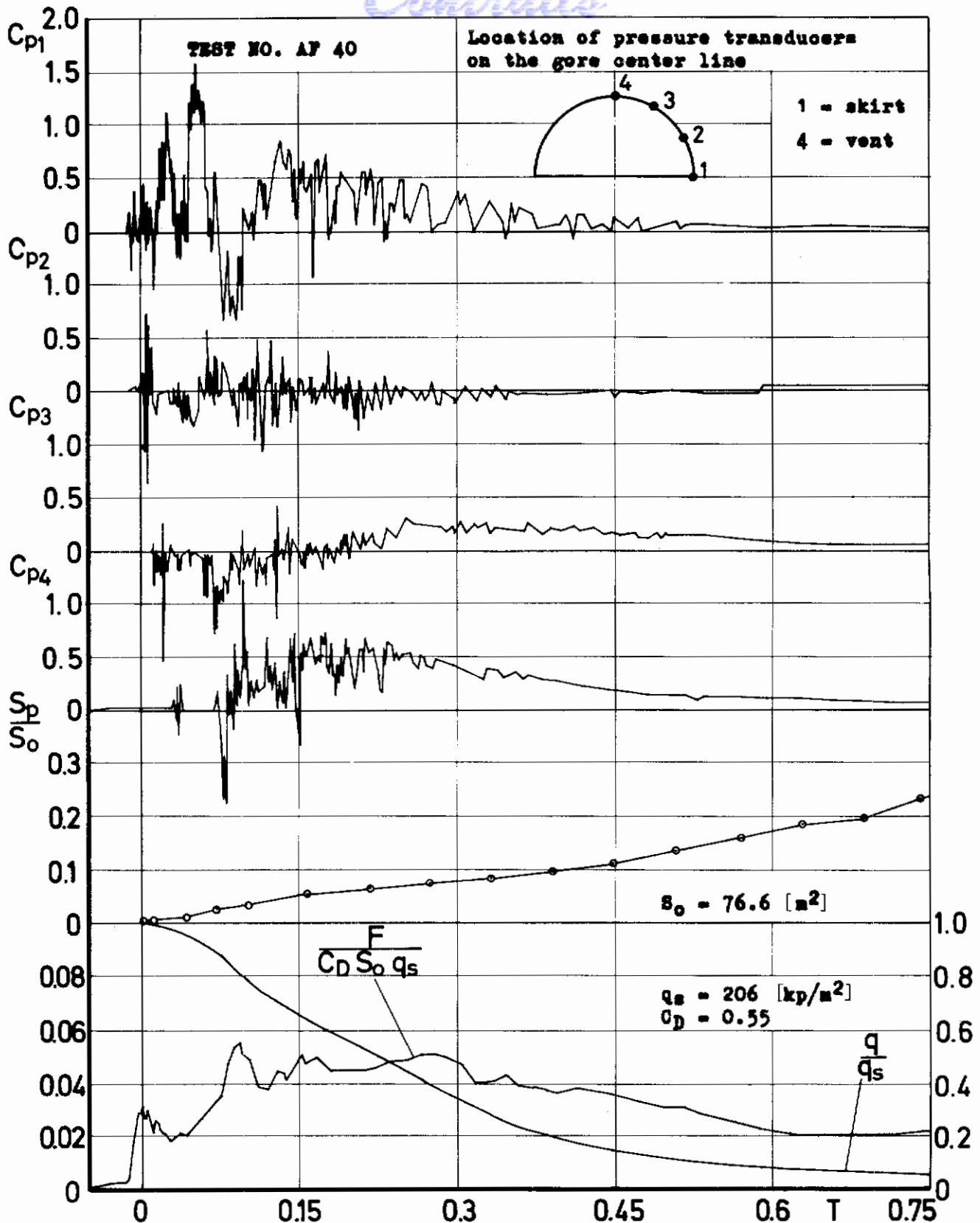


Fig. 20 Differential pressure coefficient  $C_p = \Delta p/q_s$  and corresponding projected area ratio  $S_p/S_0$ , opening shock factor  $F/C_D S_0 q_s$  and dynamic pressure coefficient  $q/q_s$  versus time ratio for 32 ft Ringslot Parachute (G). Filling time  $t_f = 3.79 \text{ [sec]}$



**Fig. 21** Differential pressure coefficient  $C_p = \Delta p/q_s$  and corresponding projected area ratio  $S_p/S_0$ , opening shock factor  $F/C_D S_0 q_s$  and dynamic pressure coefficient  $q/q_s$  versus time ratio for 32 ft Ringslot Parachute (US). Filling time  $t_f = 3.37 \text{ [sec]}$

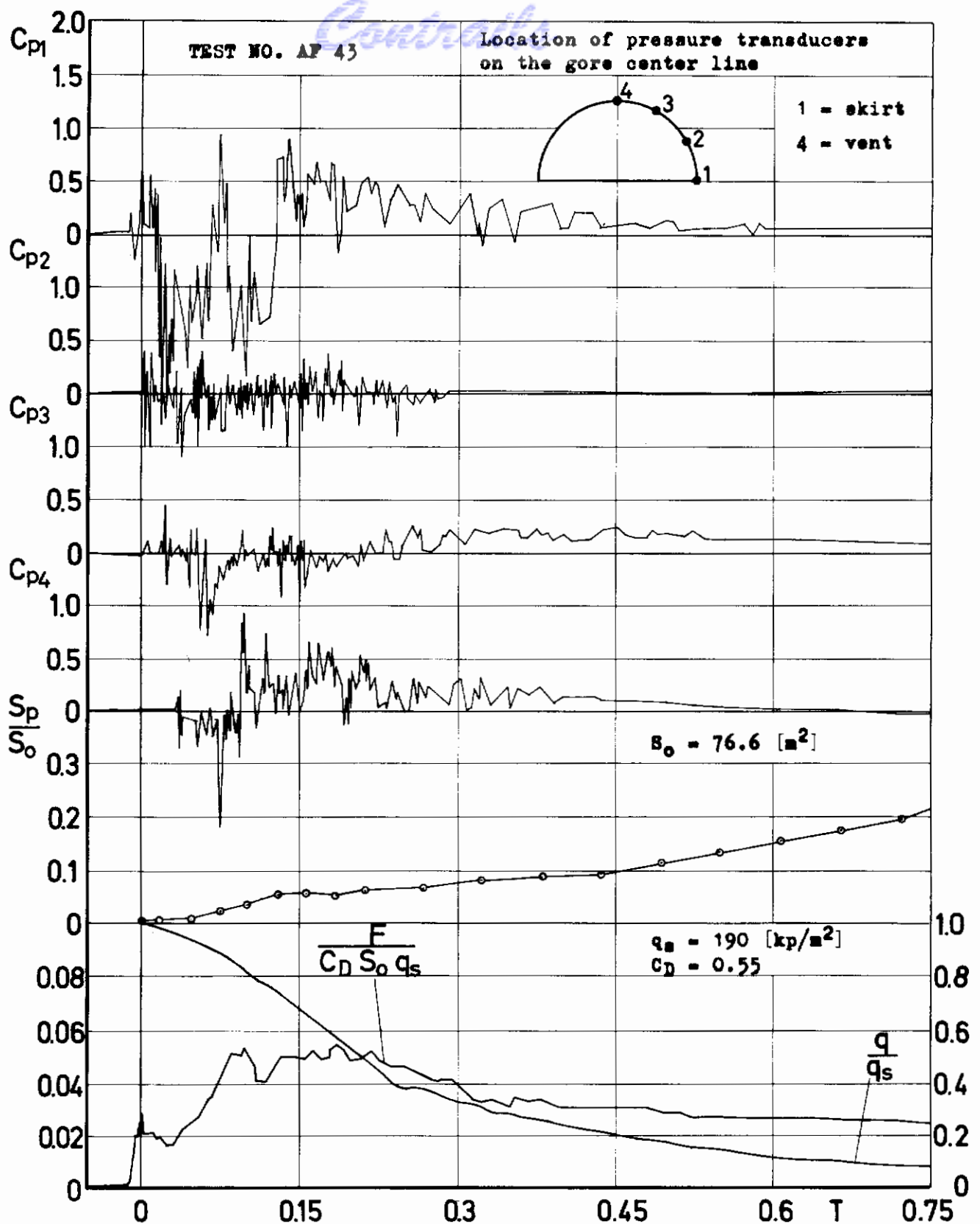


Fig. 22 Differential pressure coefficient  $C_p = \Delta p/q_s$  and corresponding projected area ratio  $S_p/S_0$ , opening shock factor  $F/C_D S_0 q_s$  and dynamic pressure coefficient  $q/q_s$  versus time ratio for 32 ft Ringslot Parachute (US). Filling time  $t_f = 3.62 \text{ [sec]}$

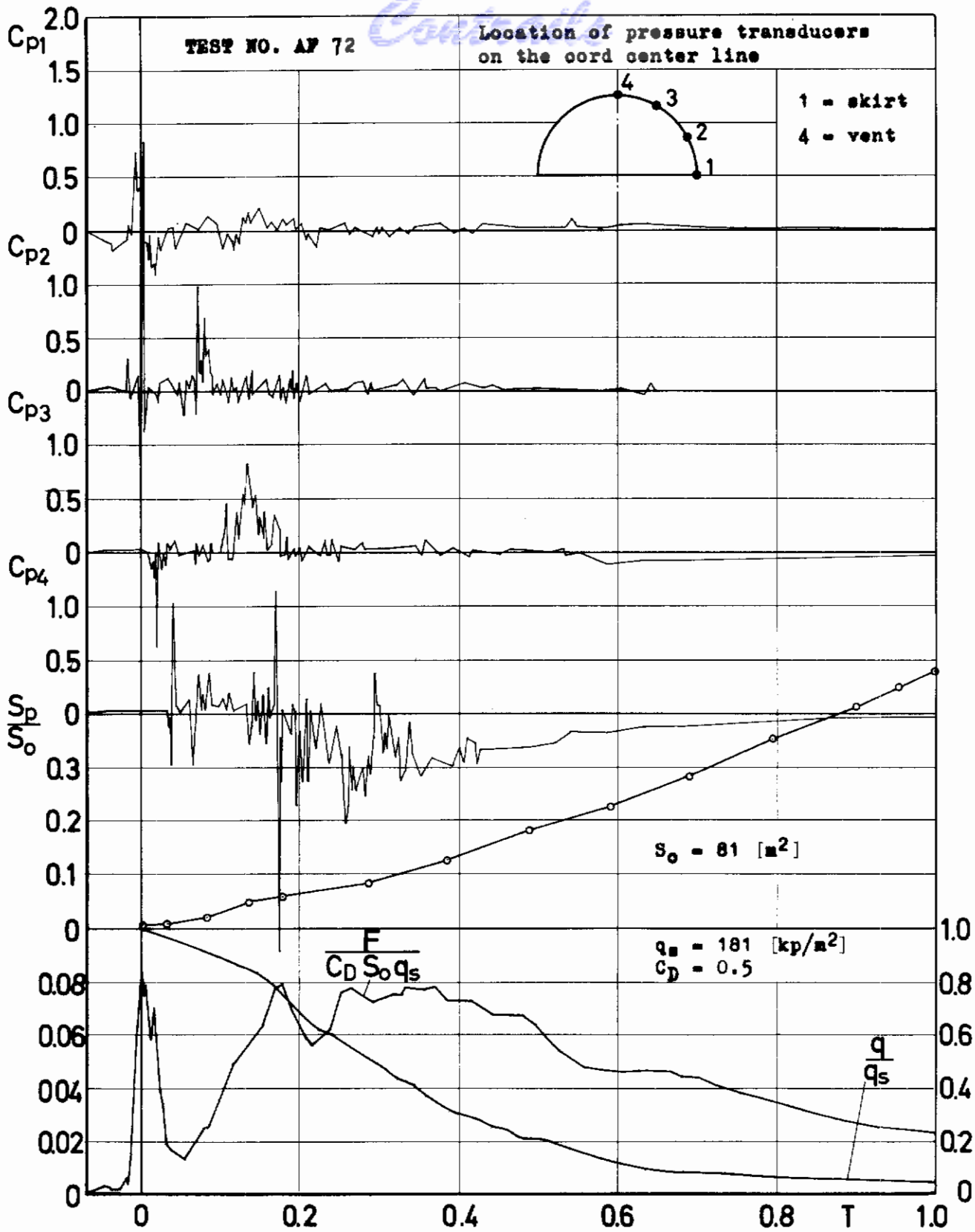
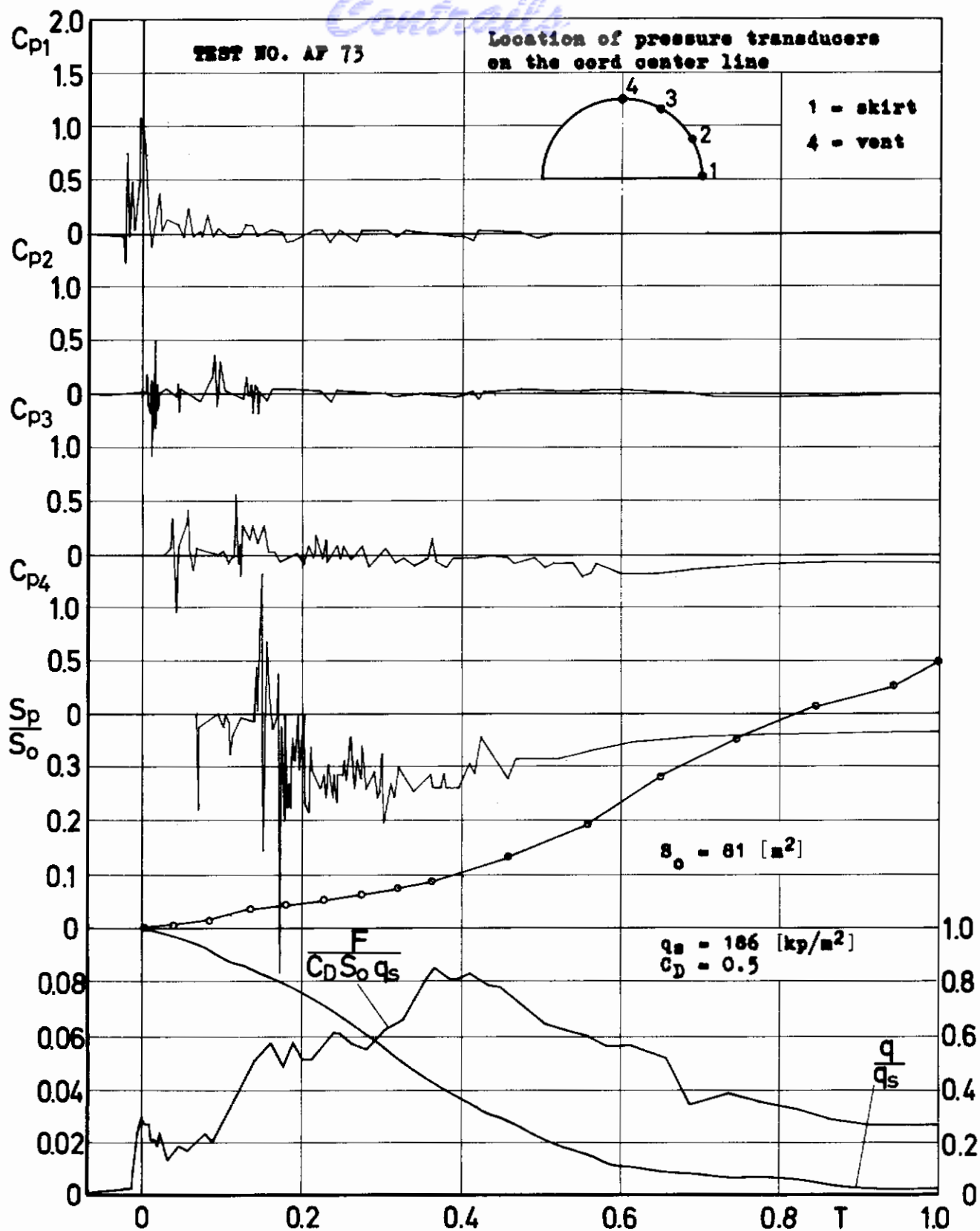


Fig. 23 Differential pressure coefficient  $C_p = \Delta p/q_s$  and corresponding projected area ratio  $S_p/S_0$ , opening shock factor  $F/C_D S_0 q_s$  and dynamic pressure coefficient  $q/q_s$  versus time ratio for 34 ft Circular Flat Ribbon Parachute (G). Filling time  $t_f = 2.04$  [sec]





**Fig. 24** Differential pressure coefficient  $C_p = \Delta p/q_d$  and corresponding projected area ratio  $S_p/S_0$ , opening shock factor  $F/C_D S_0 q_d$  and dynamic pressure coefficient  $q/q_d$  versus time ratio for 34 ft Circular Flat Ribbon Parachute (C). Filling time  $t_f = 2.52 \text{ [sec]}$

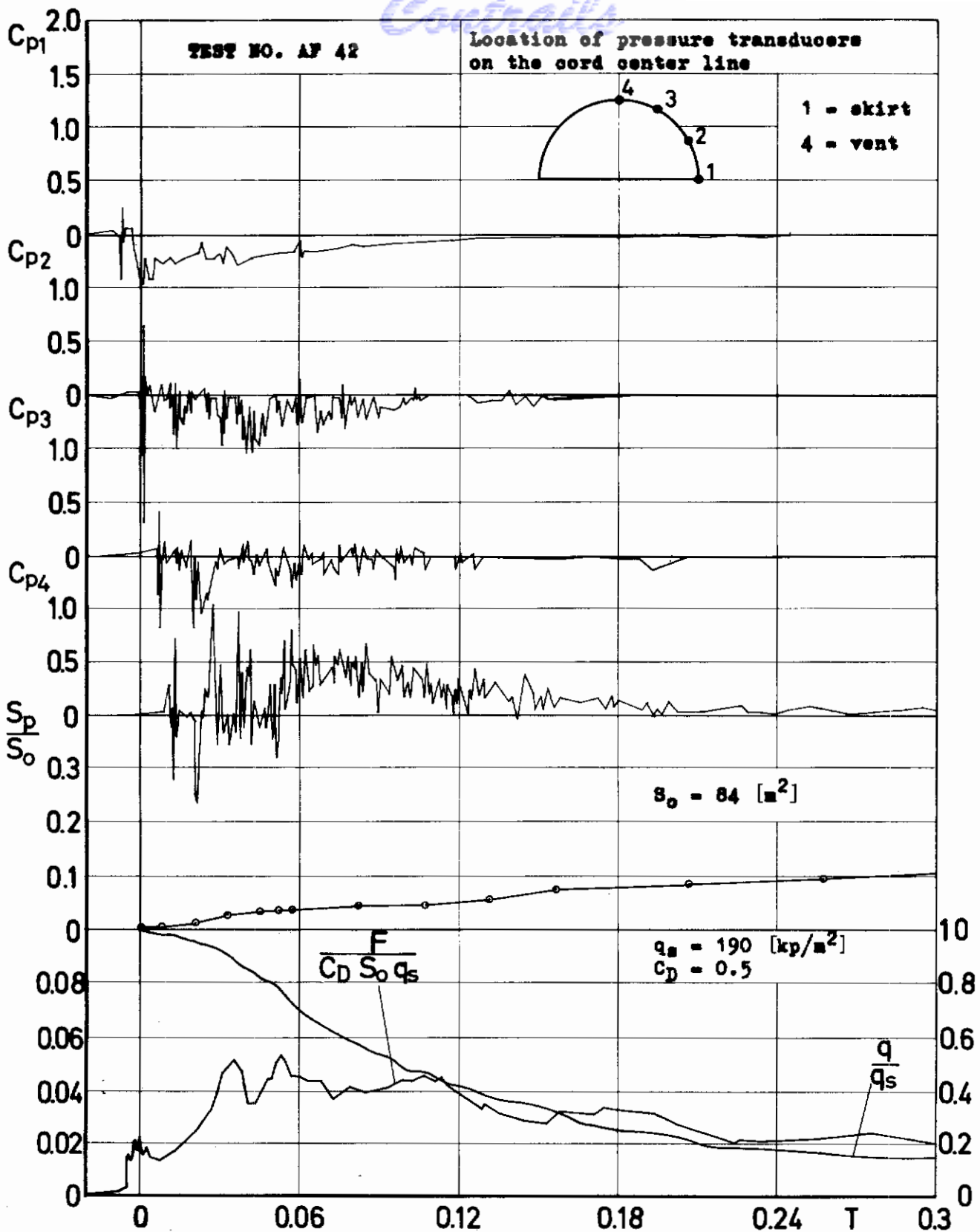
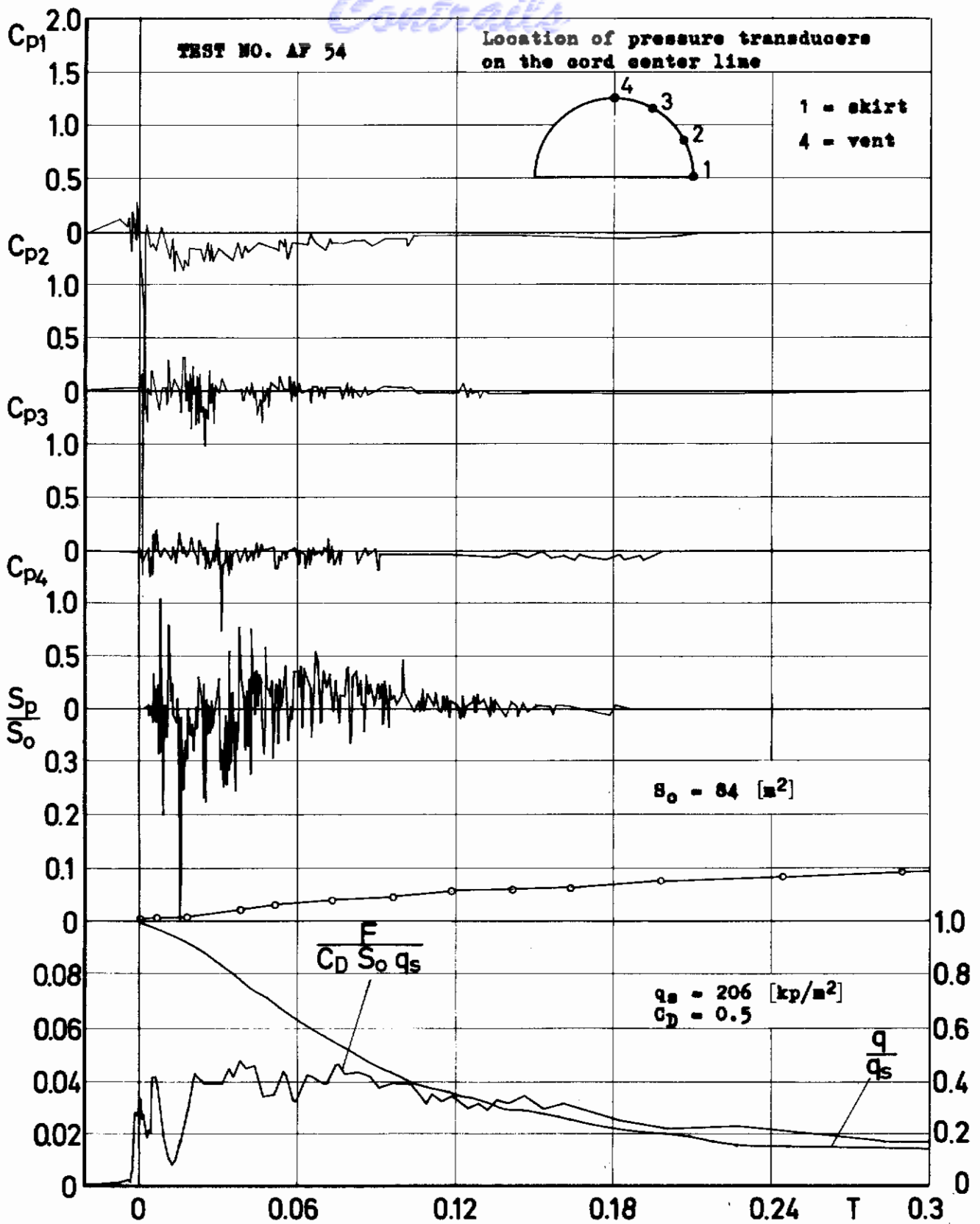


Fig. 25 Differential pressure coefficient  $C_p = \Delta p/q_s$  and corresponding projected area ratio  $S_p/S_0$ , opening shock factor  $F/C_D S_0 q_s$  and dynamic pressure coefficient  $q/q_s$  versus time ratio for 34 ft Circular Flat Ribbon Parachute (US). Filling time  $t_f = 9.37 \text{ [sec]}$



**Fig. 26** Differential pressure coefficient  $C_p = \Delta p/q_s$  and corresponding projected area ratio  $S_p/S_0$ , opening shock factor  $F/C_D S_0 q_s$  and dynamic pressure coefficient  $q/q_s$  versus time ratio for 34 ft Circular Flat Ribbon Parachute (US). Filling time  $t_f = 10.98$  [sec]

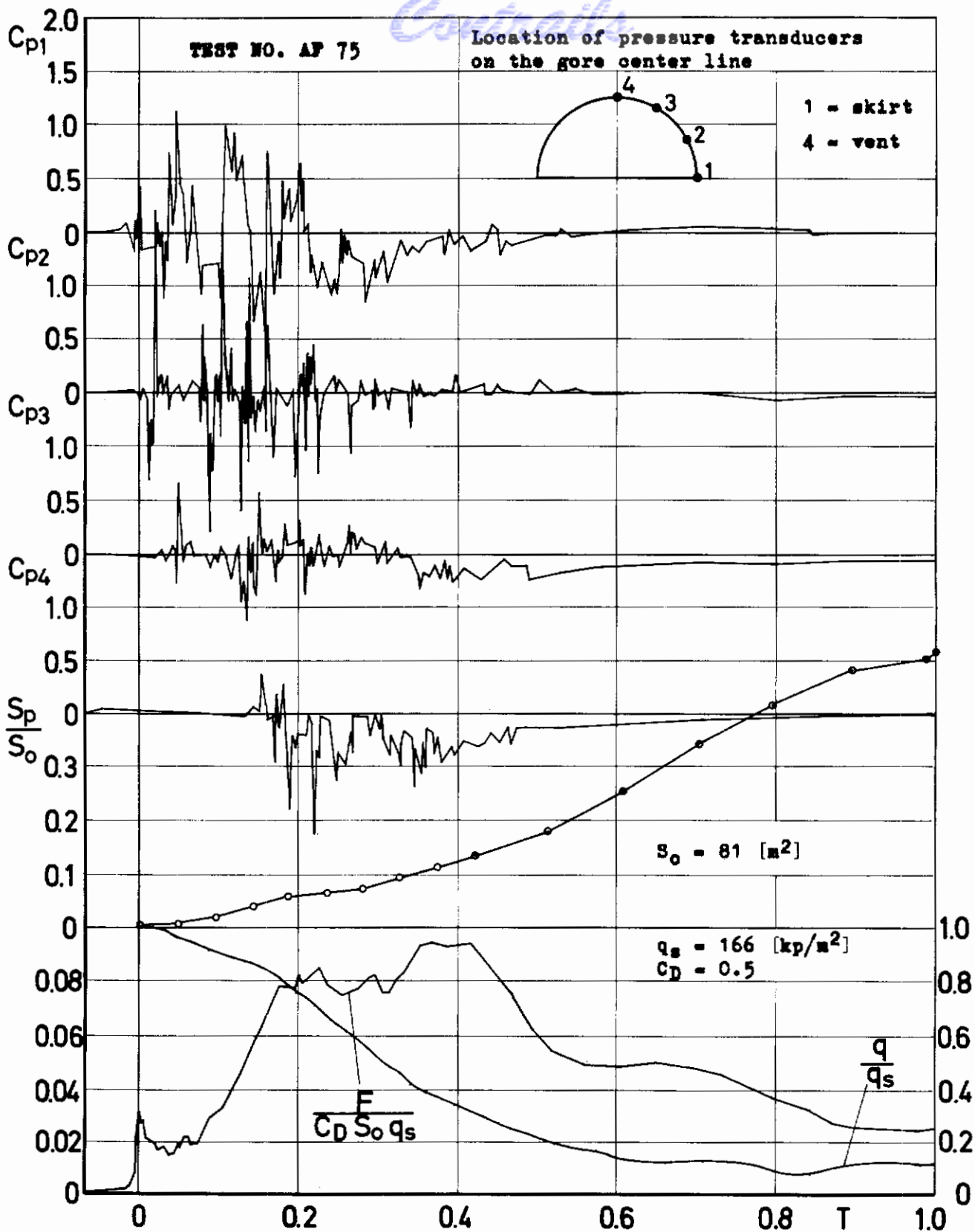


Fig. 27 Differential pressure coefficient  $C_p = \Delta p/q_s$  and corresponding projected area ratio  $S_p/S_o$ , opening shock factor  $F/C_D S_o q_s$  and dynamic pressure coefficient  $q/q_s$  versus time ratio for 34 ft Circular Flat Ribbon Parachute (G). Filling time  $t_f = 2.26$  [sec]

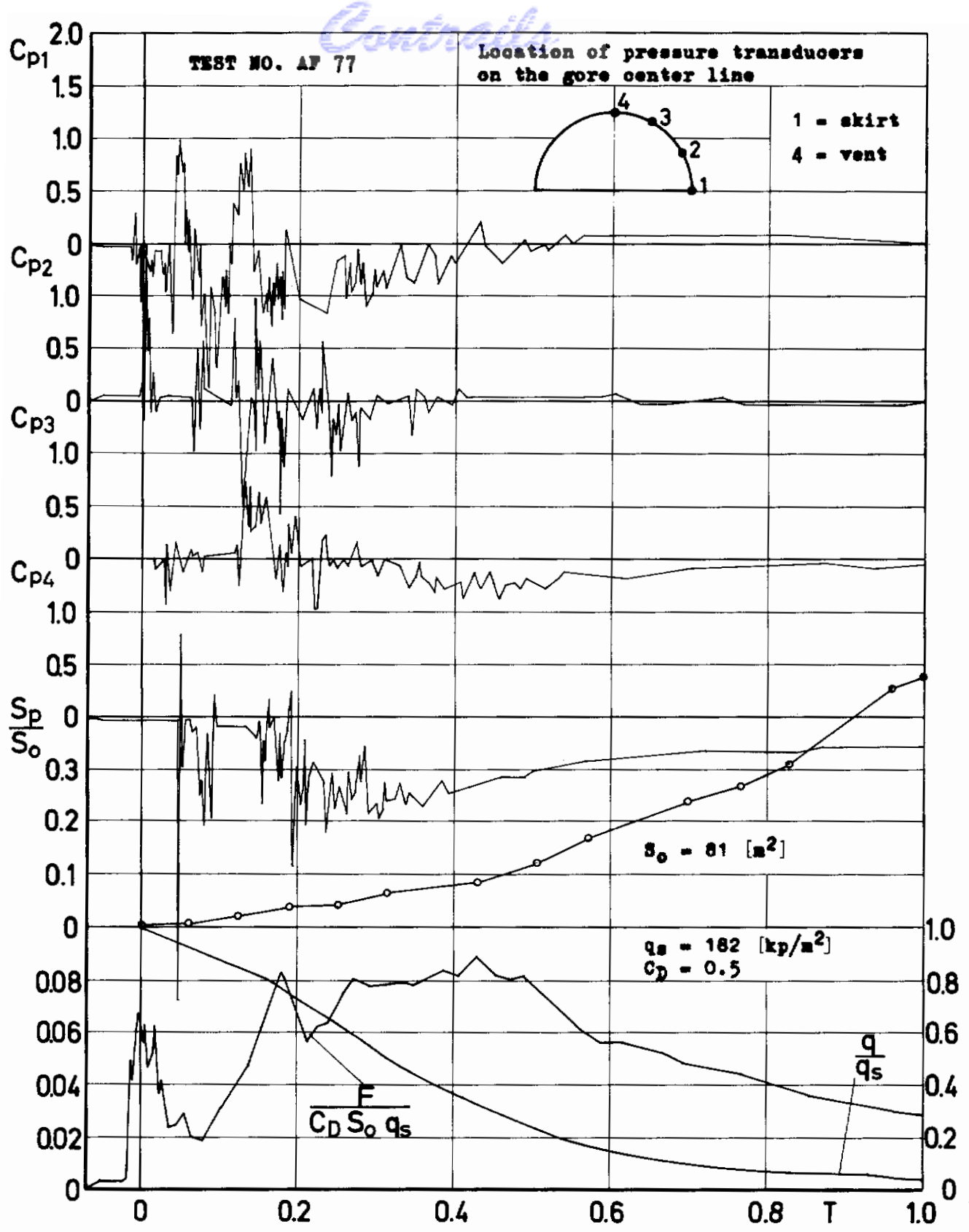
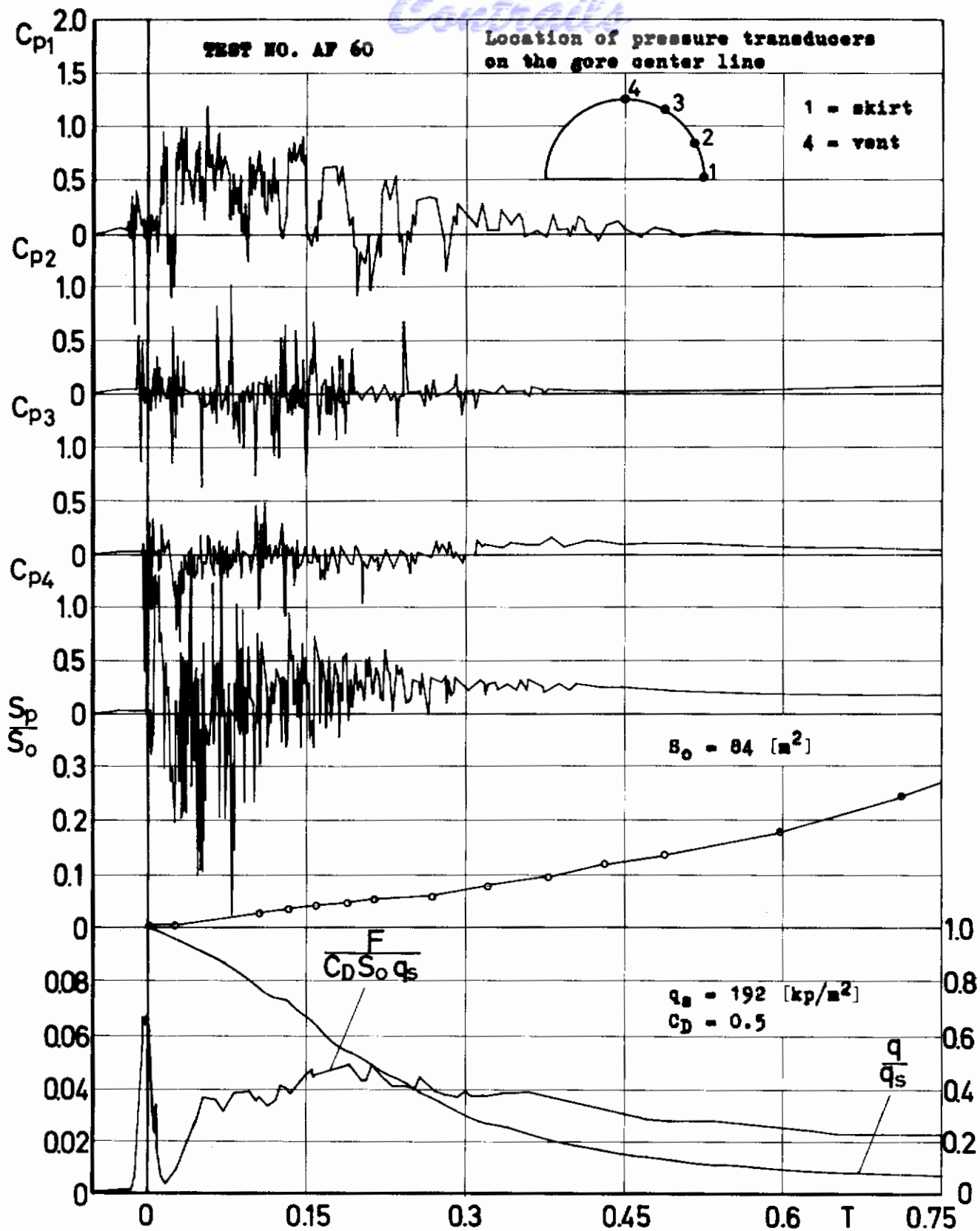


Fig.28 Differential pressure coefficient  $C_p = \Delta p/q_s$  and corresponding projected area ratio  $S_p/S_0$ , opening shock factor  $F/C_D S_0 q_s$  and dynamic pressure coefficient  $q/q_s$  versus time ratio for 34 ft Circular Flat Ribbon Parachute (O). Filling time  $t_f = 1.94$  [sec]

*Continued*



**Fig. 29** Differential pressure coefficient  $C_p = \Delta p/q_s$  and corresponding projected area ratio  $S_p/S_0$ , opening shock factor  $F/C_D S_0 q_s$  and dynamic pressure coefficient  $q/q_s$  versus time ratio for 34 ft Circular Flat Ribbon Parachute (US). Filling time  $t_f = 4.46 \text{ [sec]}$

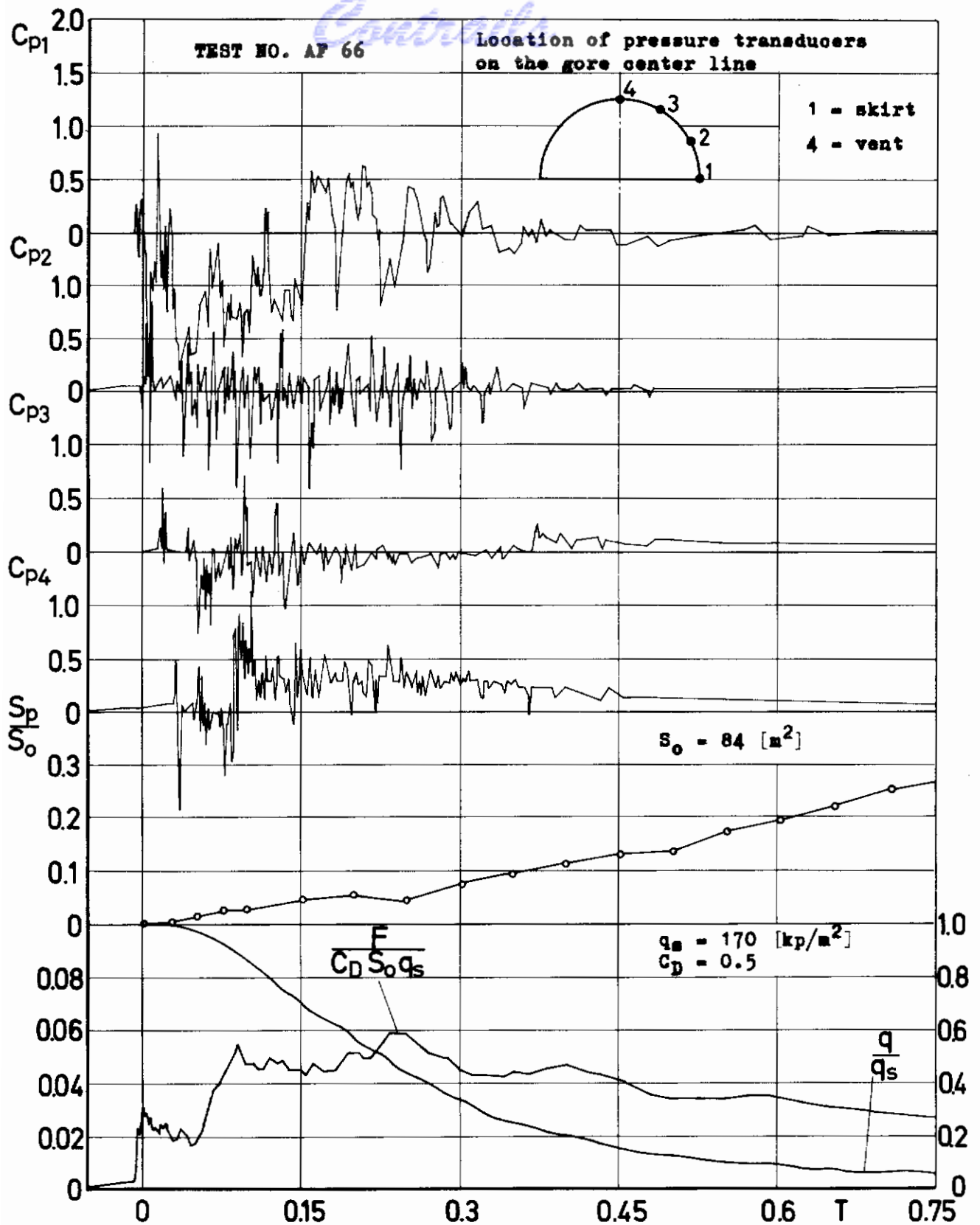


Fig. 30 Differential pressure coefficient  $C_p = \Delta p/q_s$  and corresponding projected area ratio  $S_p/S_o$ , opening shock factor  $F/C_D S_o q_s$  and dynamic pressure coefficient  $q/q_s$  versus time ratio for 34 ft Circular Flat Ribbon Parachute (US). Filling time  $t_f = 4.18 \text{ [sec]}$

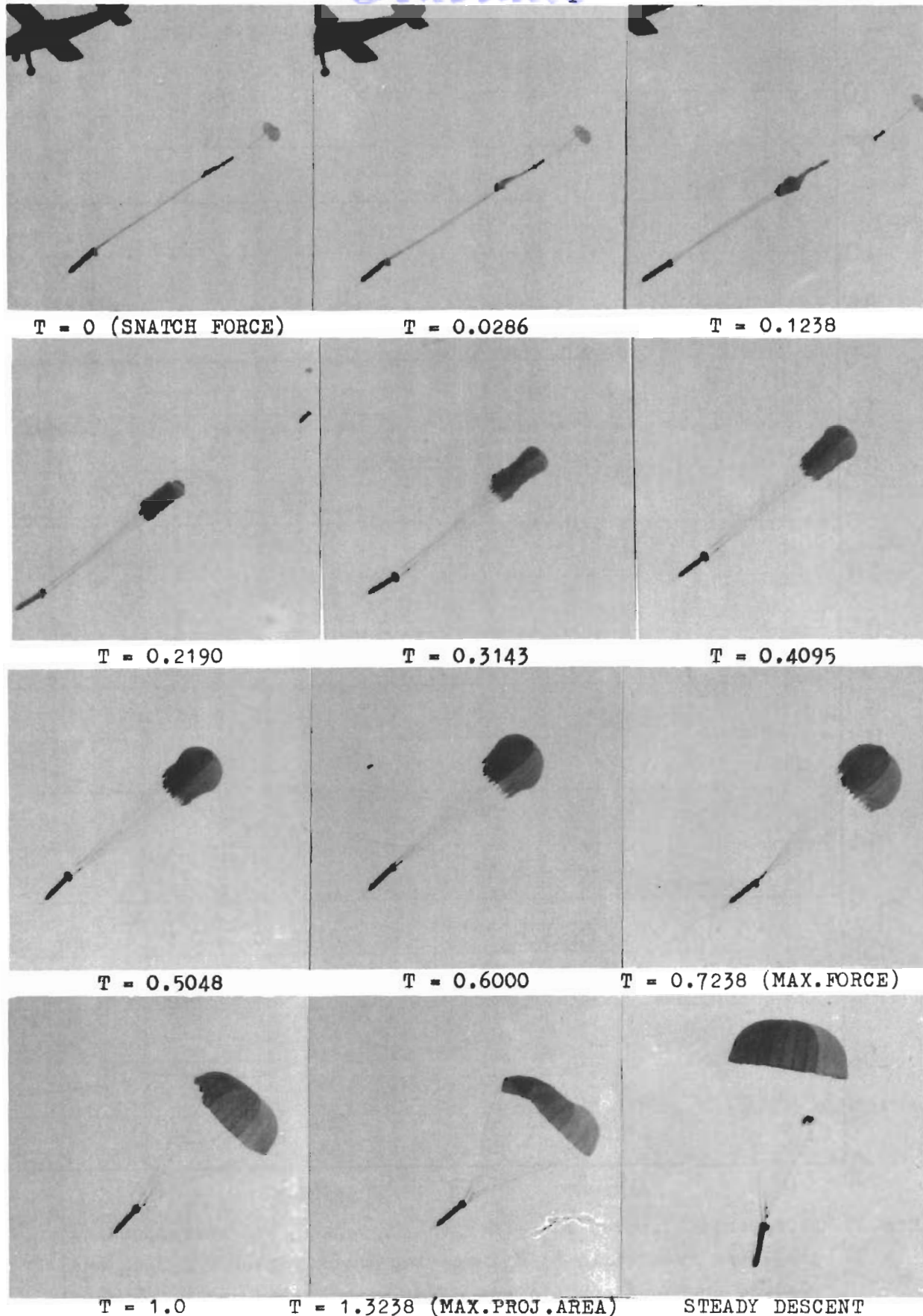


FIG.31 EVOLVEMENT OF THE CANOPY SHAPE-28 FT CIRCULAR FLAT PARACHUTE



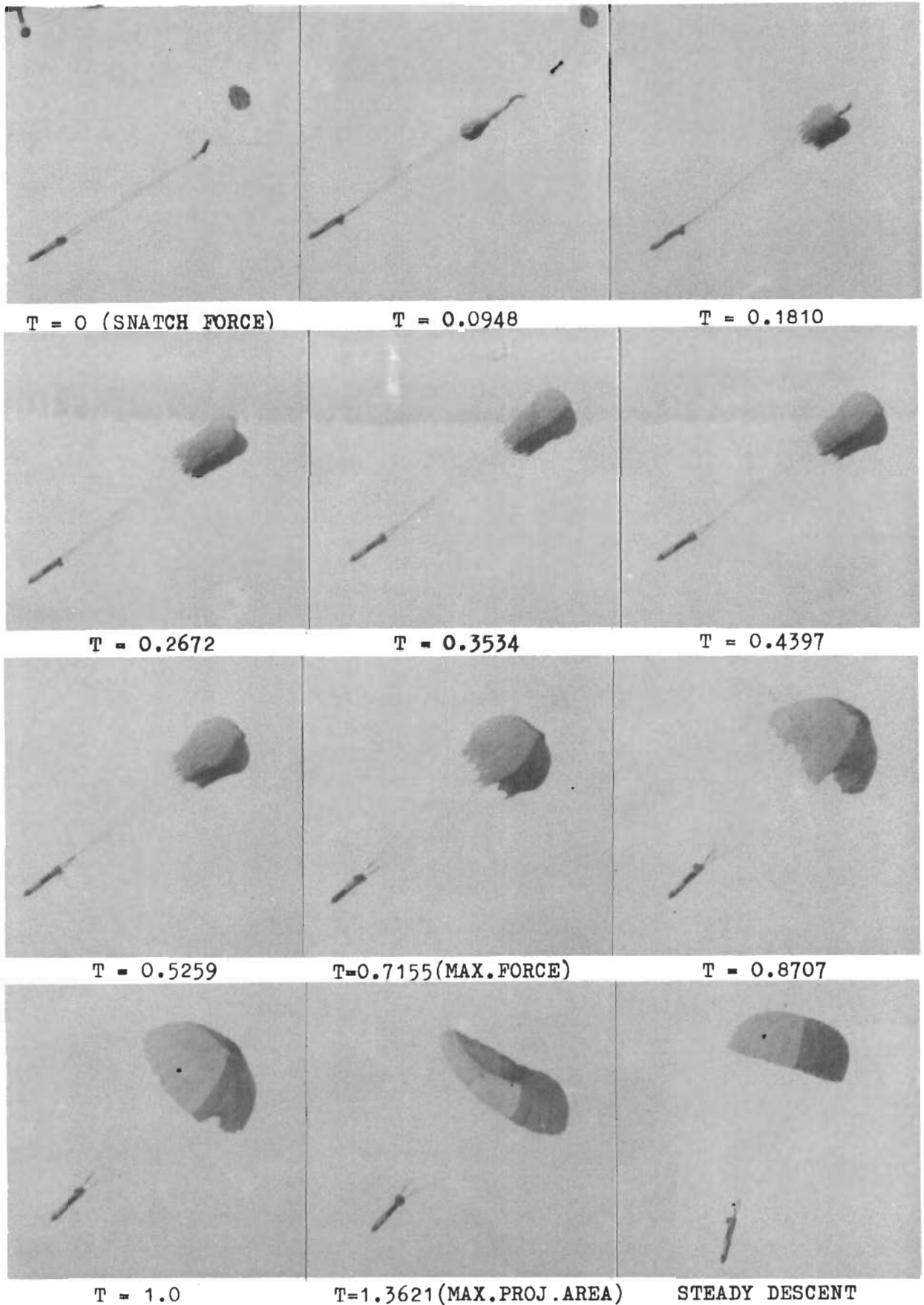


FIG. 32 EVOLVEMENT OF THE CANOPY SHAPE-28 FT CIRCULAR FLAT PARACHUTE

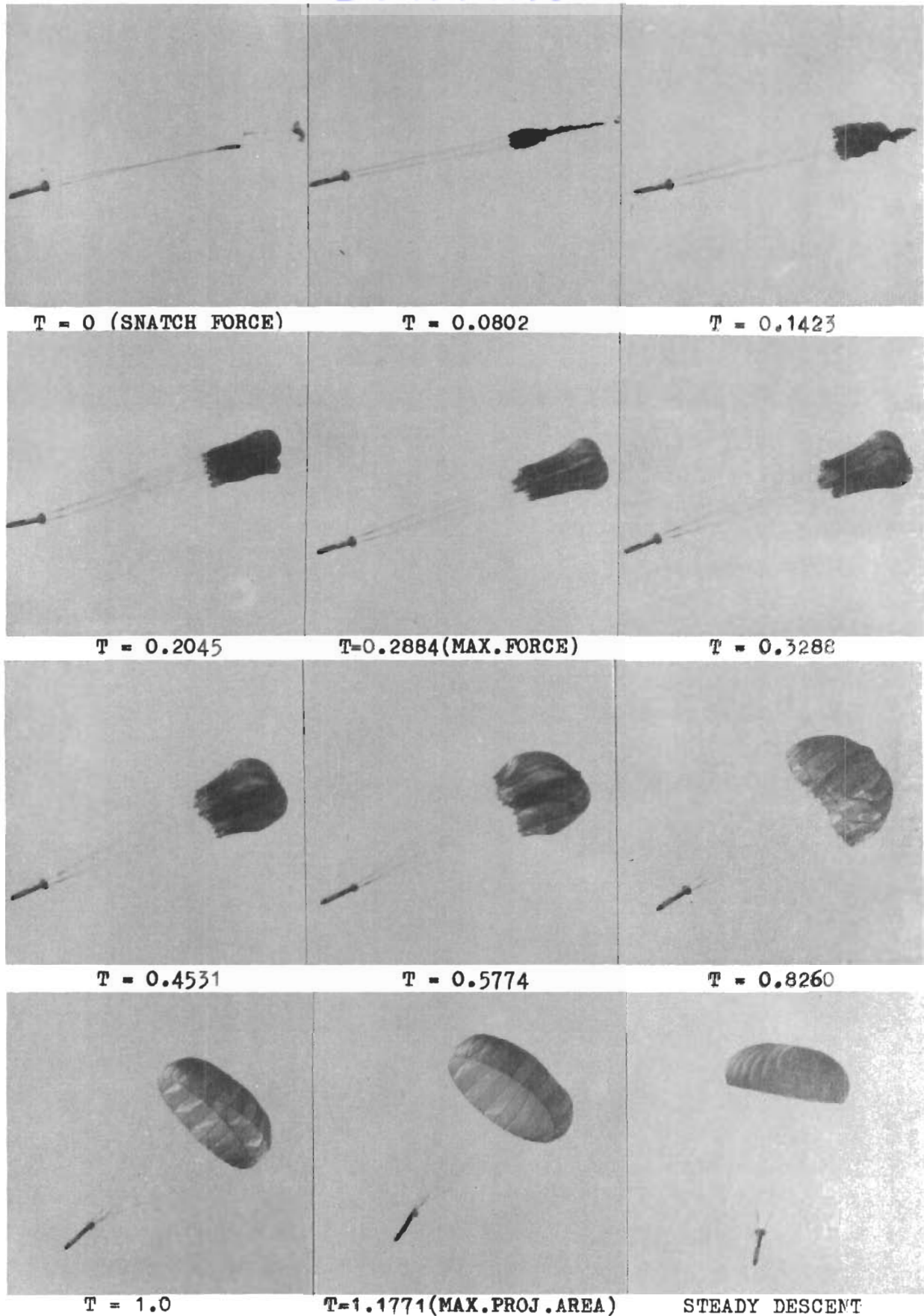


FIG. 33 EVOLVEMENT OF THE CANOPY SHAPE-35 FT EXTENDED SKIRT PARACHUTE

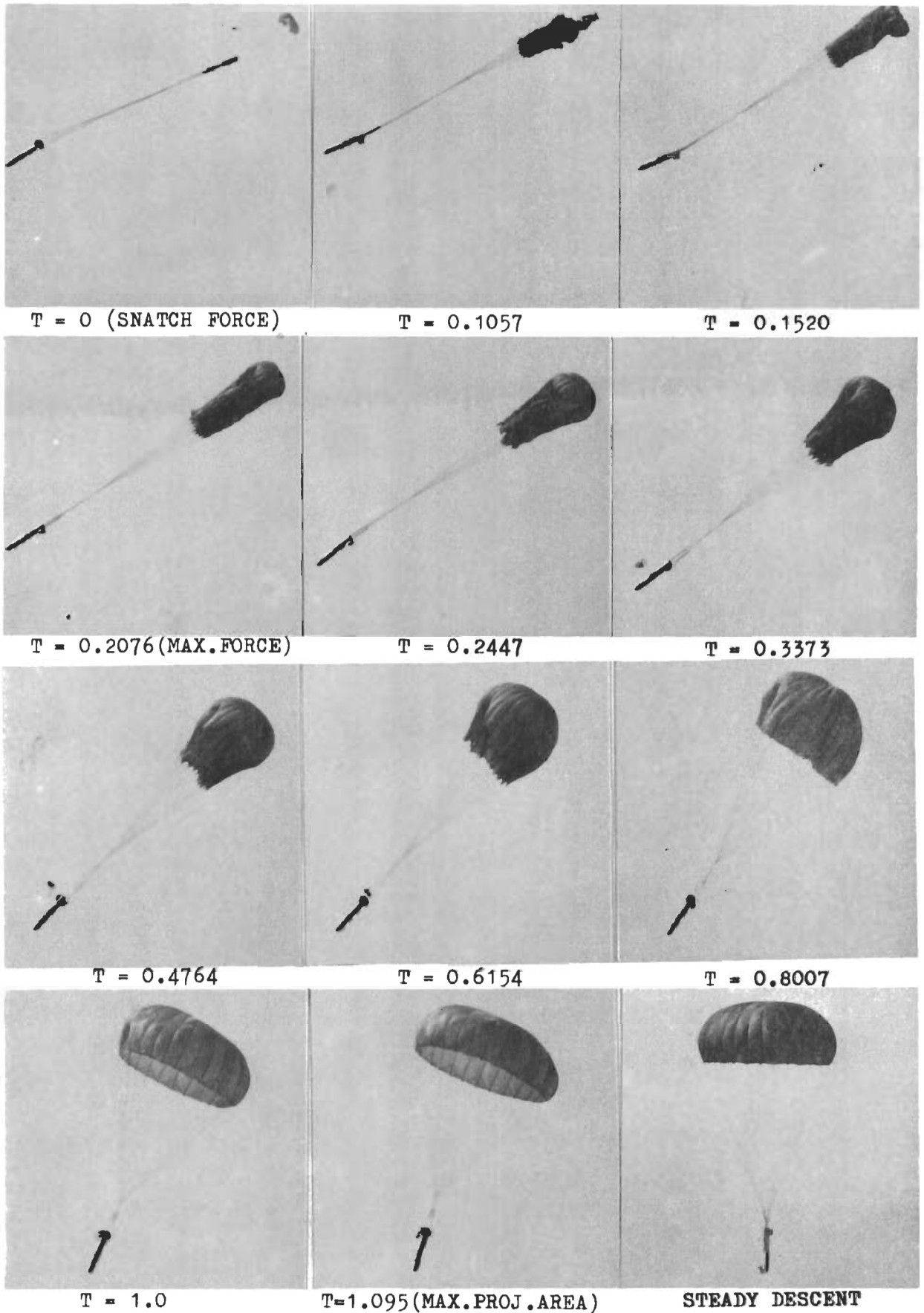


FIG. 34 EVOLVEMENT OF THE CANOPY SHAPE-35 FT EXTENDED SKIRT PARACHUTE

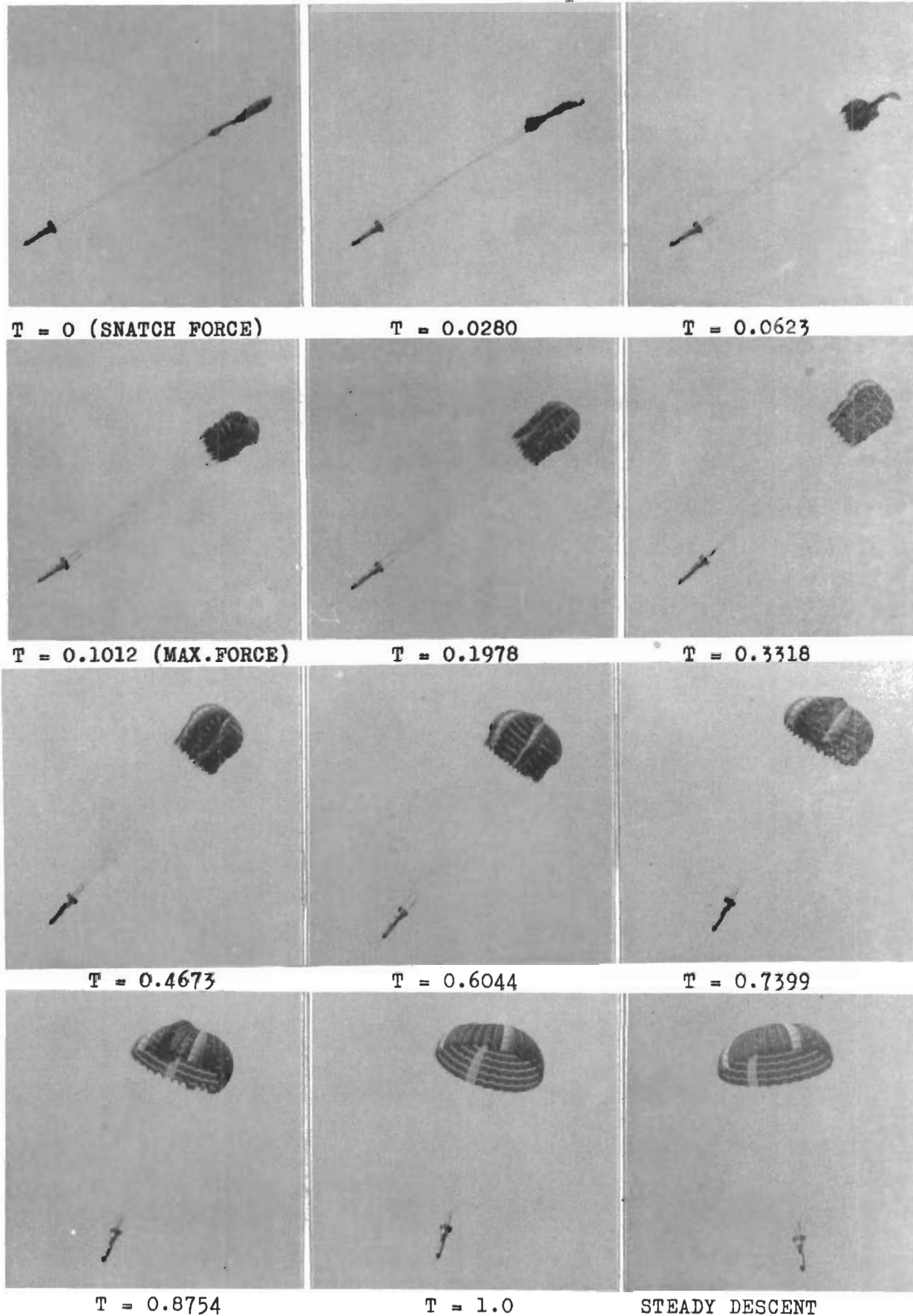


FIG.35 EVOLVEMENT OF THE CANOPY SHAPE-32 FT RINGSLOT PARACHUTE (G)

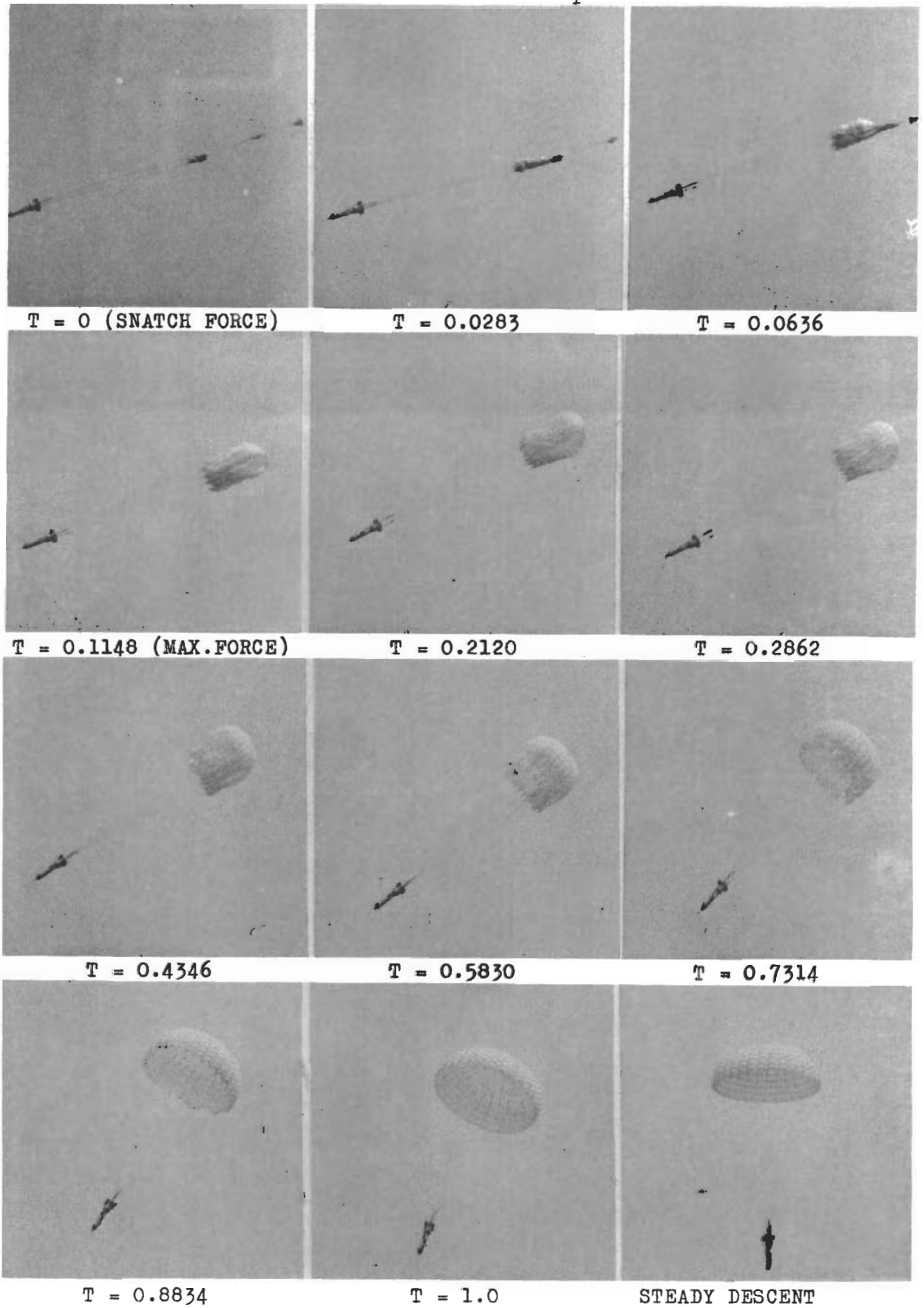


FIG. 36 EVOLVEMENT OF THE CANOPY SHAPE-32 FT RINGSLLOT PARACHUTE (US)

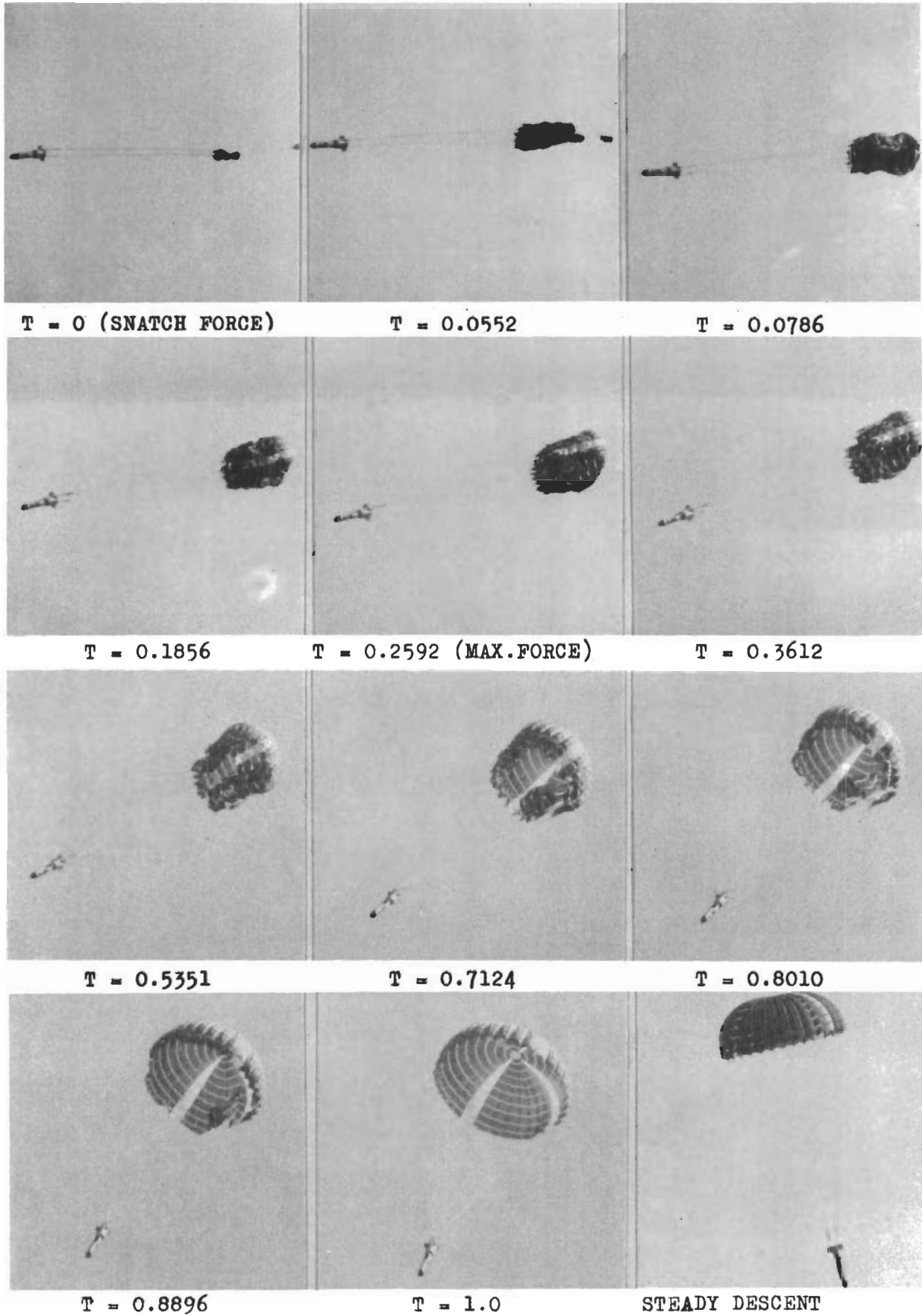


FIG. 37 EVOLVEMENT OF THE CANOPY SHAPE-32 FT RINGSLLOT PARACHUTE (G)

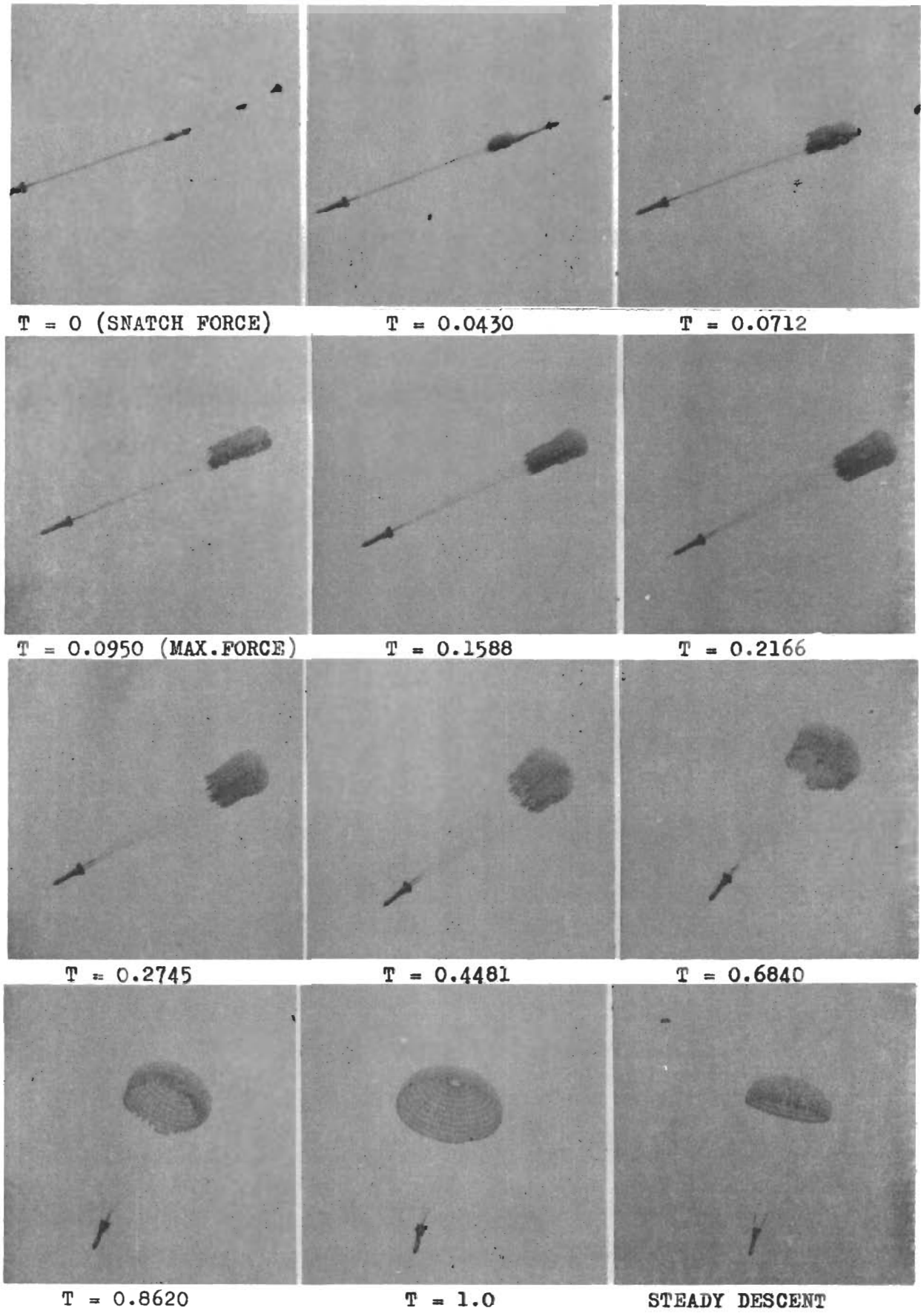


FIG.38 EVOLVEMENT OF THE CANOPY SHAPE-32 FT RINGSLLOT PARACHUTE (US)

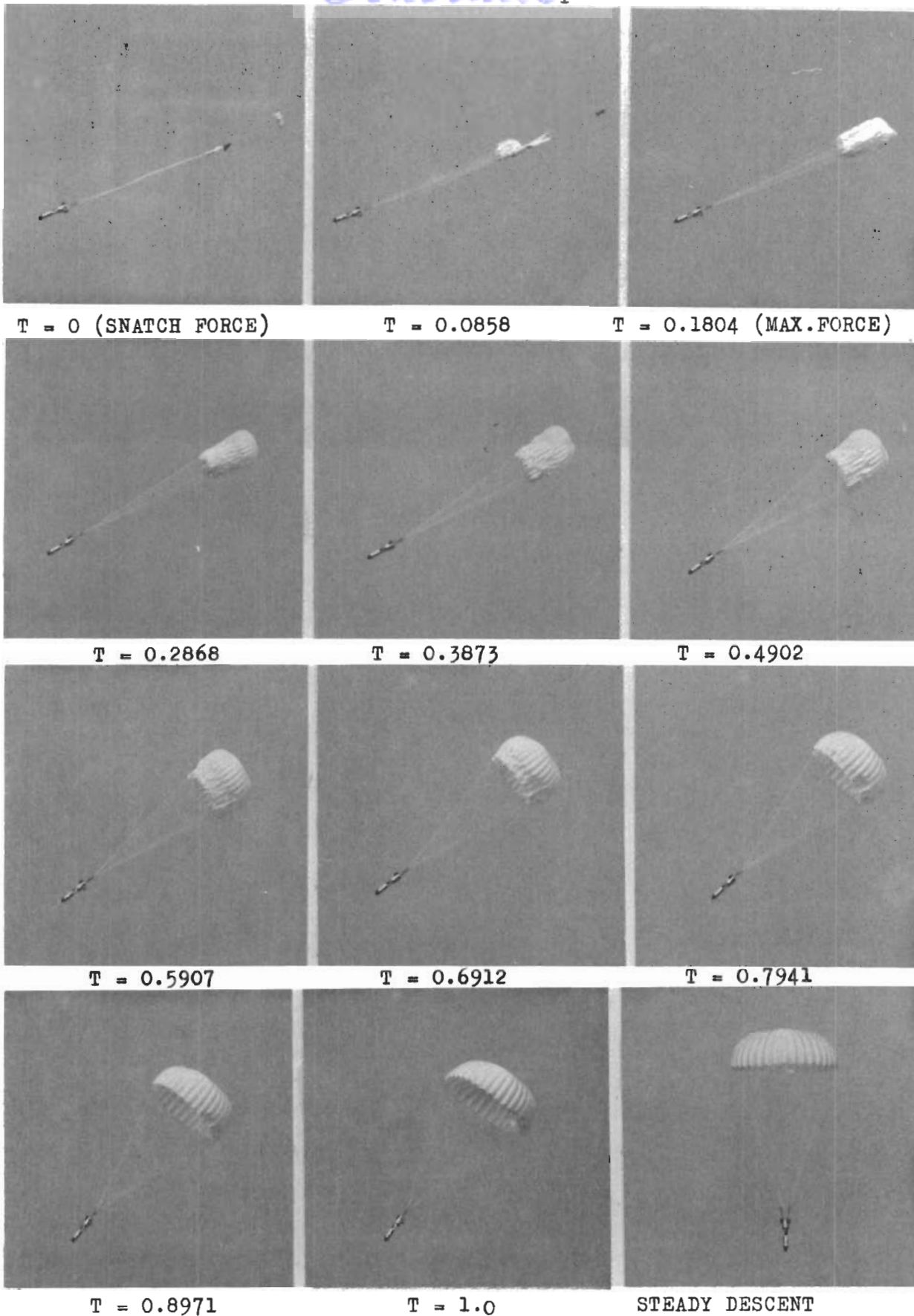


FIG.39 EVOLVEMENT OF THE CANOPY SHAPE-34 FT CIRCULAR FLAT RIBBON PARACHUTE (G)



*Controls*

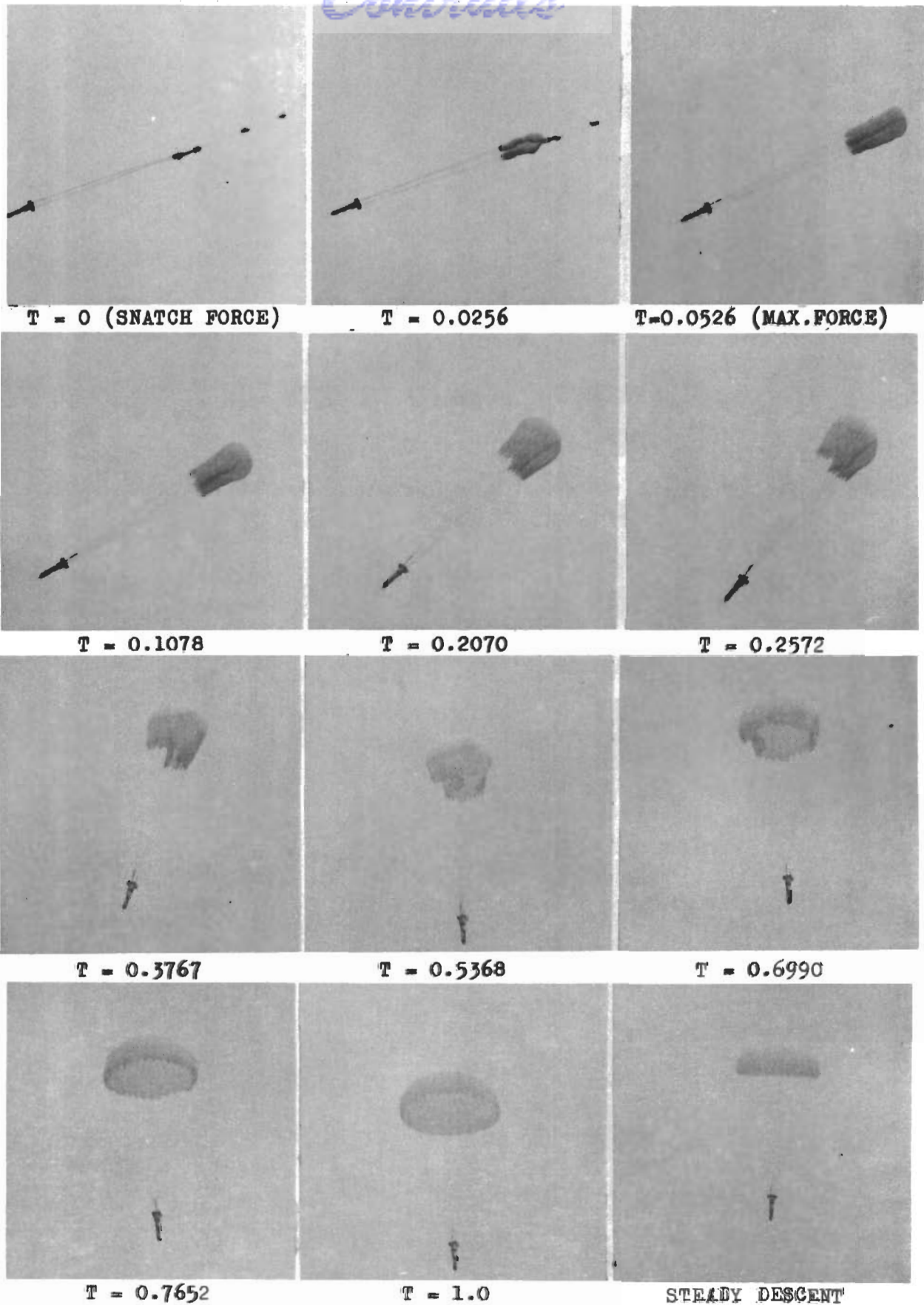


FIG.40 EVOLVEMENT OF THE CANOPY SHAPE-34 FT CIRCULAR FLAT RIBBON PARACHUTE(US)

*Controls*

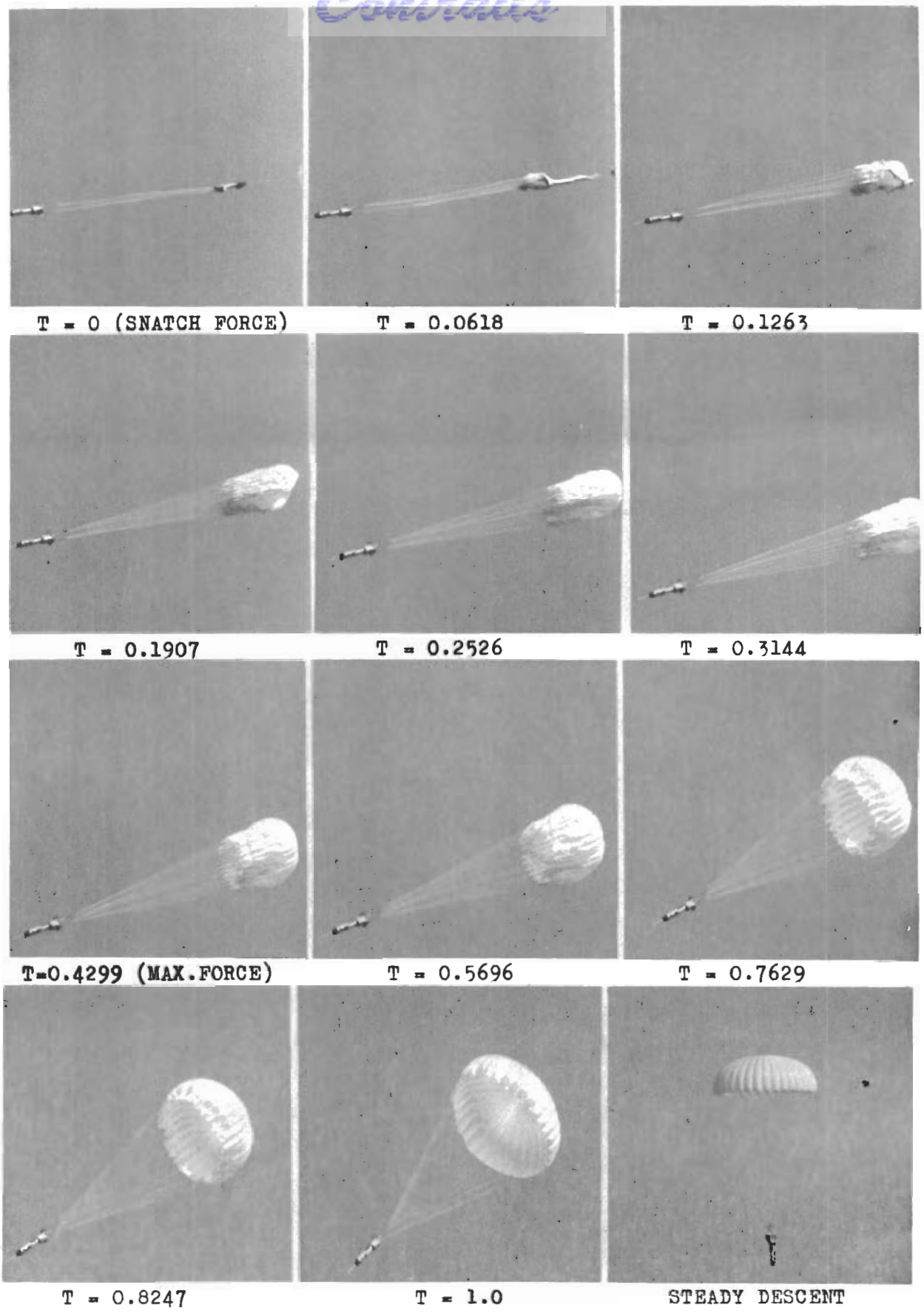


FIG.41 EVOLVEMENT OF THE CANOPY SHAPE-34 FT CIRCULAR FLAT RIBBON PARACHUTE (G)

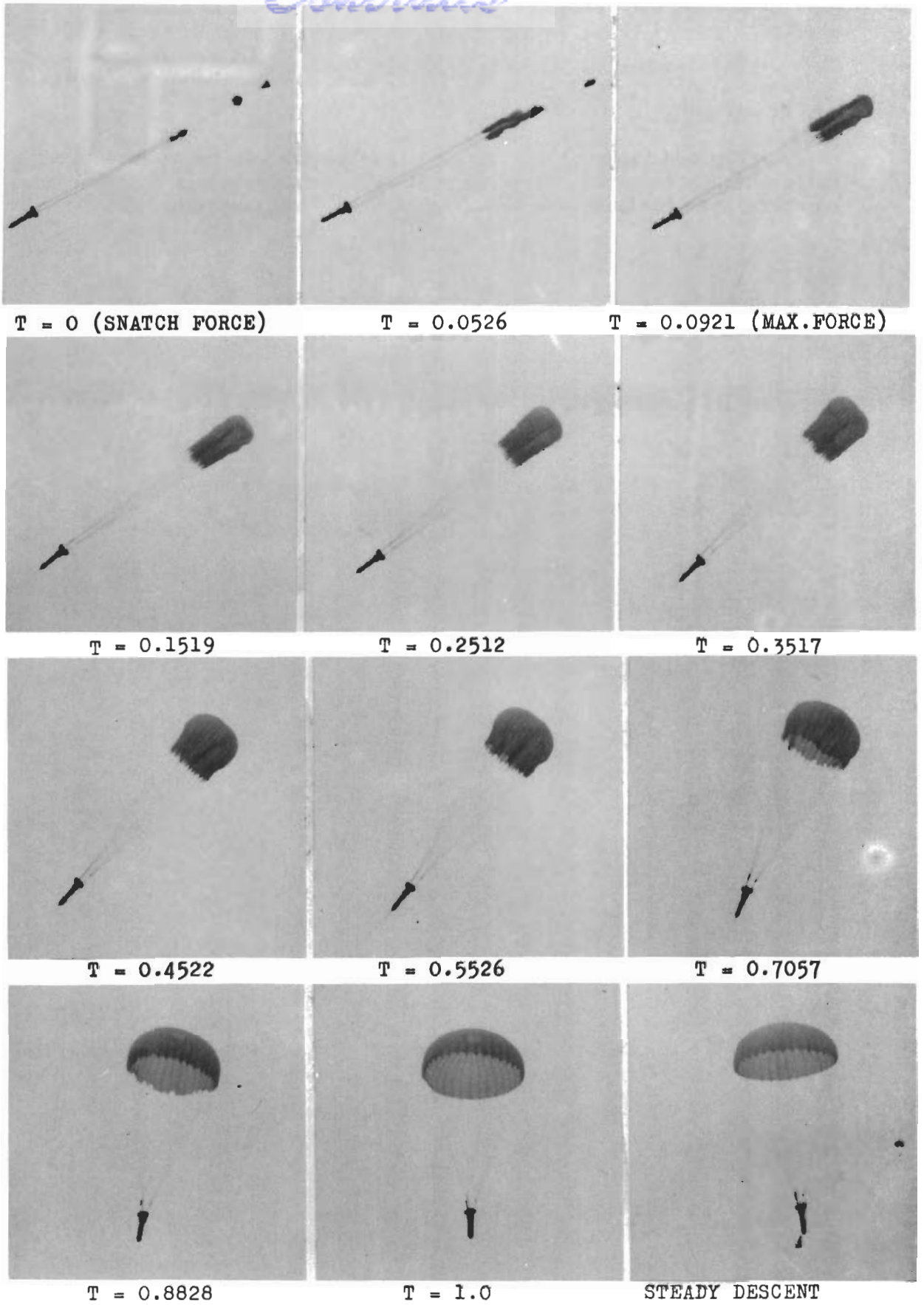


FIG.42 EVOLVEMENT OF THE CANOPY SHAPE-34 FT CIRCULAR FLAT RIBBON PARACHUTE (US)

# Contrails

## 6. APPENDIX

Reproductions of the original oscillographic recordings with differential pressures, force, dynamic pressure, openings of the camera shutters and time base are shown in Figures 43 through 66.

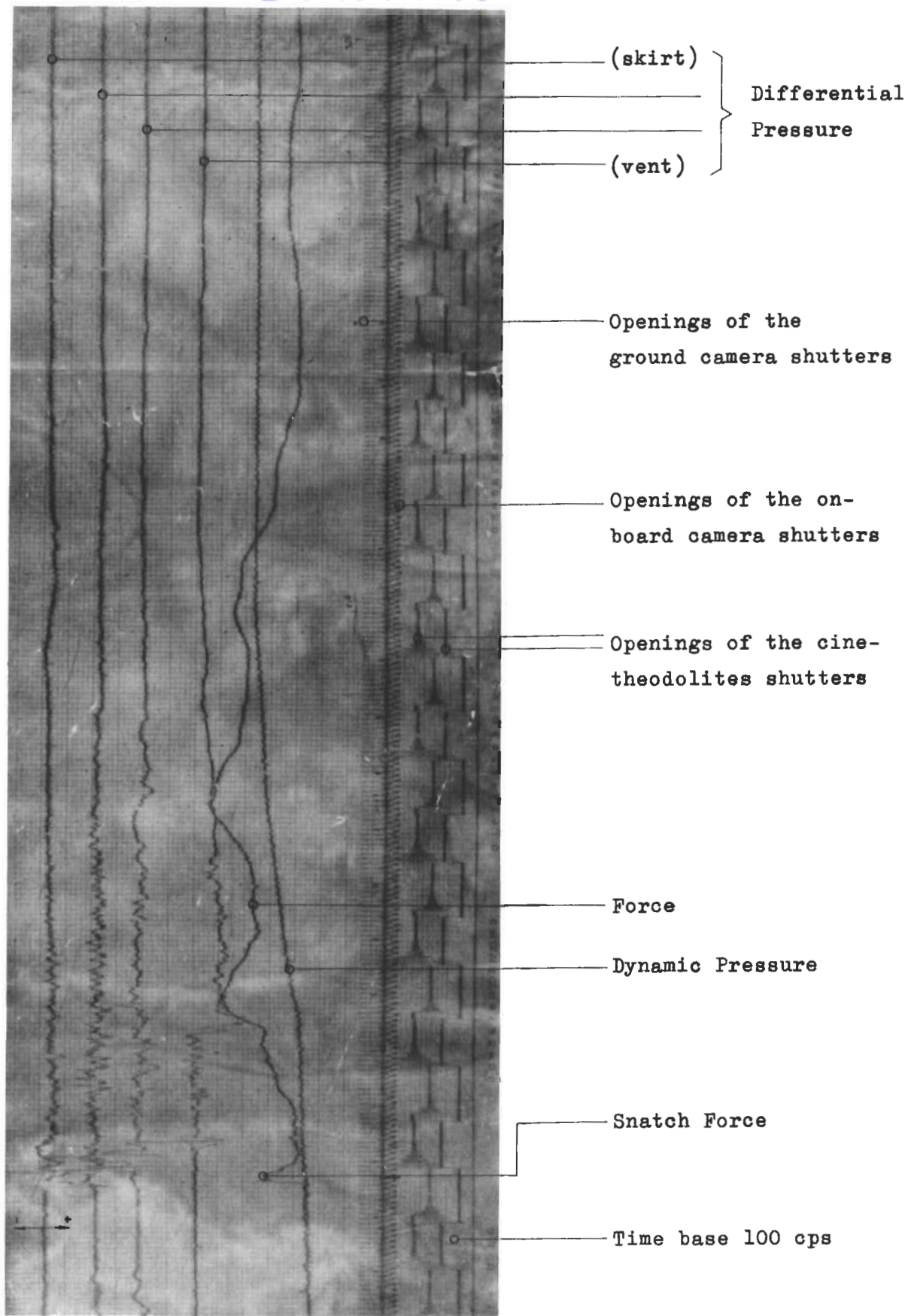


Fig. 43 Original registration. Pressure transducers on the cord center line

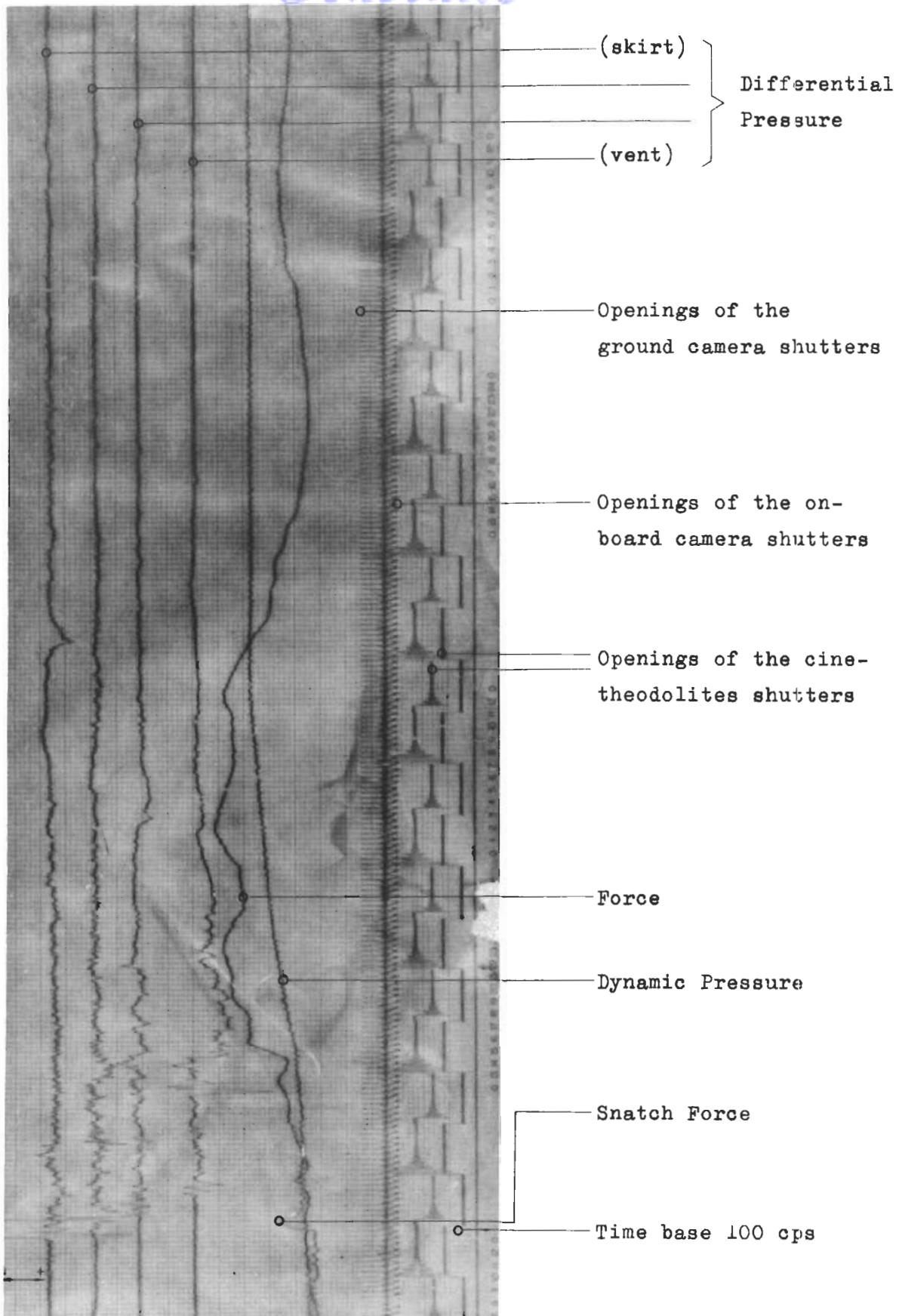


Fig. 44 Original registration. Pressure transducers on the cord center line

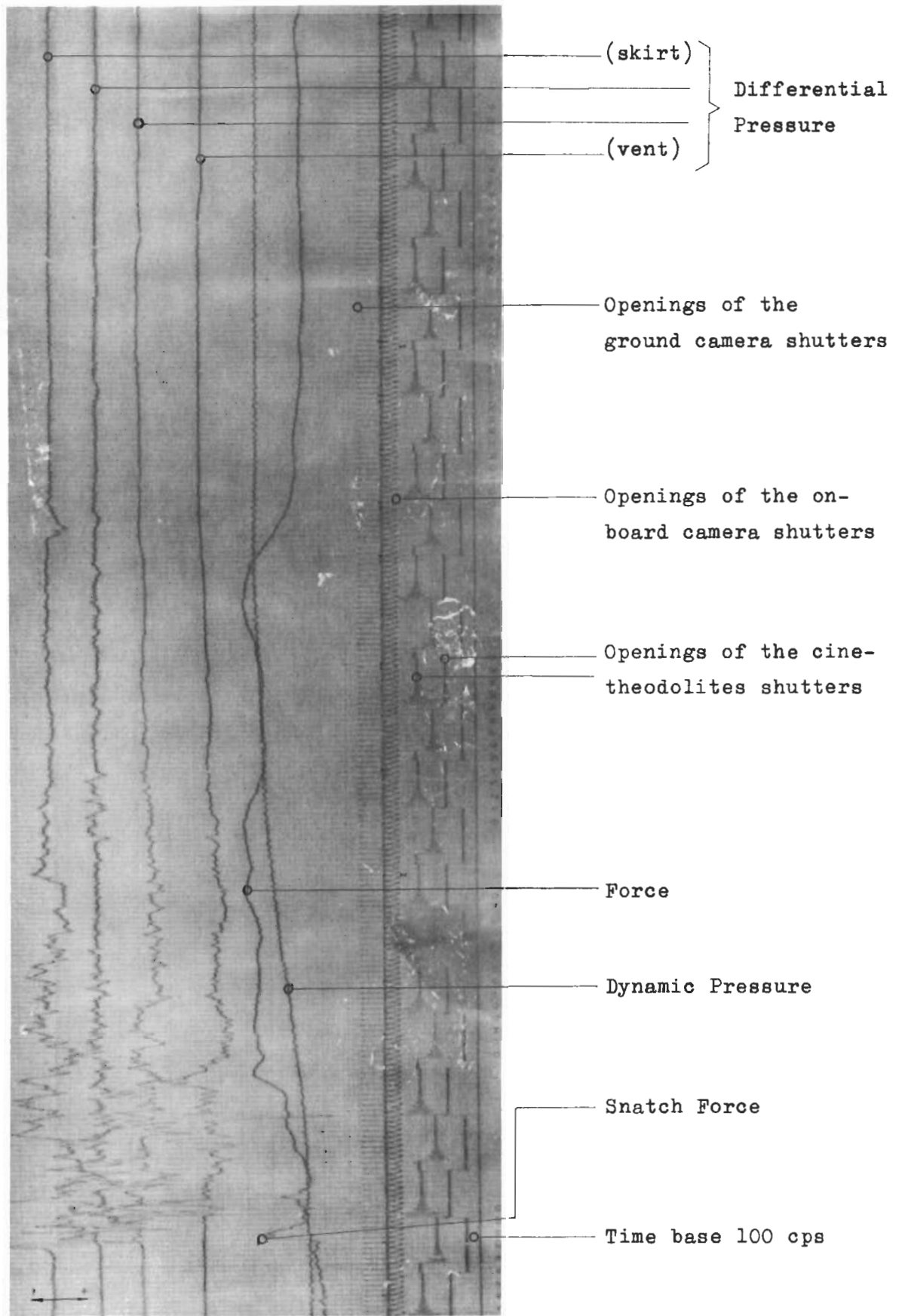


Fig. 45 Original registration. Pressure transducers on the gore center line

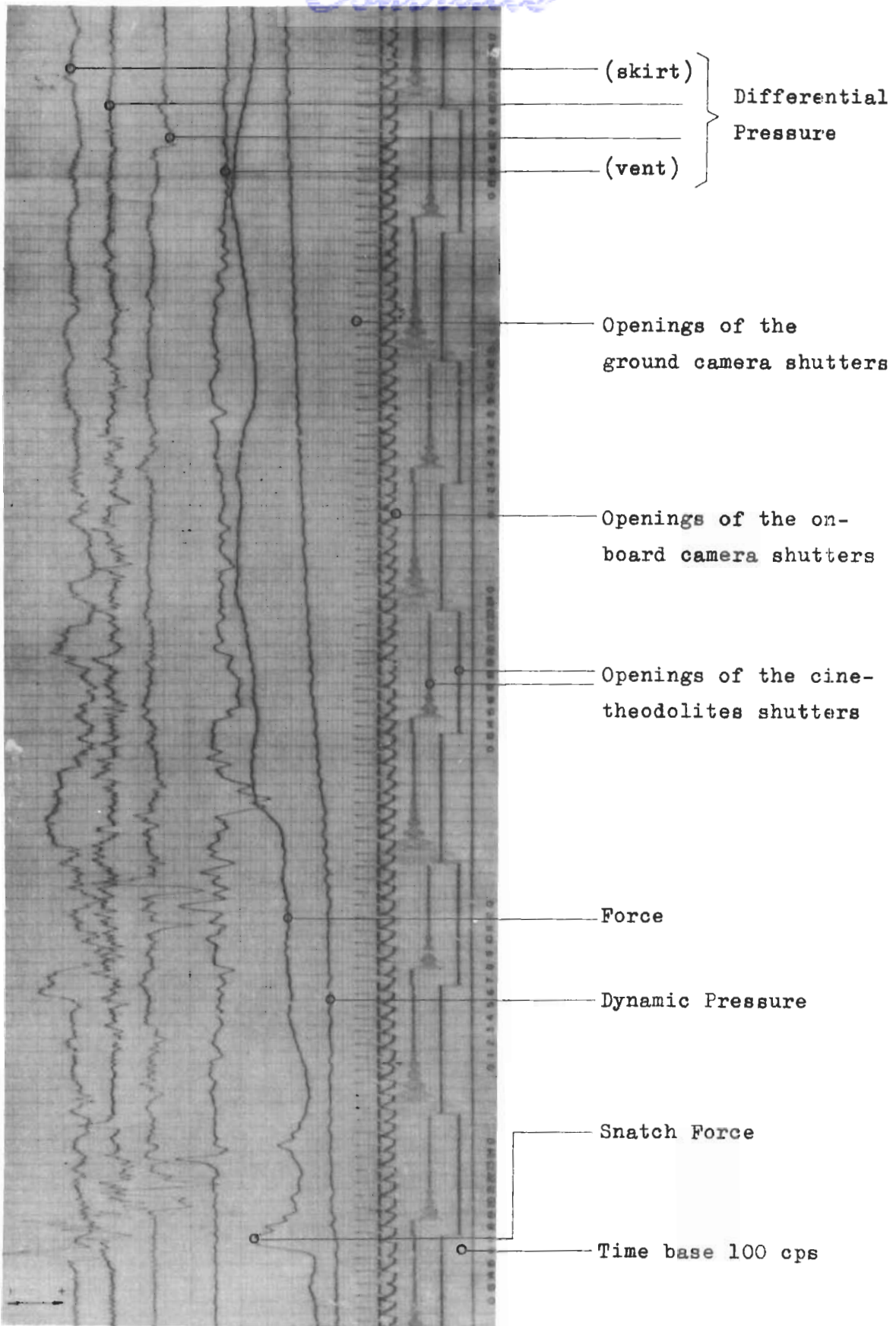


Fig. 46 Original registration. Pressure transducers on the gore center line



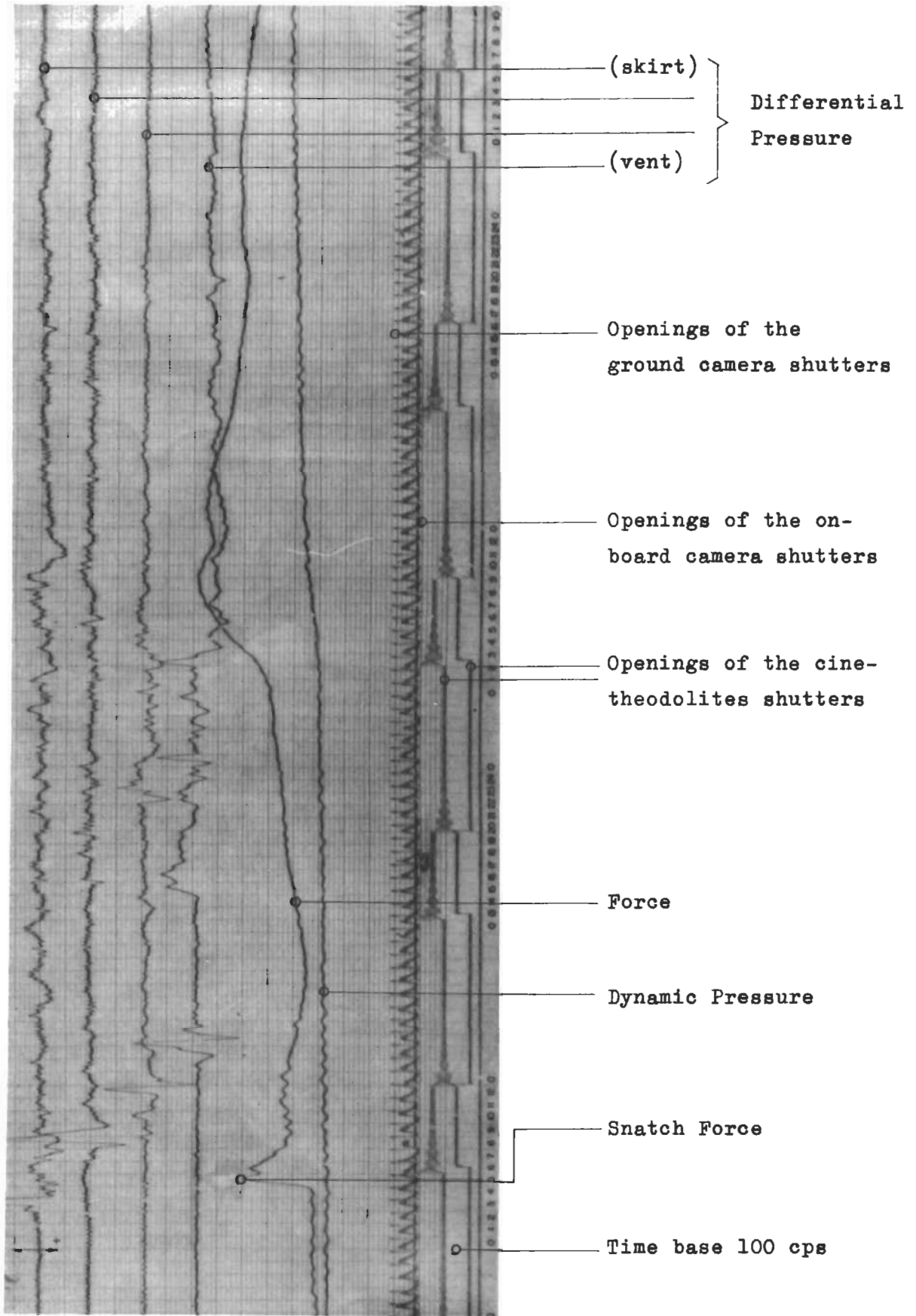


Fig. 47 Original registration. Pressure transducers on the cord center line

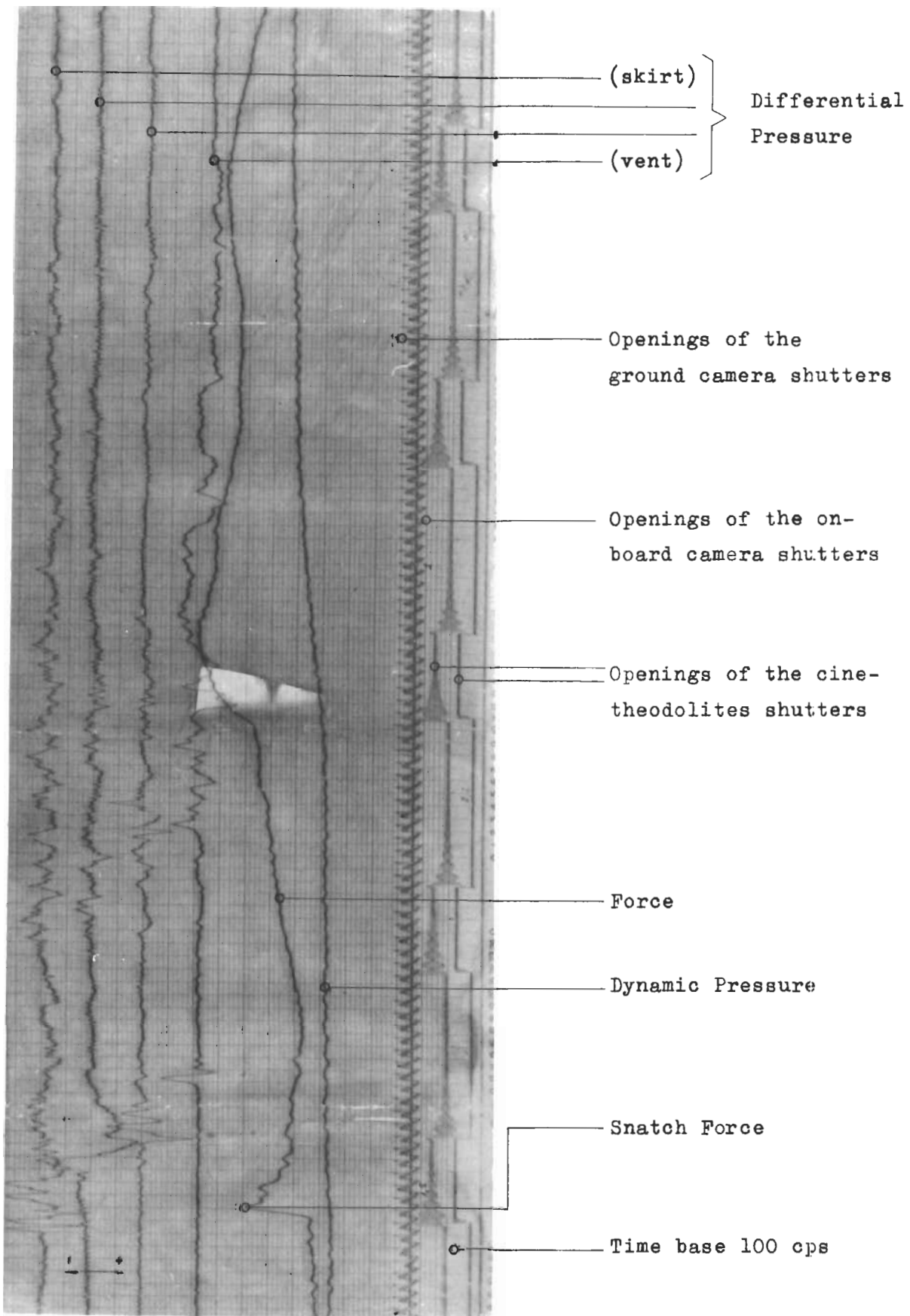


Fig. 48 Original registration. Pressure transducers on the cord center line

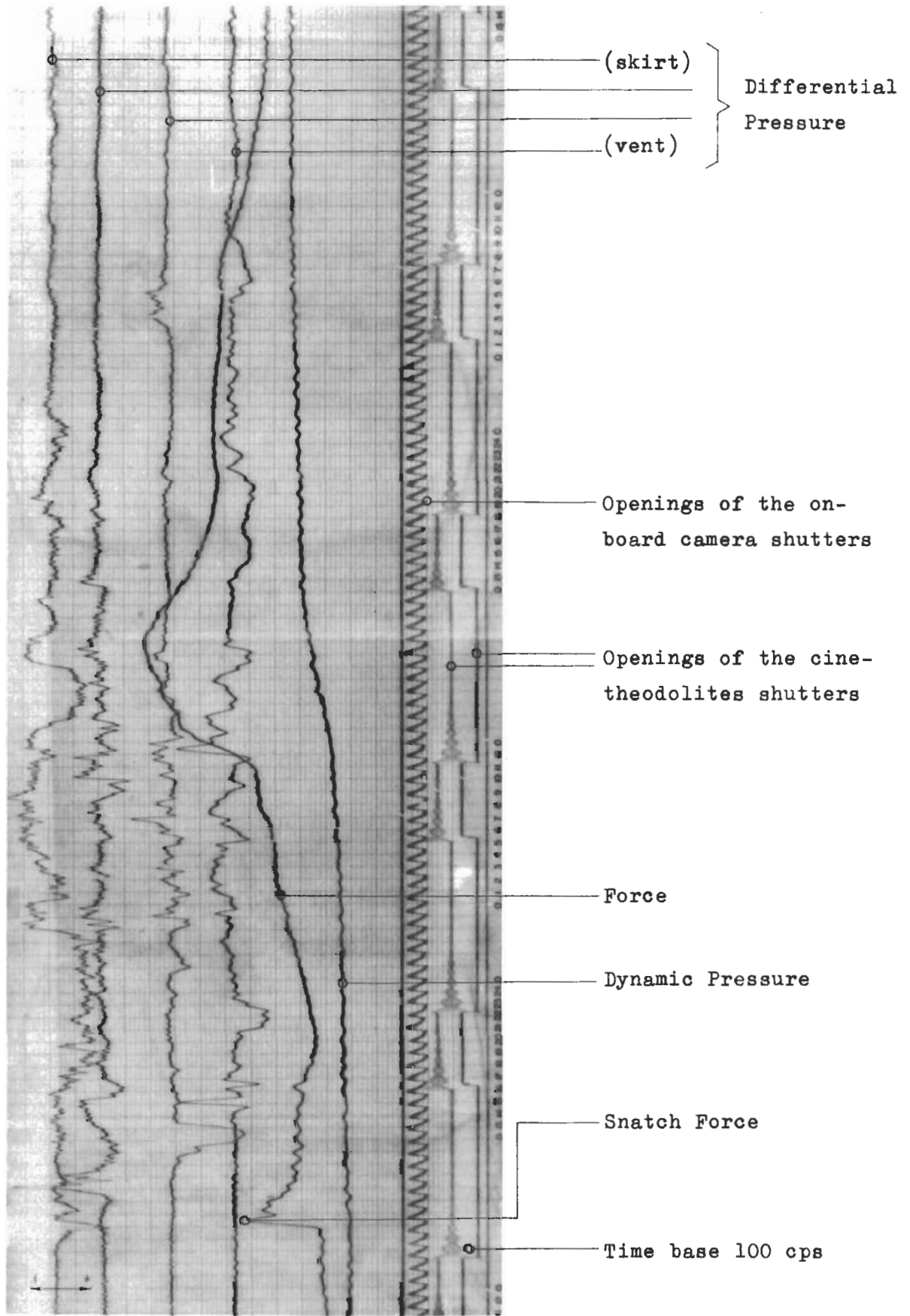


Fig. 49 Original registration. Pressure transducers on the gore center line

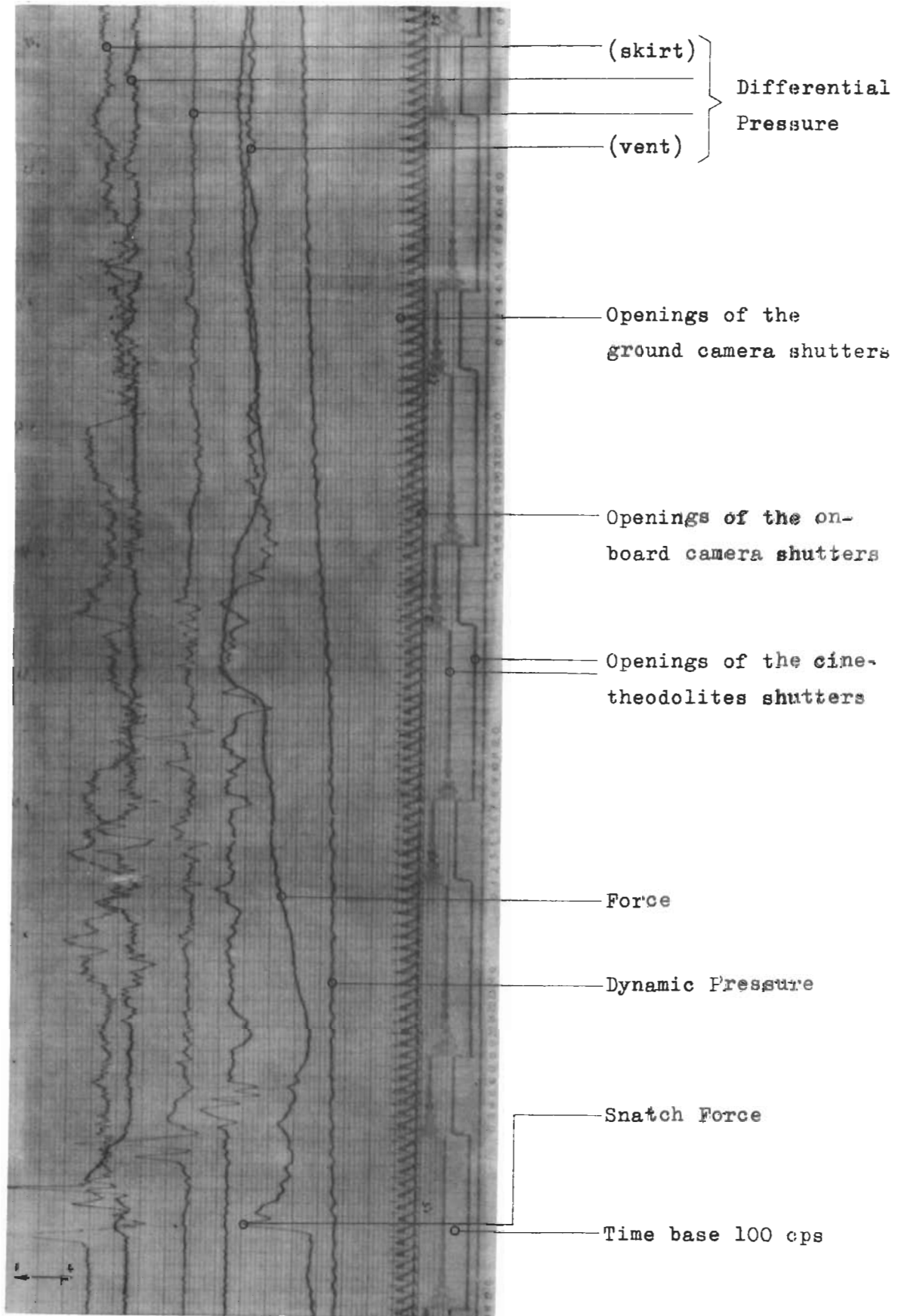


Fig. 50 Original registration. Pressure transducers on the gore center line

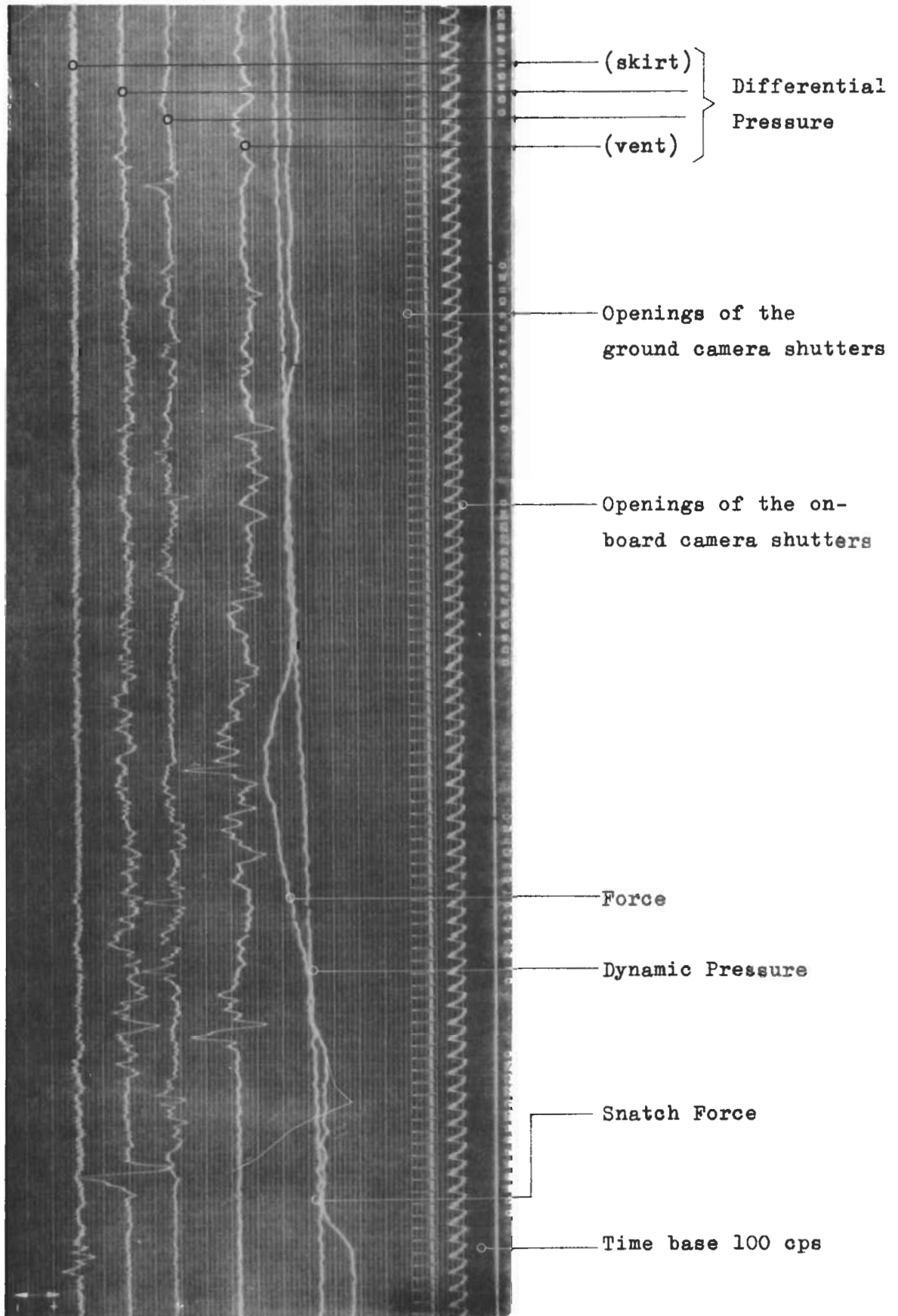


Fig. 51 Original registration. Pressure transducers on the cord center line

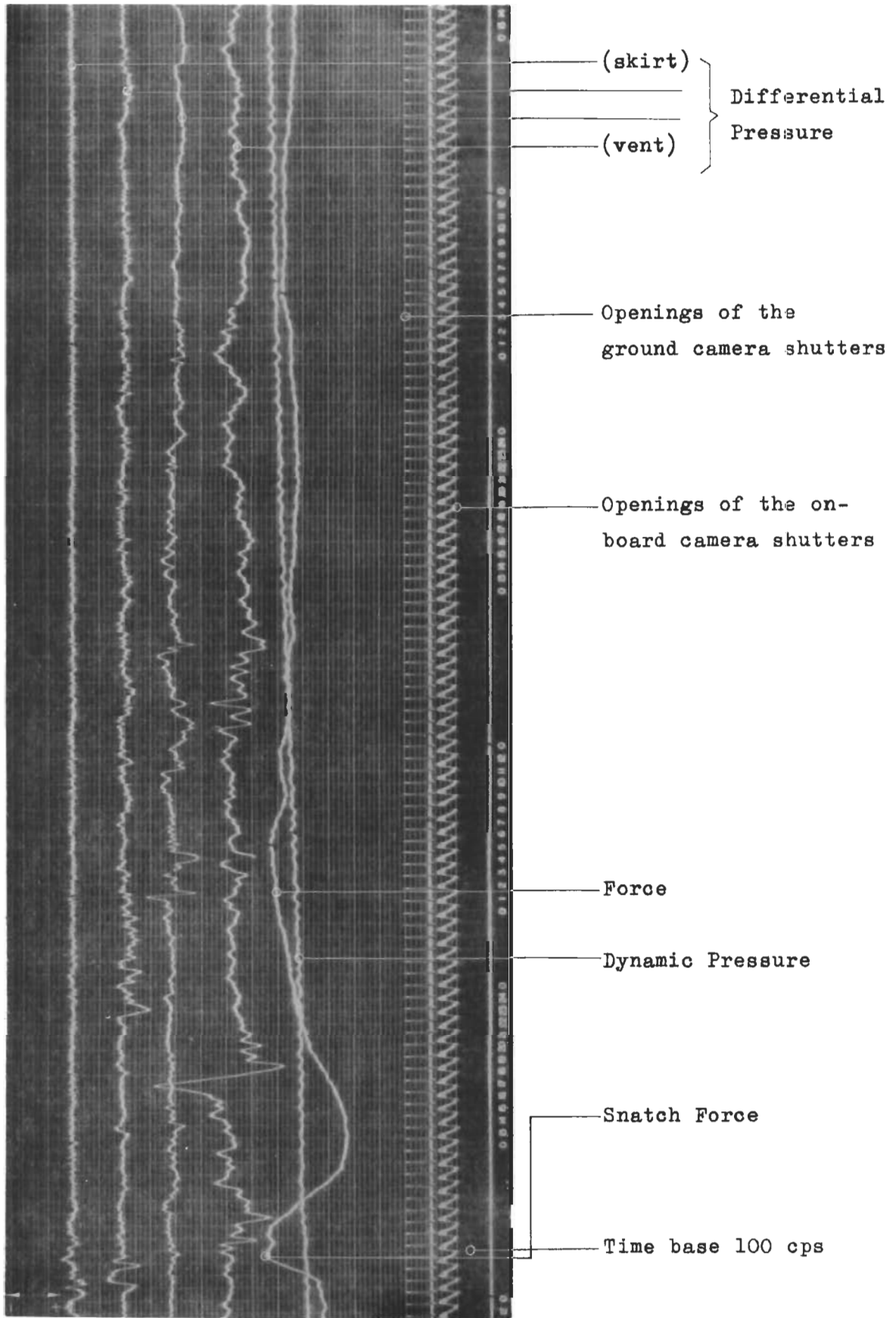


Fig. 52 Original registration. Pressure transducers on the cord center line

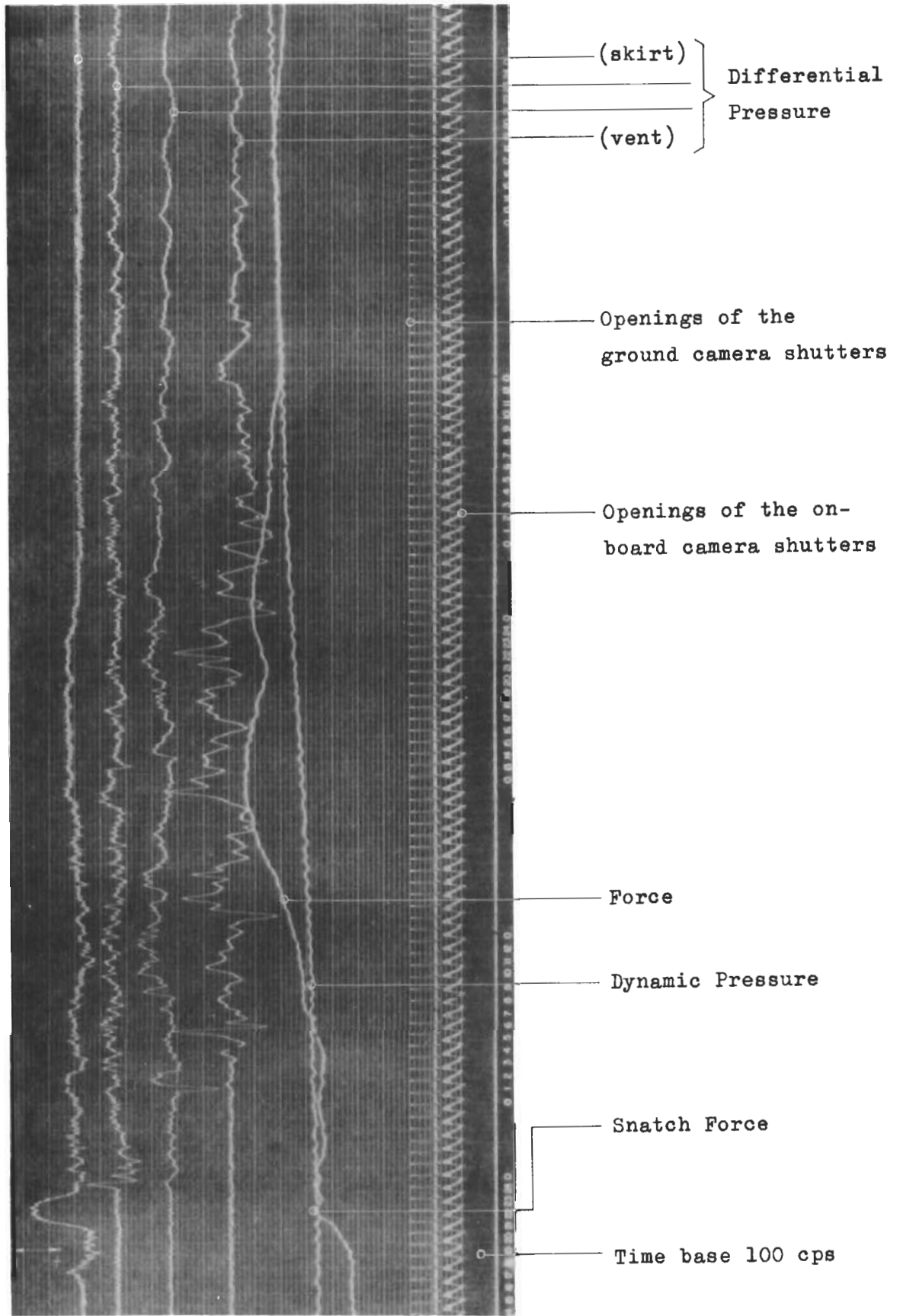


Fig. 53 Original registration. Pressure transducers on the cord center line

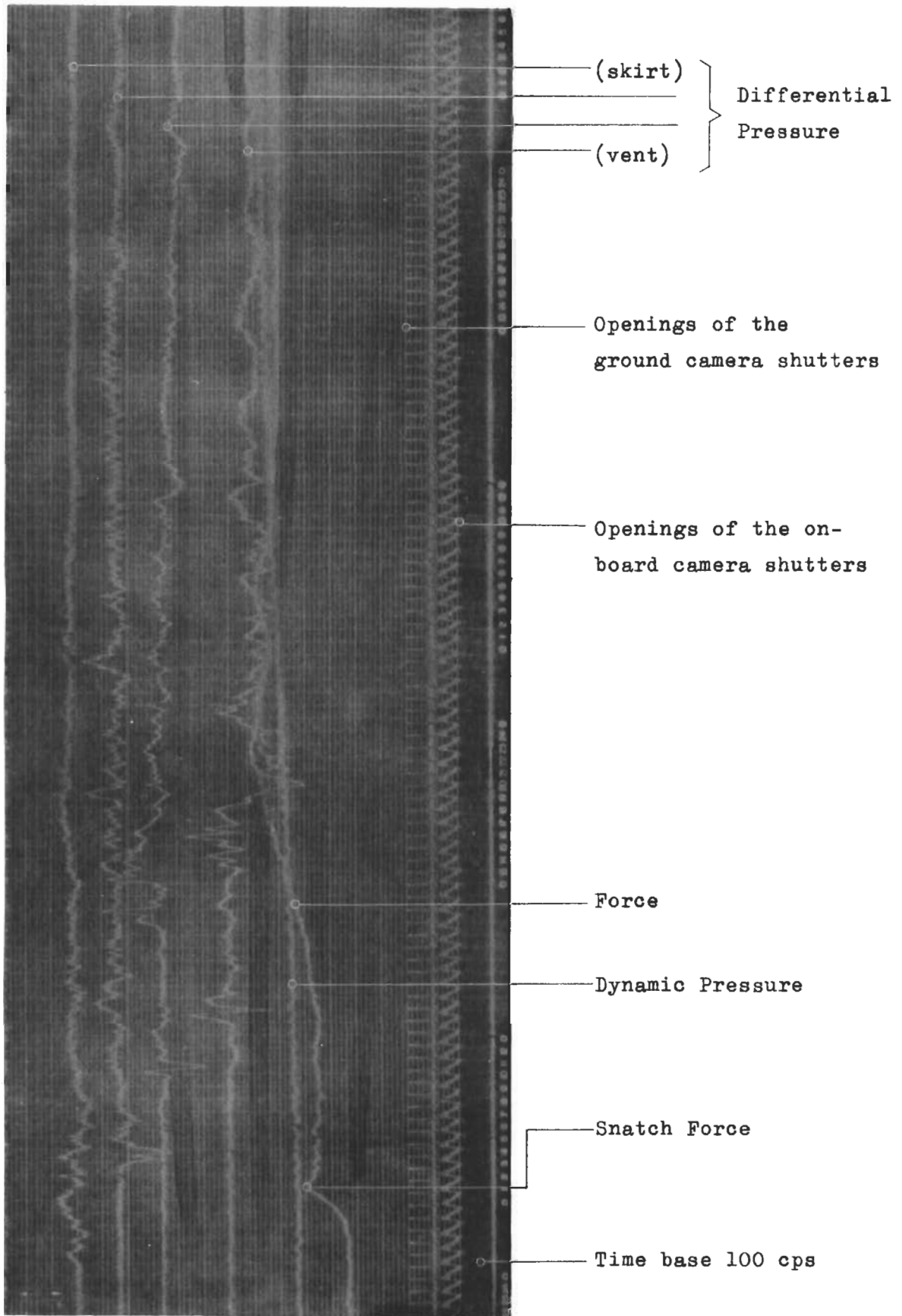


Fig. 54 Original registration. Pressure transducers on the cord center line



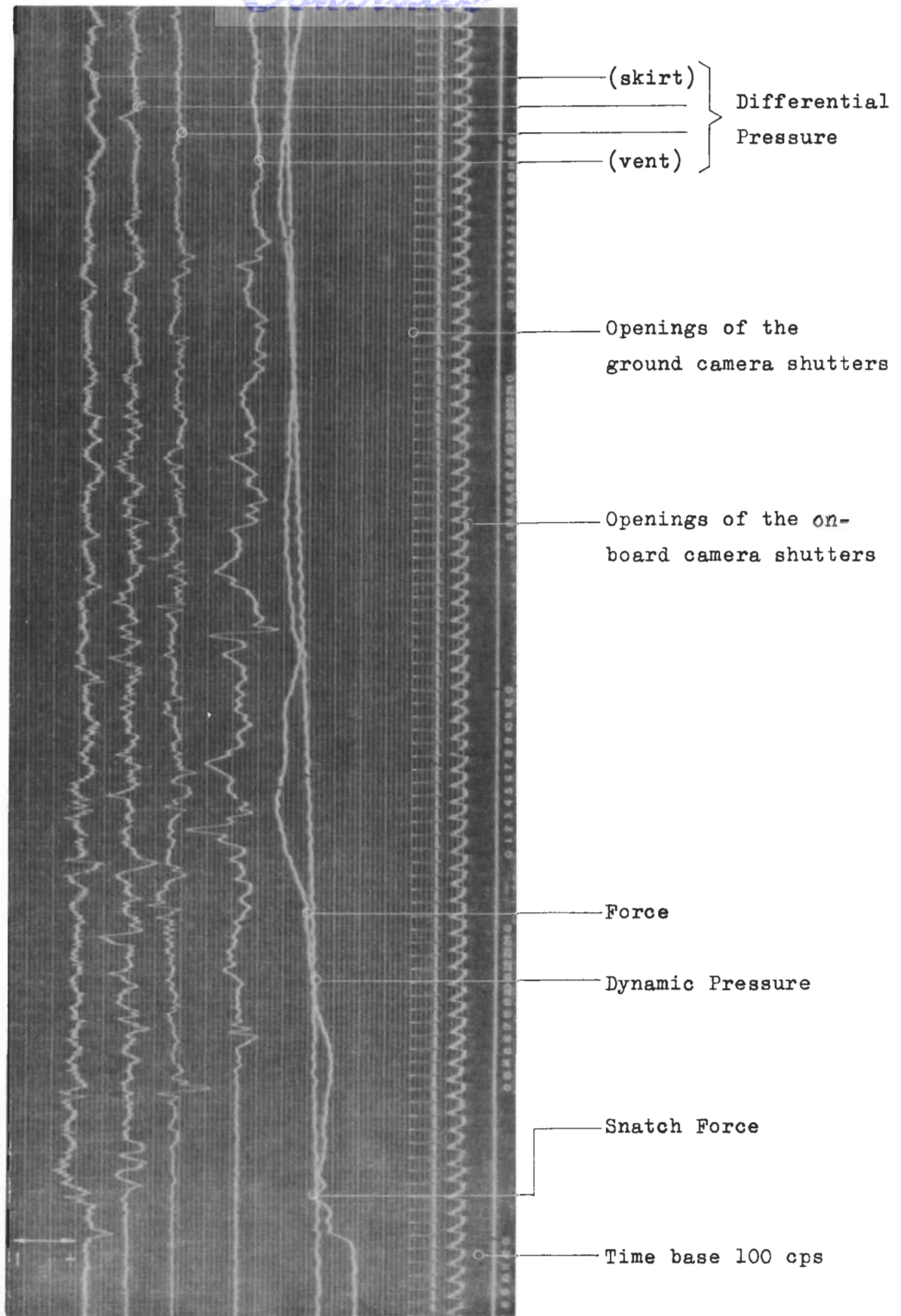


Fig. 55 Original registration. Pressure transducers on the gore center line

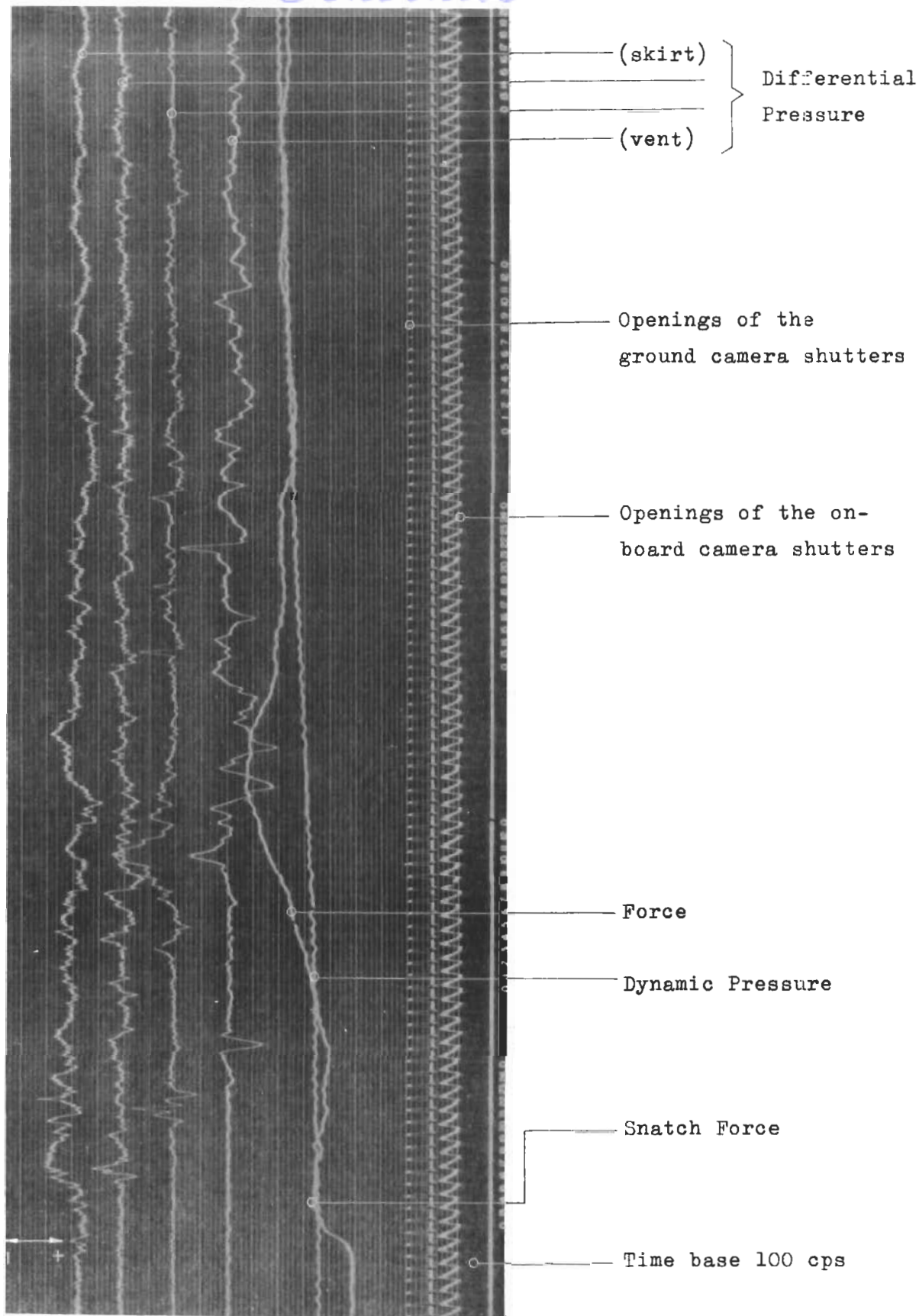


Fig. 56 Original registration. Pressure transducers on the gore center line

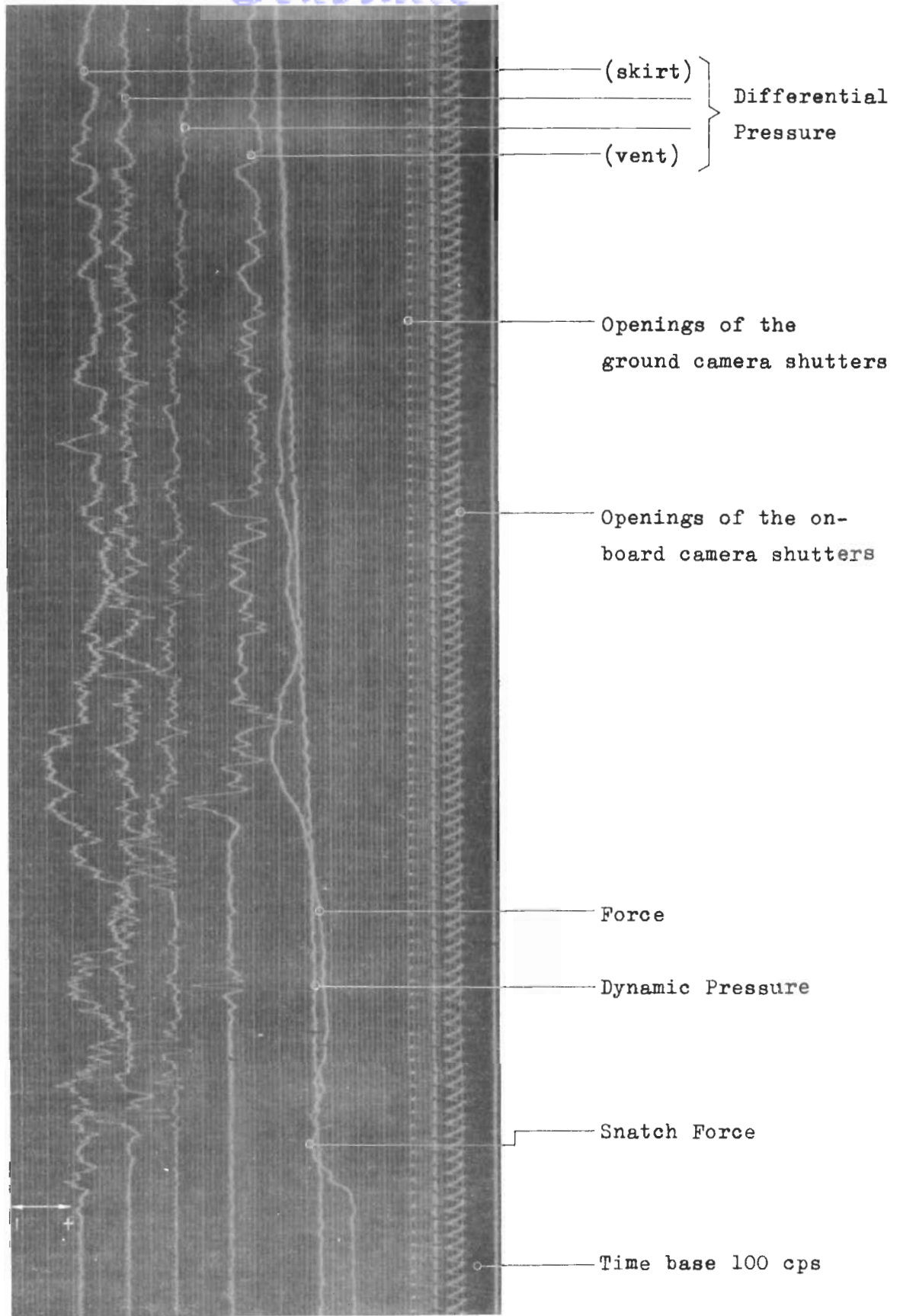


Fig. 57 Original registration. Pressure transducers on the gore center line

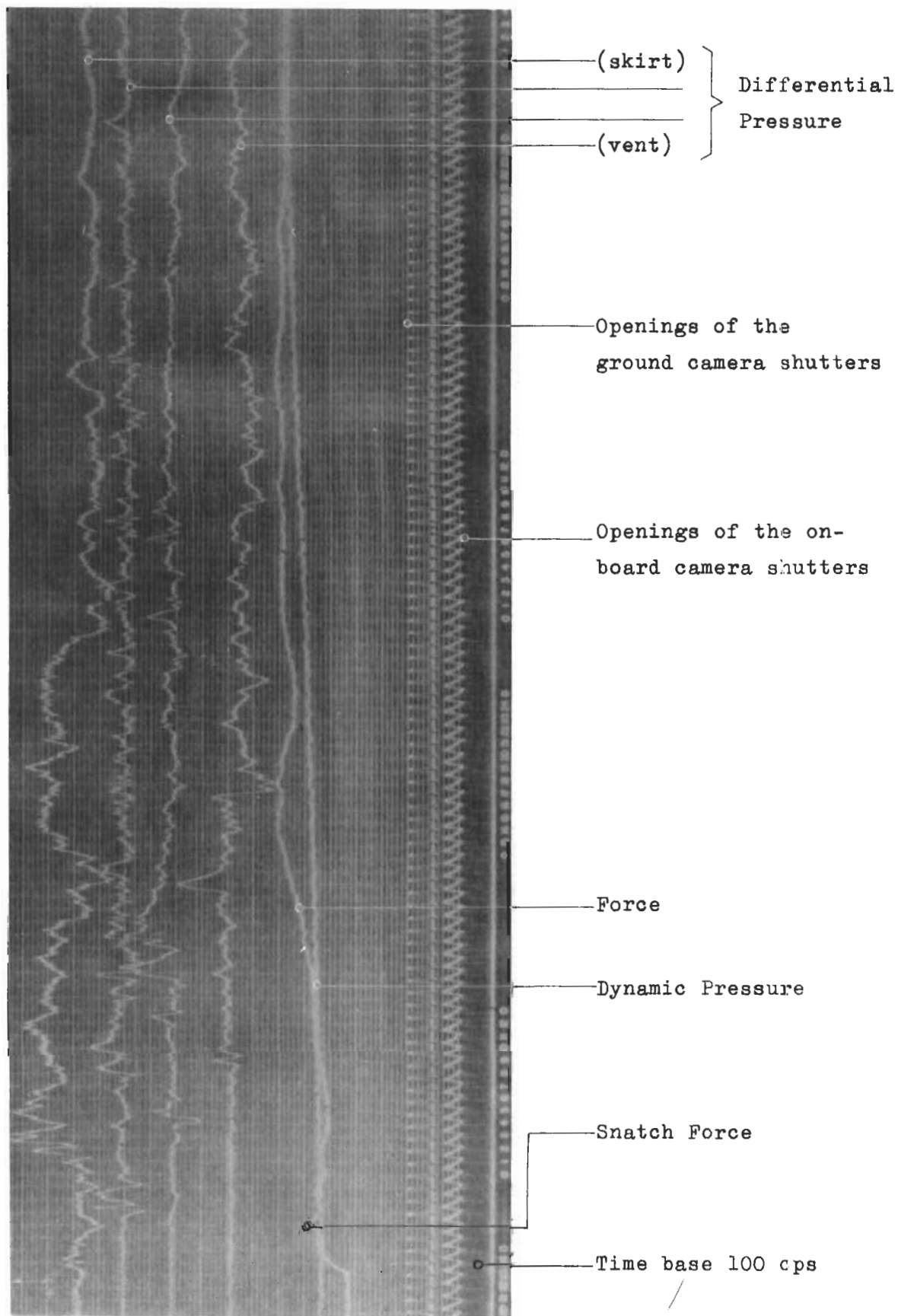


Fig. 58 Original registration. Pressure transducers on the gore center line

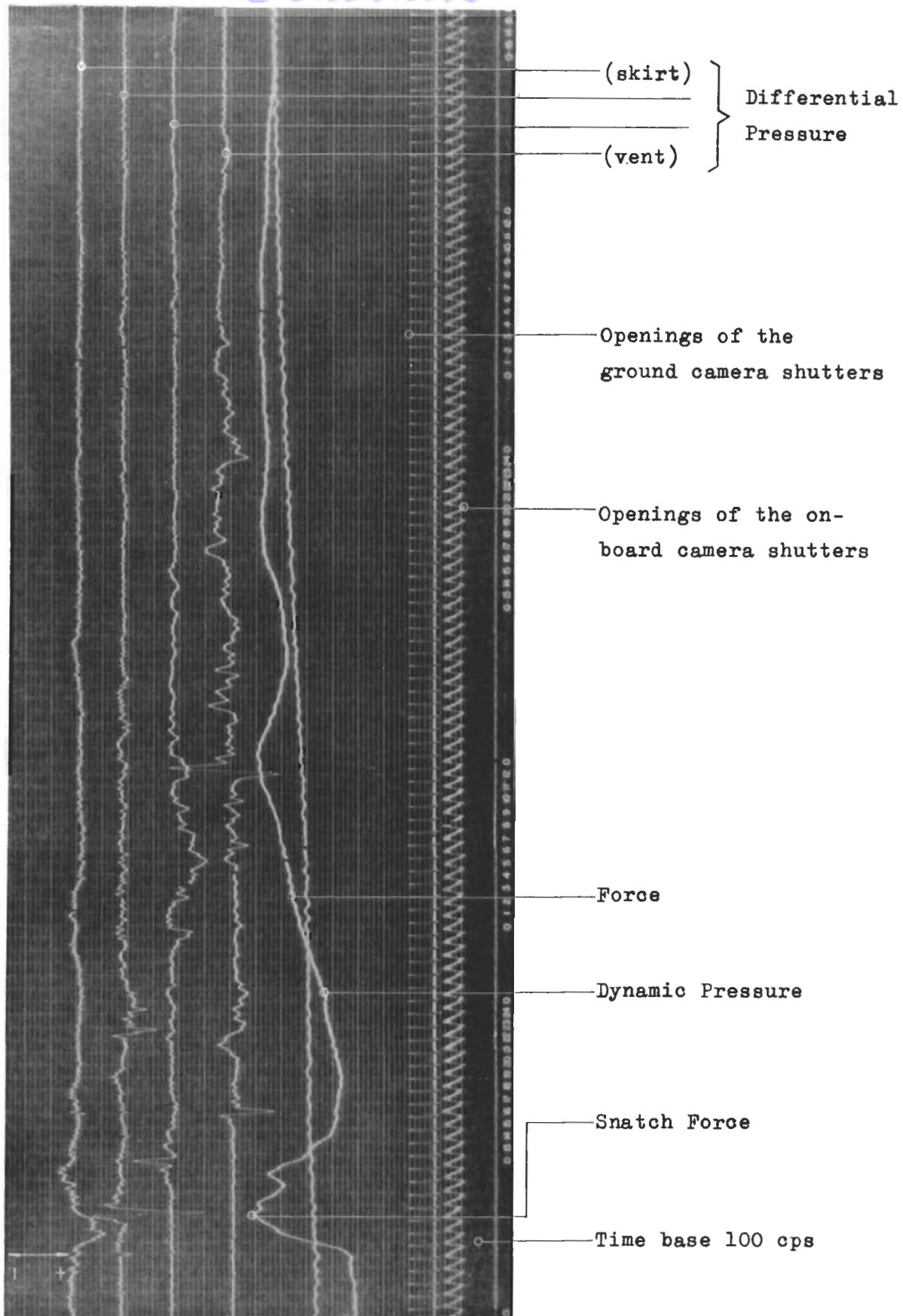


Fig. 59 Original registration. Pressure transducers on the cord center line

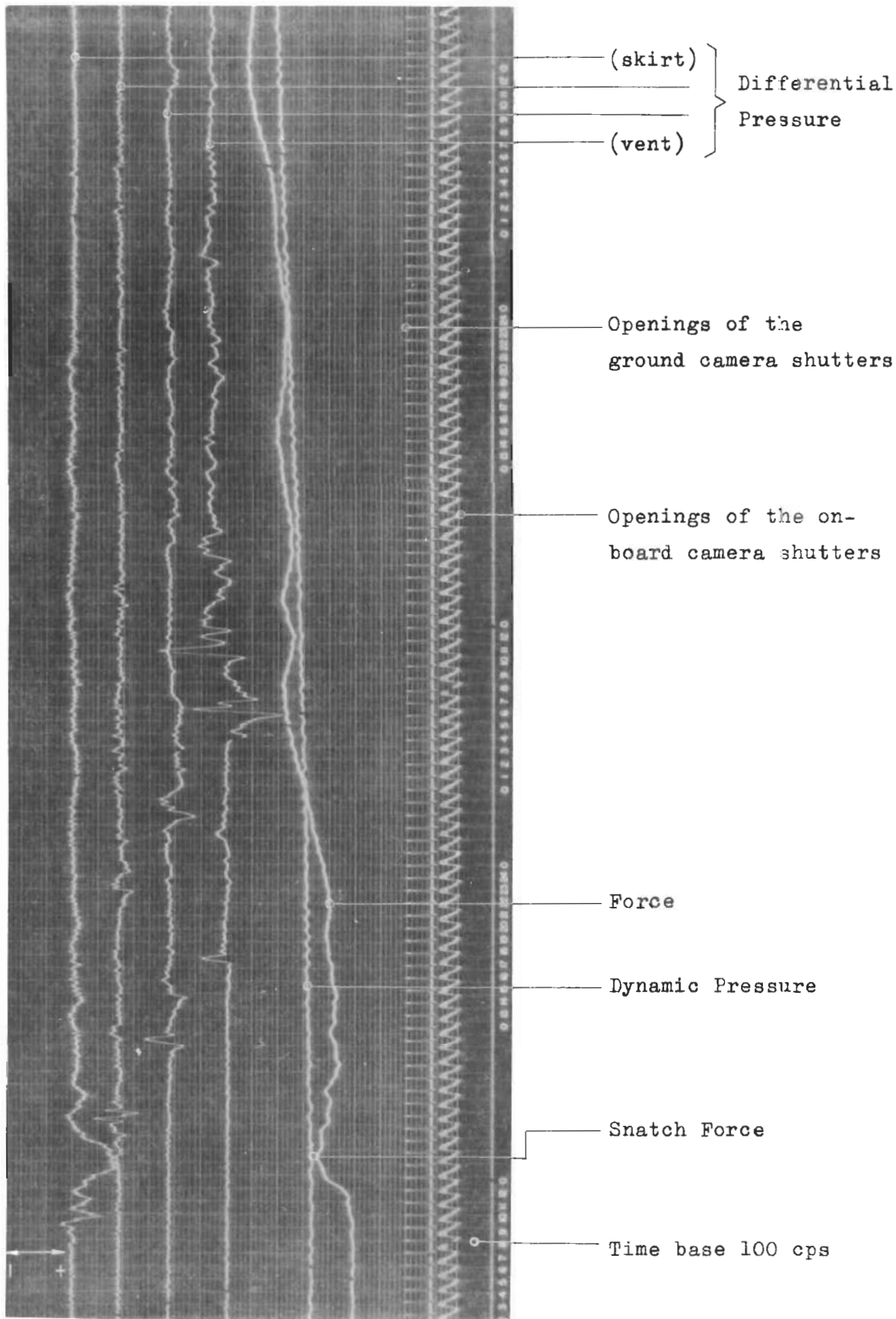


Fig. 60 Original registration. Pressure transducers on the cord center line

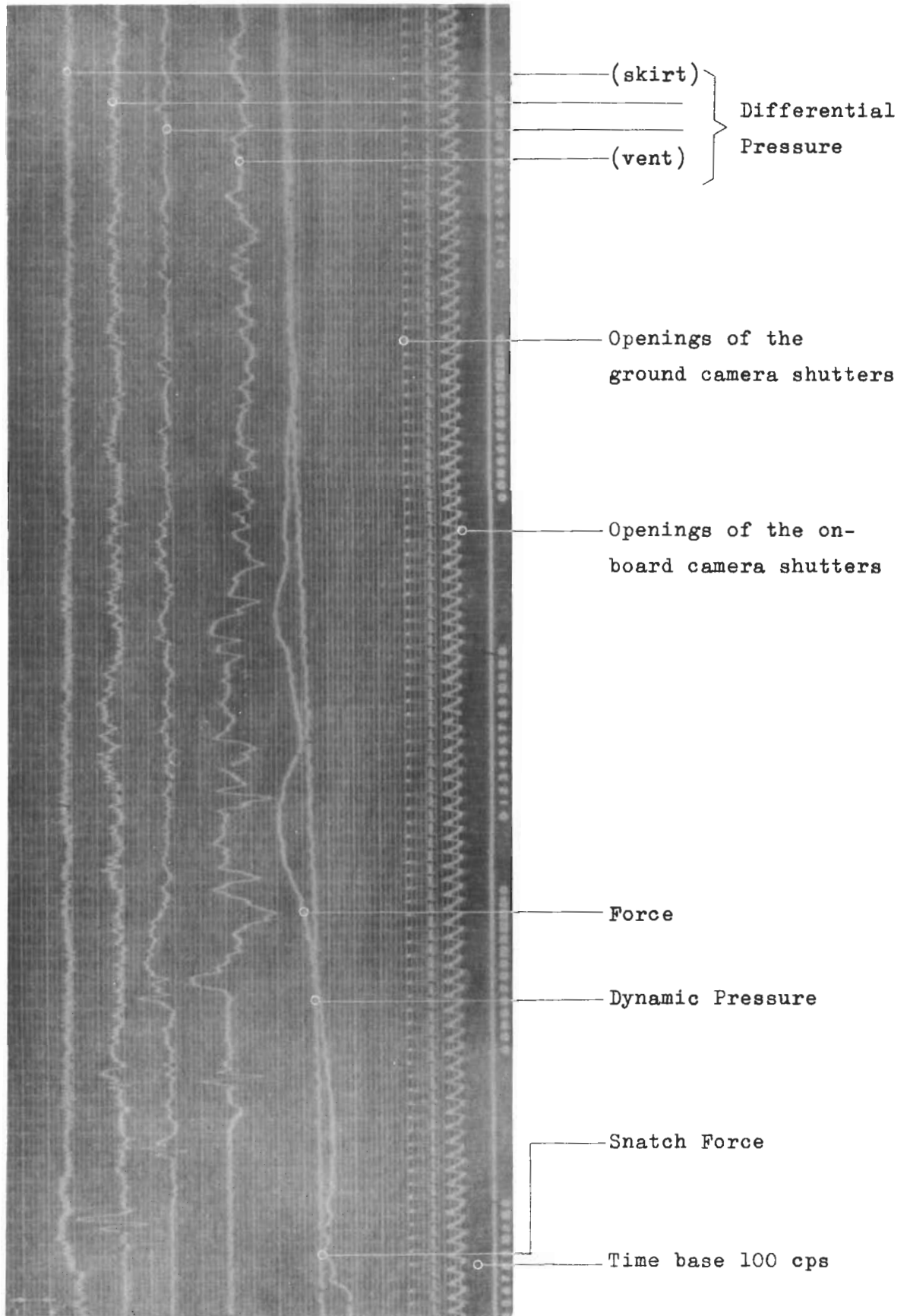


Fig. 61 Original registration. Pressure transducers on the cord center line

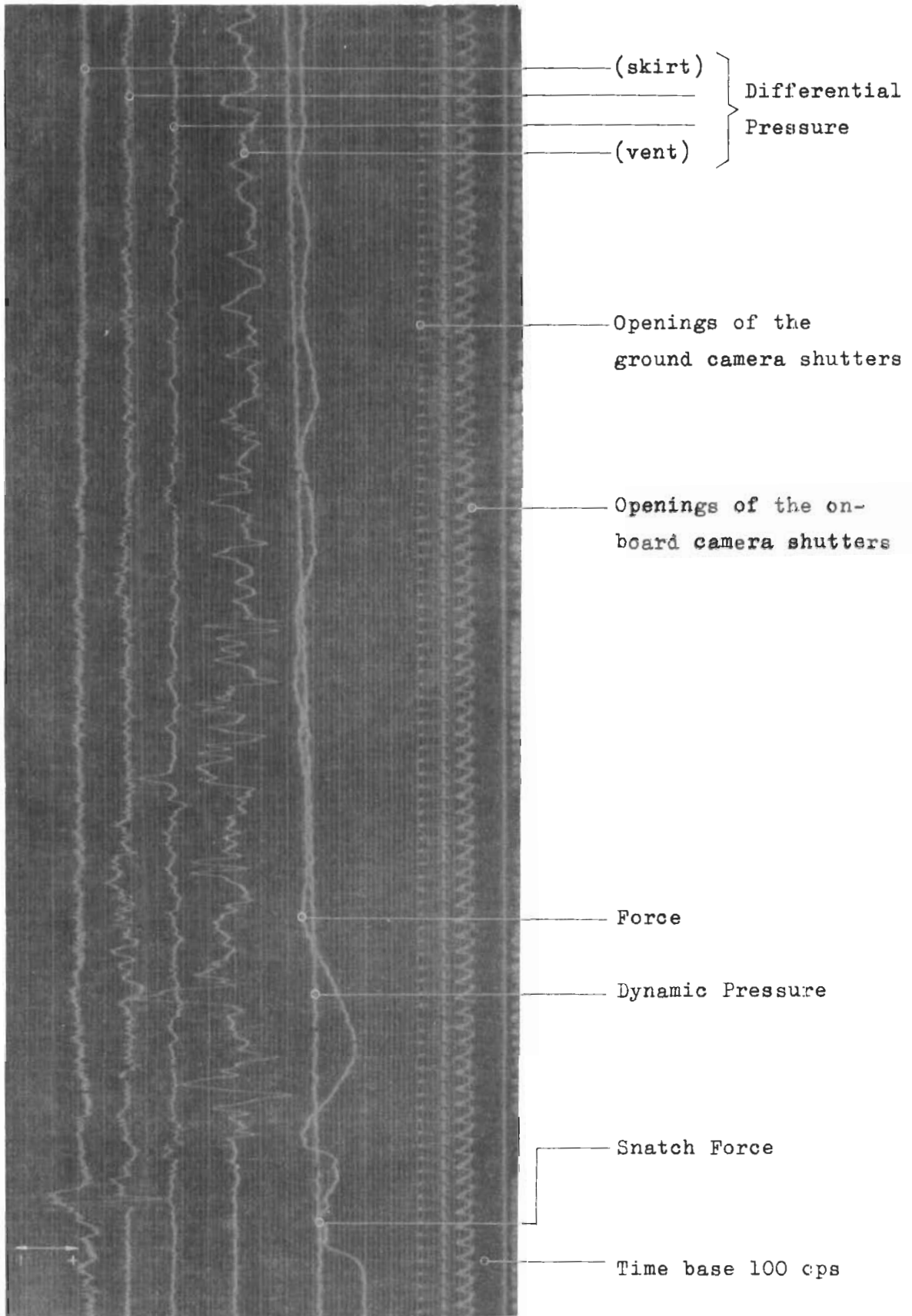


Fig.62 Original registration. Pressure transducers on the cord center line



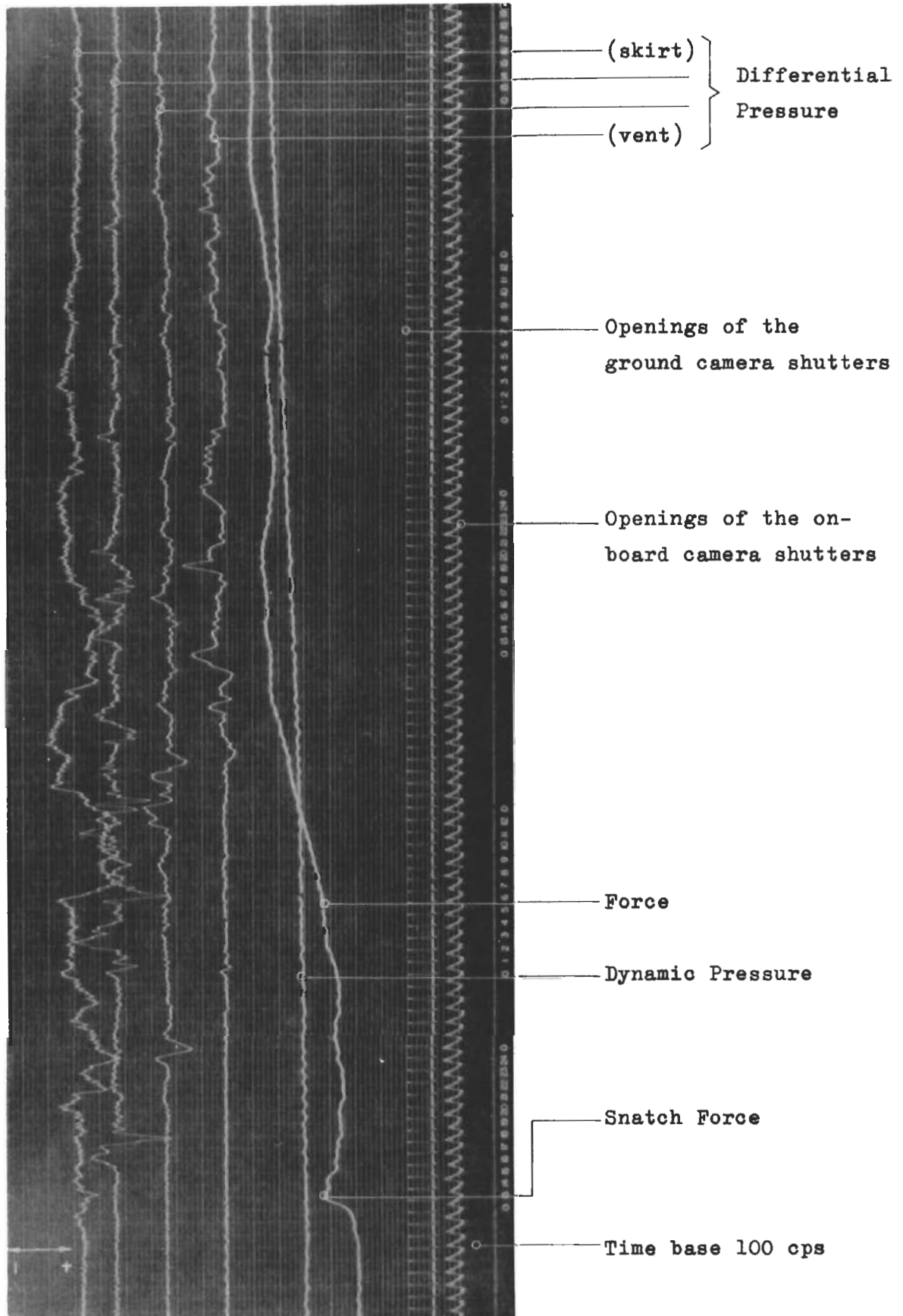


Fig.63 Original registration. Pressure transducers on the gore center line

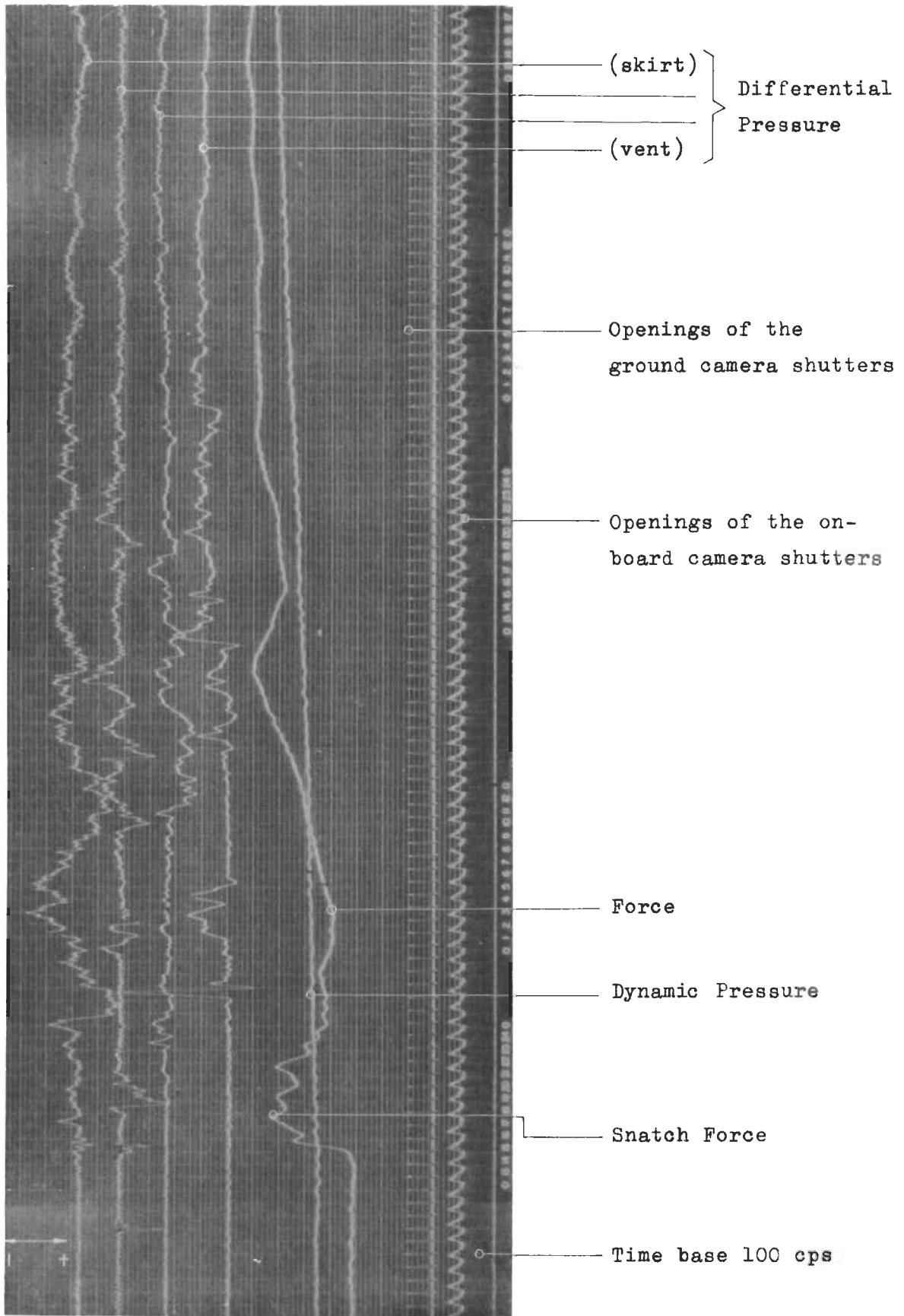


Fig. 64 Original registration. Pressure transducers on the gore center line

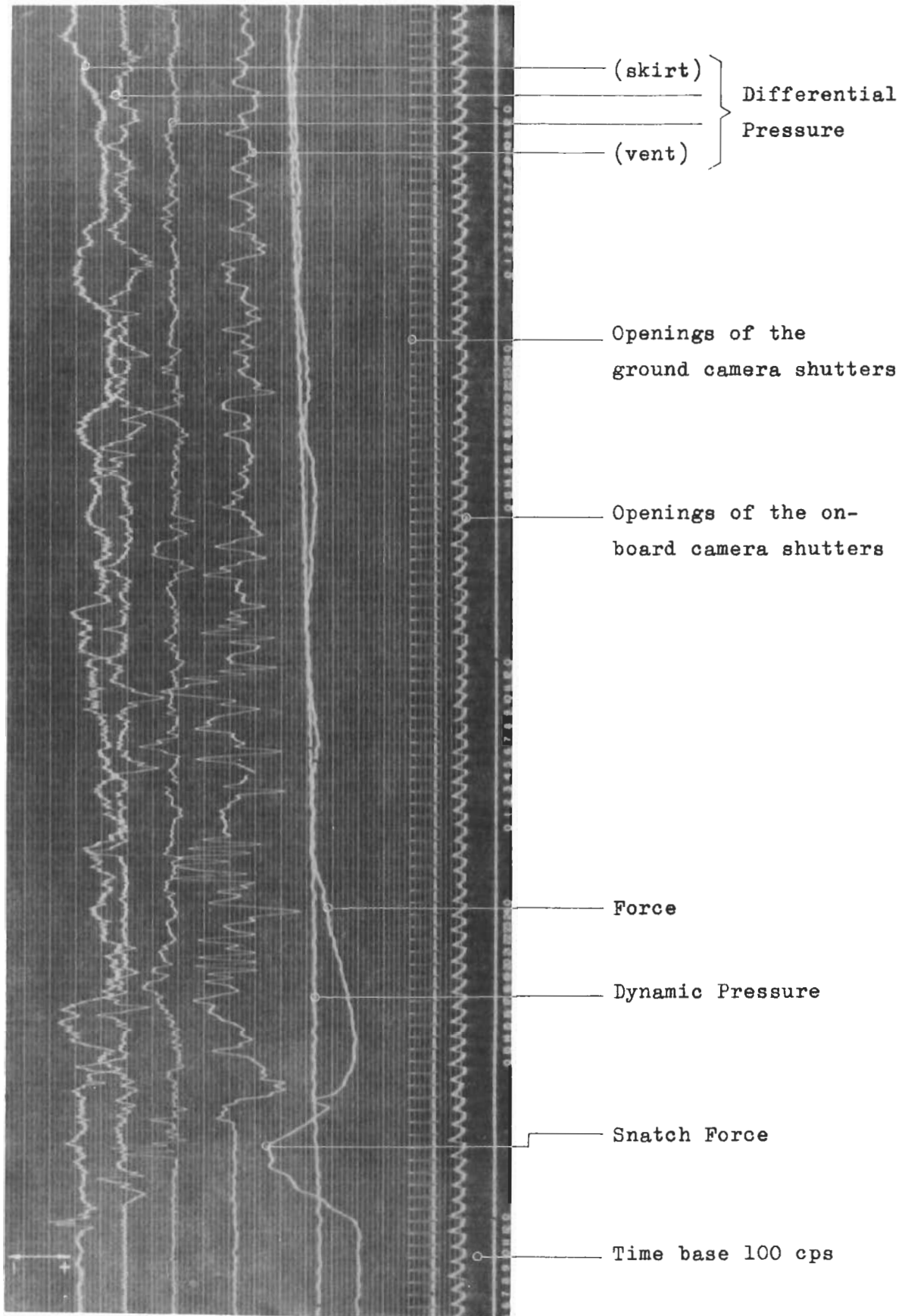


Fig.65 Original registration. Pressure transducers on the gore center line

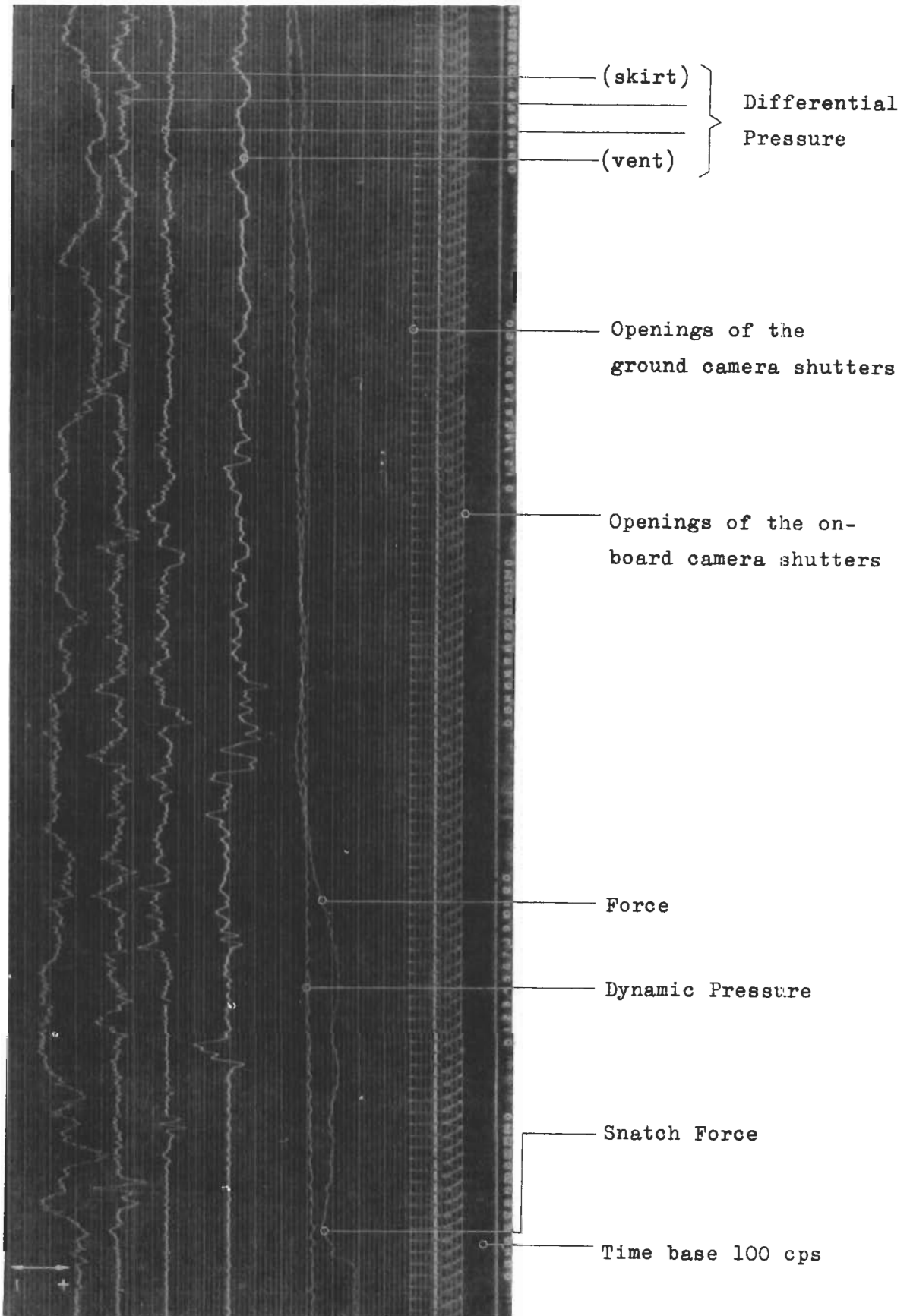


Fig. 66 Original registration. Pressure transducers on the gore center line

UNCLASSIFIED

Security Classification

DOCUMENT CONTROL DATA - R & D

(Security classification of title, body of abstract and indexing annotation must be entered when the overall report is classified)

1. ORIGINATING ACTIVITY (Corporate author) Deutsche Forschungsanstalt fuer Luft-und Raumfahrt E. V. (DFLR), Braunschweig, Flughafen, Germany		2a. REPORT SECURITY CLASSIFICATION UNCLASSIFIED	
		2b. GROUP N/A	
3. REPORT TITLE Pressure Distribution During Parachute Opening Phase II - Finite Mass Operating Case			
4. DESCRIPTIVE NOTES (Type of report and inclusive dates) Final Scientific Report February 1966 - February 1968			
5. AUTHOR(S) (First name, middle initial, last name) H. D. Melzig and C. Saliavis			
6. REPORT DATE February 1969		7a. TOTAL NO. OF PAGES 78	7b. NO. OF REFS 4
8a. CONTRACT OR GRANT NO. AF61(052)-922		9a. ORIGINATOR'S REPORT NUMBER(S)	
b. PROJECT NO. 6065			
c. Task No. 606503		9b. OTHER REPORT NO(S) (Any other numbers that may be assigned this report) AFFDL TR-68-135	
d.			
10. DISTRIBUTION STATEMENT This document is subject to special export controls and each transmittal to foreign governments or foreign nationals may be made only with prior approval of the Vehicle Equipment Division, AF Flight Dynamics Laboratory (PDF) Wright-Patterson AFB, Ohio.			
11. SUPPLEMENTARY NOTES		12. SPONSORING MILITARY ACTIVITY AFFlight Dynamics Laboratory Wright-Patterson AFB, Ohio 45433	
13. ABSTRACT  An experimental investigation was conducted to determine the differential pressure distribution over the surface of parachute canopies during the period of inflation under finite mass conditions.  Full scale parachute canopies of the Circular Flat, 10% Extended Skirt, Ringslot and Ribbon types were utilized during the free-flight test program, and differential pressures on the gore centerline and on the cord line were measured by means of four pressure transducers distributed over the canopy in equal distances from the skirt to the vent.  In order to analyze the relationships and dependencies between the pressure distribution, projected canopy area, canopy shape, generated force, and dynamic pressure, graphical displays of these quantities were made as a function of time for each type of parachute canopy.  The results of the pressure distribution measurements permit a better understanding of the physical nature of the dynamic process of parachute inflation. The stress distribution in a parachute canopy can be calculated if the corresponding canopy shape is known. For this purpose, the evolution of the canopy shape with the corresponding time is presented for each of the canopy types.  (The distribution of this Abstract is unlimited).			

DD FORM 1473  
1 NOV 65

UNCLASSIFIED

Security Classification

# Contrails

UNCLASSIFIED

Security Classification

14. KEY WORDS	LINK A		LINK B		LINK C	
	ROLE	WT	ROLE	WT	ROLE	WT
Parachute Opening Dynamics Parachute Filling Pressure Distribution						

UNCLASSIFIED

Security Classification